Distribution Agreement

In presenting this thesis or dissertation as a partial fulfillment of the requirements for an advanced degree from Emory University, I hereby grant to Emory University and its agents the non-exclusive license to archive, make accessible, and display my thesis or dissertation in whole or in part in all forms of media, now or hereafter known, including display on the world wide web. I understand that I may select some access restrictions as part of the online submission of this thesis or dissertation. I retain all ownership rights to the copyright of the thesis or dissertation. I also retain the right to use in future works (such as articles or books) all or part of this thesis or dissertation.

Signature:

_____ _____

Shang-Hsun Yang Date

Developing a Nonhuman Primate Model of Huntington's Disease

By

Shang-Hsun Yang
Doctor of Philosophy

Graduate Division of Biological and Biomedical Sciences
Genetics and Molecular Biology

_____

Anthony W. S. Chan
Advisor

_____

Andrew P. Escayg
Committee Member

_____

Carlos S. Moreno
Committee Member

_____

Joseph Cubells
Committee Member

_____

Xiao-Jiang Li
Committee Member

Accepted:

_____

Lisa A. Tedesco, Ph.D.
Dean of the Graduate School

_____

Date

Developing a Nonhuman Primate Model of Huntington's Disease

By

Shang-Hsun Yang

B.S., National Chung-Hsing University, 1998
M.Sc., National Taiwan University, 2000

Advisor: Anthony W. S. Chan, Ph.D.

An abstract of

A dissertation submitted to the Faculty of the Graduate School of Emory University in partial fulfillment of the requirements for the degree of Doctor of Philosophy

in

Graduate Division of Biological and Biomedical Sciences
Genetics and Molecular Biology

2008

Abstract

Developing a Nonhuman Primate Model of Huntington's Disease

By Shang-Hsun Yang

Huntington's disease (HD) is an inherited autosomal-dominant disease, manifesting itself as a loss of striatal medium spiny neurons leading to a neurodegenerative disorder in humans. Transgenic mice carrying mutant *huntingtin* (*HTT*) provide an *in vivo* mechanism for HD; however, there are limitations in recapitulating the process of HD in mouse models. In my dissertation work, we developed a non-human primate model of HD that expresses polyglutamine-expanded HTT. Hallmark features of HD, including nuclear inclusions and neuropil aggregates, were observed in the brains of the HD transgenic monkeys. The transgenic monkeys also showed key clinical features observed in human HD patients, including dystonia and chorea. In addition, the microRNA (miRNA) expression profile of HD monkeys was investigated in a high-throughput manner, showing that four potential miRNA candidates, Hsa-mir-196a, Hsa-mir-451, Hsa-mir-486 and Hsa-mir-429, and one target gene, CUG triplet repeat RNA binding protein 2 (CUGBP2), may be correlated to HD. The development of behavioral and pathological phenotypes in the HD monkeys without medical intervention suggests

our studies could emulate the natural course of human HD. The goal of this study is to better understand the underlying biology of HD and to develop potential therapies for HD.

Developing a Nonhuman Primate Model of Huntington's Disease

By

Shang-Hsun Yang

B.S., National Chung-Hsing University, 1998
M.Sc., National Taiwan University, 2000

Advisor: Anthony W. S. Chan, Ph.D.

A dissertation submitted to the Faculty of the Graduate School of Emory University in partial fulfillment of the requirements for the degree of Doctor of Philosophy

In

Graduate Division of Biological and Biomedical Sciences
Genetics and Molecular Biology

2008

Acknowledgments

I would like to thank my advisor, Dr. Anthony W. S. Chan, for his guidance, enthusiasm, encouragement and patience for my Ph.D. study. I would also like to thank my committee members, Drs. Andrew P. Escayg, Carlos S. Moreno, Joseph Cubells and Xiao-Jiang Li, for their guidance, suggestions, and valuable enthusiasm during the course of my dissertation projects. Additionally, I would also express my sincere thanks to all the members in my excellent lab for discussion, technical support and recommendations: Pei-Hsun Cheng, Jinjing Yang, Heather Banta, Eric Ching-Hsun Cheng, Karolina Piotrowska-Nitsche, Brooke Snyder, Jun Liu, Katherine Larkin, Adam P. Neumann, Sarah Ward, Chuti Laowtammathron, Andrew M. Chiu,Elizabeth K. Chu, , Joseph J. Ling, Kanya Singhapakdi and Jessica Li. I also like to thank to Shi-Hua Li, Peng Jin, Keith Edward Szulwach for their guidance for my experiments, and thank for Brooke Snyder, Katherine Larkin, ChangHui Pak, Keith Edward Szulwach, and Jennifer Bradford for revising English of this dissertation. Finally, I would like to thank my wife, Pei-Hsun Cheng, and my family in Taiwan for their endless support for my Ph.D. study.

TABLE OF CONTENTS

FIGURES AND TABLES

CHAPTER I

General Introduction

General information on Huntington's disease:

Huntington's disease (HD), an inherited autosomal-dominant disease which causes neurodegeneration in humans, was first described by the American physician, George Huntington in 1872. HD affects the central nervous system (CNS), resulting in distinct clinical symptoms related to neuron and brain dysfunction (Li and Li, 2006). The prevalence of HD is approximately 7 to 10 out of 100,000 people in the Caucasian population; whereas prevalence decreases in other ethnic groups, such as the African and Asian population (Walker, 2007b). The progression of HD is evident by the degeneration of gray and white matter in the brain, resulting in the loss of neurons (DiFiglia *et al.*, 1997). Classical HD symptoms include personality changes, emotional disturbances, mental deterioration, involuntary movements, progressive cognitive dysfunction, chorea, dystonia, weight loss and motor deficits (Li and Li, 2006; Walker, 2007a, 2007b).

The *Huntingtin (HTT)* gene was first cloned in 1993, and is located at the 4p16.3 region of the short arm of chromosome 4 (Gusella *et al.*, 1983). *HTT* is expressed ubiquitously in the body with the highest levels in the brain and testis

(DiFiglia *et al.*, 1995; Li and Li, 2006; Li and Li, 2004; Sharp *et al.*, 1995; Trottier *et al.*, 1995). The human *HTT* gene (also called *IT15*) has 67 exons spanning more than 200 kb, and wild-type HTT protein is approximately 350-kDa with a polymorphic stretch of 6 to 35 glutamine residues in the N-terminal domain of exon 1 (1993). HD is the result of an expansion of CAG trinucleotide repeats (polyglutamine; polyQ; >37 residues) in the *HTT* gene (Li and Li, 2006; Walker, 2007a). The number of CAG repeats is highly correlated to the severity of the disease. HD patients with > 60 CAG repeats develop symptoms at ~15-20 years of age. Such patients are categorized as juvenile HD patients. Individuals with CAG repeats in the range of 37-60 develop HD later in life, and are categorized as adult HD patient (Estrada Sanchez *et al.*, 2008).

This mutant *HTT* gene results in a toxic gain-of-function by eliciting cytotoxicity of affected cells, primarily in the brain. Mutant HTT causes neurodegeneration, particularly in the striatum region and deeper layers of the cortex (Li and Li, 2006; Walker, 2007a). The key feature of the early stages of HD is the degeneration of striatal medium spiny neurons (MSNs); however cortical

degeneration may also be observed prior to the development of clinical features (Rosas *et al.*, 2005; Vonsattel and DiFiglia, 1998). Other brain regions, such as the hippocampus, the hypothalamus and the cerebellum, are also affected in HD patients (Vonsattel *et al.*, 1985).

Another key determining factor of HD is the size of the HTT fragment, which is highly correlated to the severity and pathogenesis of HD in patients and animal models. Smaller HTT fragments result in more severe phenotypes and earlier onset of HD in transgenic mouse models of HD (DiFiglia *et al.*, 1997; Graham *et al.*, 2006; Gutekunst *et al.*, 1999; Li and Li, 2006; Schilling *et al.*, 1999). In human HD patient and transgenic mouse studies, the N-terminal HTT fragments were misfolded, forming aggregates and inclusions in the brain (DiFiglia *et al.*, 1997; Gutekunst *et al.*, 1999). These studies suggest the proteolysis of full-length HTT to smaller fragments is important in HD pathogenesis. The *HTT* gene contains numerous unique protease cleavage sites within the first 550 amino acids (Graham *et al.*, 2006; Li and Li, 2006; Wellington *et al.*, 2002). These cleavage sites are specific for capsase-3, caspase-6, calpain, and several unknown aspartic

proteases (Gafni and Ellerby, 2002; Kim *et al.*, 2006; Kim *et al.*, 2001; Li and Li, 2006; Lunkes *et al.*, 2002; Wellington *et al.*, 2002). When the caspase-6 site was blocked in HD transgenic mice, neuronal function was protected and striatal neurodegeneration was ameliorated (Graham *et al.*, 2006). This suggests proteolysis of full-length HTT contributes to neurodegeneration and HD pathogenesis. Lysosomal proteases, such as cathepsins D, B and L, also regulate the processing of mutant HTT and the levels of cleavage products (Kim *et al.*, 2006), suggesting their roles in the generation of N-terminal HTT fragments and the clearance of mutant HTT.

Cellular and neuropathology of HD:

HTT plays an important role in intracellular trafficking and interacts with proteins that are related to transcription, intracellular signaling, trafficking, endocytosis and metabolism (Cowan and Raymond, 2006; Li and Li, 2004). Based on previous studies, wild-type HTT participates in protein trafficking between the Golgi and the extracellular space (Strehlow *et al.*, 2007). Additionally, mutant HTT

can sequester dynactin p150 and kinesin to influence axonal transport (Gunawardena *et al.*, 2003; Szebenyi *et al.*, 2003) and affects vesicle transport, such as the transport of brain-derived neurotrophic factor (BDNF) along microtubules (Gauthier *et al.*, 2004). The impairment of cellular transport caused by mutant HTT leads to neuronal toxicity and the loss of neurotrophic support, which results in neuronal cell death (Gauthier *et al.*, 2004). Therefore, mutant HTT may lead to HD via impairment of cellular transport.

Another important set of factors affecting the progression of HD at the cellular level are the proteins that interact with mutant HTT. In the past 15 years, a number of cytoplasmic proteins, such as HTT-associated protein 1 (HAP1) and HTT-interacting protein 1 (HIP1), have been identified that interact with HTT based on a yeast two-hybrid screen and *in vitro* binding assays (Borrell-Pages *et al.*, 2006; Li and Li, 2006; Li *et al.*, 1995). These proteins have been shown to be involved in the HD pathogenesis. For example, the binding of HAP1 with HTT is enhanced by an expansion of polyQ repeats, which regulates the intracellular trafficking of mutant HTT (Li *et al.*, 1995; Rong *et al.*, 2007b; Rong *et al.*, 2006).

HIP1, p150 and 14-3-3 are all involved in the cascade of protein trafficking (Gauthier *et al.*, 2004; Rong *et al.*, 2007a), similar to HTT itself. Additionally, HIP1 is involved in the functions of neuronal cytoskeleton and endocytosis, and also regulates the normal function of HTT with weak binding affinity (Kalchman *et al.*, 1997; Li and Li, 2006). Other cytoplasmic proteins, like Huntingtin associated protein of 40 kDa (HAP40) and Rab protein 5 (Rab5), are involved in modulating the aggregation and toxicity of mutant HTT through macroautophagy (Pal *et al.*, 2008; Pal *et al.*, 2006; Ravikumar *et al.*, 2008). Furthermore, nuclear factors, such as the coactivators, cAMP response element-binding protein (CREB)-binding protein (CREBBP) and specificity protein 1 (Sp1), and transcription factors, such as TATA-binding protein (TBP) and TBP-associated factors 130 (TAF 130), also play a critical role in HD (Li and Li, 2006; Mantamadiotis *et al.*, 2002; Sugars and Rubinsztein, 2003). These studies suggest various cytoplasmic and nuclear proteins play a regulatory role in HD pathogenesis.

The hallmark neuropathological feature of HD is neuronal loss in the caudate and putamen, especially targeting MSNs (Vonsattel *et al.*, 1985). In the

pathological diagnosis of HD, two signature characteristics are neuropil aggregates and intranuclear inclusions in neurons (Li and Li, 2006; Maat-Schieman *et al.*, 2007; Walker, 2007a). In the postmortem brains of HD patients and transgenic mice, HTT aggregates are primarily observed in the nucleus, and mutant HTT accumulates in striatal neurons as HD progresses (Li and Li, 2006; Lin *et al.*, 2001). Based on a structural biology study, mutant HTT is involved in the aggregation process, forming dimers, trimers and oligomers inside the cells (Walker, 2007a). In addition, HTT inclusions are the result of protein misfolding which is caused by the mutant polyQ expansion (Li and Li, 2006). The expression pattern of HTT also relates to the progression of HD, especially in neurons. In healthy individuals, HTT protein is primarily located in the cytoplasm; whereas mutant HTT protein forms aggregates in the nucleus (Li and Li, 2006). In early-stage HD, patients' brains have more neuropil aggregates than nuclear inclusions (DiFiglia *et al.*, 1997; Gutekunst *et al.*, 1999); in late-stage HD, more nuclear inclusions develop. This transition of HTT expression and aggregation may be related to the development of HD and neural degeneration in the brain.

Furthermore, the truncated N-terminal proteins also misfold, aggregate, and form inclusions in HD patients' brains (DiFiglia *et al.*, 1997; Gutekunst *et al.*, 1999), which results in the accumulation of toxic mutant HTT leading to neurodegeneration and cell death.

Aberrant gene regulation in HD:

Although the relationship between polyQ repeats, N-terminal size, and the severity of HD has been determined in different model systems, the effect of mutant HTT on gene regulation remains unclear. Normally, the HTT complex is involved in cellular gene regulation; therefore, mutant HTT is expected to influence gene expression. Based on previous reports, mutant HTT interacts with transcription factors and coactivators at different binding sites, and several transcription factors also contain the polyQ-rich domains, which may interact with other polyQ protein resides (Li and Li, 2006; Ryu *et al.*, 2006). For example, mutant HTT represses the transcription of the p53-regulated promoters, p21 (WAF1/CIP1) and MDR-1 (Bae *et al.*, 2005; Steffan *et al.*, 2000), and also interacts

with transcription factors carrying polyQ or proline-rich domains, such as CREBBP, TBP and TAF130 (Li and Li, 2006; Perez *et al.*, 1998; Shimohata *et al.*, 2000; Steffan *et al.*, 2001). The CAG repeats in HTT also change the normal nuclear location of CREBBP to the nuclear aggregates of HD (Nucifora *et al.*, 2001; Steffan *et al.*, 2000). Transcription activator, Sp1, and coactivator, TAFII130, are also suppressed by mutant HTT, resulting in transcriptional inhibition of the dopamine D2 receptor gene, which causes cellular toxicity (Chen-Plotkin *et al.*, 2006; Dunah *et al.*, 2002). By sequestering transcription factors, such as Sp1, mutant HTT reduces the availability for binding to the promoter region, thus downregulating the expression of target genes (Chen-Plotkin *et al.*, 2006). Furthermore, TBP was found in the HTT aggregates and interacted with polyQ-containing proteins. With the abnormal interaction with these proteins essential for the survival of target neurons, mutant HTT aggregates lead to neuronal death in HD (Huang *et al.*, 1998). Since the aberrant expression of mutant HTT protein was also detected ubiquitously and affected gene expression patterns in peripheral tissues, such as the muscle and blood (Borovecki *et al.*, 2005; Luthi-Carter *et al.*, 2002a), the gene

regulation pathway may also cause dysfunction in peripheral tissues.

HTT interacts with several essential transcription repressors to regulate gene expression. REST (Repressor Element 1 Silencing Transcription Factor, also known as NRSF, Neuron-Restrictive Silencing Factor) is normally expressed in the cytoplasm of neurons; however, in HD, REST is sequestered by mutant HTT and accumulates in the nucleus of neurons. These changes repress the expression BDNF, a REST target gene, and decrease the survival of striatal neurons by altering the cooperation of chromatin-modifying proteins (Ooi and Wood, 2007; Zuccato *et al.*, 2003). REST potentially interacts with more than 1000 sites in the human or mouse genome, and some sites are putative targets related to neuronal function and differentiation (Bruce *et al.*, 2004; Johnson *et al.*, 2006b; Zuccato *et al.*, 2007), thus the regulation of REST may contribute to the development of HD. These studies suggest that mutant HTT may have a compound effect on regulating gene expression via transcription factors and cofactors.

Recently, post-transcriptional regulation of non-coding RNAs in metazoan, mice and humans, especially in the area of miRNAs, has been found. miRNAs are

~21bp non-coding RNAs processed from 70-100bp hairpin precursors by the nuclear ribonuclease III enzyme “Dicer”. The hairpin precursors are from the primary miRNA transcript processed by the nuclear ribonuclease III enzyme “Drosha”. miRNAs interact with an RNA-induced silencing complex (RISC) to silence/modulate gene expression at the post-transcriptional level (Ambros, 2004; Bartel, 2004; He and Hannon, 2004; Kosik, 2006). Several miRNAs have been identified and involved in neuronal functions and development (Lim *et al.*, 2005; Vo *et al.*, 2005; Yu *et al.*, 2008). In several neuronal diseases, such as Fragile X syndrome (Jin *et al.*, 2004; Li *et al.*, 2008; Qurashi *et al.*, 2007), Parkinson’s and Alzheimer’s disease (Kim *et al.*, 2007; Lukiw, 2007), miRNAs play a critical role in pathogenesis. Therefore, it is tempting to speculate that miRNA also plays a role in neuropathogenesis of HD.

Several miRNAs are expressed during brain development; for example, miR-124 is preferentially expressed in brain (Lim *et al.*, 2005; Yu *et al.*, 2008) and miR-132 is enriched in neurons (Vo *et al.*, 2005). These miRNAs are involved in the control of the neuronal transcriptome, and regulation of neuronal

morphogenesis and dendrite development (Lim *et al.*, 2005; Vo *et al.*, 2005; Yu *et al.*, 2008), suggesting a regulatory role of miRNAs in the brain. Another polyglutamine disease, spinocerebellar ataxia type 3 (SCA3), is also modulated by the miRNA, bantam, which acts downstream of SCA3 to prevent degeneration (Bilen *et al.*, 2006). Mutations of Dicer in SCA3 enhance polyQ toxicity in both Drosophila and HeLa cells (Bilen *et al.*, 2006). In a similar study, the depletion of Dicer led to dysfunction in miRNA processing and resulted in the death of Purkinje cells (Schaefer *et al.*, 2007). This evidence implies a neuroprotective role of miRNAs in neural diseases (Schaefer *et al.*, 2007) and gives insight to the miRNA pathway in HD.

Due to the interaction between HTT and the transcriptional repressor, REST, HD may be regulated by miRNAs while REST regulates the expression of several neuronal miRNAs (Conaco *et al.*, 2006). REST suppresses the expression of miR-124a in non-neuronal cells and neural progenitors, leading to the existence of non-neuronal transcripts (Conaco *et al.*, 2006). In the brain tissue of HD mice and human patients, upregulation of REST enhanced the repression of

neuronal-specific miRNA, mir-132, leading to higher levels of p250GAP mRNA (Johnson *et al.*, 2008). It is possible that other miRNAs may also be involved in the pathogenesis of HD at the post-transcriptional level.

Epigenetic modification also contributes to HD pathogenesis by altering nucleosome dynamics, chromatin remodeling and subsequent transcriptional dysregulation. Histone modification is one epigenetic change that is important in HD. Several studies have shown aberrant histone modification patterns in HD patients and animal models. For example, the extent of acetylation and deacetylation of histones differs between HD and wild-type in cell, fly and mouse models based on the expression level of histone acetyltransferase (Giorgini *et al.*, 2008; Sadri-Vakili *et al.*, 2007; Steffan *et al.*, 2001). In addition, altered histone methylation and histone methyltransferase are important for transcription-induced neuronal death in HD (Ryu *et al.*, 2006). Recently, treatments targeting epigenetic modification in HD have been developed, including histone H3 (K9) methyltransferase and histone deacetylase inhibitors (Dompierre *et al.*, 2007; Ryu *et al.*, 2006). These studies support a potential role of mutant HTT in global gene

dysregulation at an epigenetic level (McCampbell *et al.*, 2001; Ryu *et al.*, 2006; Steffan *et al.*, 2001).

The development of HD may be dependent on the effect of mutant HTT on gene regulation; therefore, studies of gene regulation are important in fully understanding HD. The genome-wide DNA microarray analysis in HD is a powerful tool to monitor thousands of gene expression profiles in relation to their pathological status. As a result, several genomic profiling studies using microarray technologies have demonstrated the effect of mutant HTT overexpression on the gene expression profile in different HD mice and patients (Chan *et al.*, 2002; Crocker *et al.*, 2006; Luthi-Carter *et al.*, 2002a; Luthi-Carter *et al.*, 2002b) (Borovecki *et al.*, 2005). There are two categories of expression changes in HD microarray studies: direct responses to mutant HTT, and indirect/secondary compensatory effects to mutant HTT. Therefore, it is a challenge to identify the most important transcripts directly related to HD. Due to the fact that cellular and molecular alterations in neurons or other somatic cells must precede clinical symptoms such as motor dysfunction, identifying a set of genes that are

specifically altered at different stages of HD could be useful in early diagnosis and determining the extent of disease progression of HD. Furthermore, elucidating the transcriptional changes throughout the course of HD will provide important information for understanding the mechanism of neurodegeneration and the development of HD.

Mouse models of HD and limitations:

Transgenic technology has led biomedical research to a new era for animal modeling, which has accelerated the understanding of gene function and disease development. Animal modeling has primarily focused on mice, a mammalian species that has a relatively similar genome to a human's and has a shorter life span than other mammals. Transgenic mice expressing mutant *HTT* controlled by different promoters, including a *HTT* promoter and a neuron-specific promoter (e.g. prion), show similar neuropathology and behavioral changes to HD. One of the most commonly used transgenic mice is the R6/2, which expresses the mutant exon 1 *HTT* with 115-156 CAG repeats under the control of human *HTT* promoter

(Davies *et al.*, 1997; Mangiarini *et al.*, 1996). These mice develop a progressive neurological phenotype, including motor and cognitive deficits (Carter *et al.*, 1999; Lione *et al.*, 1999). They also show a pathological phenotype, including a dramatic loss of MSN in the striatum and neuronal intranuclear inclusions similar to those observed in HD patients (Carter *et al.*, 1999; Li *et al.*, 2003; Li and Li, 2006; Lione *et al.*, 1999). In addition, R6/2 mice begin to lose body weight at approximately 9 weeks old, suggesting metabolic dysfunction and abnormal regulation of weight-regulating factors (van der Burg *et al.*, 2008) (Stack *et al.*, 2005). Furthermore, pre- and post-symptomatic R6/2 mice show alterations in corticostriatal synaptic transmission (Levine *et al.*, 2004) and abnormalities in dopaminergic cell function, which causes progressive motor and cognitive symptoms (Cha *et al.*, 1998; Johnson *et al.*, 2006a; Kung *et al.*, 2007). The neuropathology of R6/2 mice is consistent with the idea that N-terminal fragments of HTT with a CAG repeat expansion are toxic to neurons (Wang *et al.*, 2008). Due to the similarity of these neuropathological and clinical characteristics in HD mice to HD patients, R6/2 mice are broadly used in HD research.

Another transgenic HD mouse N171-82Q expresses the first 171 amino acids of HTT with 82 CAG repeats under the control of neuronal specific *prion* promoter (Schilling *et al.*, 1999). This transgenic line displays similar patterns of neurological symptoms with similar timing to R6/2 mice. The HTT N-terminal fragments are prone to form intranuclear inclusions and neuropil aggregates (Schilling *et al.*, 1999; Wang *et al.*, 2008). These mice also develop behavioral abnormalities, including loss of coordination, tremors, hypokinesia and abnormal gait (Schilling *et al.*, 1999). Studies on N171-82Q mice further support the neurotoxicity of N-terminal fragments of HTT with CAG repeat expansion.

YAC HD transgenic mice carry full-length *HTT* with 46 or 72 CAG repeats under the regulation of the human *HTT* promoter. YAC HD mice provide important evidence supporting the dependence of neuronal cytoplasmic toxicity in HD on the cleavage of HTT followed by nuclear translocation of HTT N-terminal fragments (Hodgson *et al.*, 1999; Van Raamsdonk *et al.*, 2007a; Van Raamsdonk *et al.*, 2007b). Mice with expanded CAG repeats show motor and cognitive impairment, striatal degeneration (Hodgson *et al.*, 1999; Van Raamsdonk *et al.*, 2005; Van

Raamsdonk *et al.*, 2007b), and exhibit a higher sensitivity to NMDA-induced apoptosis in MSNs cultured from early postnatal pups (Fernandes *et al.*, 2007; Hodgson *et al.*, 1999; Shehadeh *et al.*, 2006; Slow *et al.*, 2003). Studies on YAC HD mice provide evidence that neurodegeneration can occur in the absence of HTT aggregates, while proteolytic cleavage of HTT remains important in HD pathogenesis (Hodgson *et al.*, 1999; Li and Li, 2006).

In addition to the above HD transgenic mice, *HTT* knock-in mice representing precise genetic replicas with mutant *HTT* under the control of normal regulatory elements have also been developed. These mice display behavioral phenotypes at approximately 70 weeks, including motor deficit and gait abnormality (Heng *et al.*, 2007; Lin *et al.*, 2001). Regarding the brain, the *HTT* knock-in mouse presents reactive gliosis, the formation of neuronal intranuclear inclusions predominantly in the striatum and neurological abnormality in the striatum (Heng *et al.*, 2007; Lin *et al.*, 2001; Woodman *et al.*, 2007). Overall, the neuropathology of these mice is similar to early-stage HD in human patients (Lin *et al.*, 2001). *HTT* knock-in mice also form widespread aggregates in the brain, dysregulate gene expression in the

striatum and cerebellum and decrease the expression level of specific chaperones, similar to R6/2 mice (Woodman *et al.*, 2007). These similarities suggest that *HTT* knock-in mice develop comparable phenotypes to late-stage HD.

Although several HD mouse models are available and widely used, there are limitations in each of these mouse models. For example, transgenic HD mice do not emulate the distinct neurodegeneration process observed in HD patients even though similar neurological symptoms were observed (Davies *et al.*, 1997; Li and Li, 2006; Schilling *et al.*, 1999). Possible explanations for these limitations are: (1) The extent of neurodegeneration is limited by the short life span of mice (Li and Li, 2006), (2) Gene function may vary between rodents and humans, and (3) There are fundamental differences, especially in the brain, between rodents and humans. Therefore, it is important to develop an animal model with closer proximity to humans (Chan, 2004; Yang *et al.*, 2008a).

The importance and limitations of a non-human primate model of HD:

Non-human primates are ideal for modeling human neurodegenerative

diseases for the following reasons: (1) The development of a non-human primate's brain is similar to that of humans (Presty *et al.*, 1987; Walker *et al.*, 1988), (*2*) The complex behavior of monkeys enables advanced analysis of cognitive, social and motor phenotypes that are classic features of neurodegenerative disorders (Peters *et al.*, 1996), (3) The size of a primate brain allows for high resolution *in vivo* imaging, such as magnetic resonance imaging (MRI) and positron emission tomography (PET), which serve as powerful diagnostic tools in humans. Moreover, the monkey brain is suitable for neurochemical and histopathological analysis because the neuroanatomy is similar to that of humans (Small *et al.*, 2004), (4) Non-human primates have a high genomic and physiologic similarity to humans, thus the likelihood of identifying human ortholog genes in monkeys is higher than with any other species (Chan, 2004), and (5) By *in vivo* imaging, cognitive behavior testing and the gene expression profile monitoring in peripheral blood, a longitudinal study can be performed on monkeys, allowing detailed information to be collected throughout the course of the disease. (Chan, 2004)

Models of HD have been created through chemical induction and stereotaxic

injection of lentiviruses with mutant *HTT* into the brain of non-human primates (Burns *et al.*, 1995; Lee and Chang, 2004; Sramka *et al.*, 1992). Although such primate models develop neuropathological and behavioral changes similar to those observed in HD patients, the effect of mutant HTT on the body as well as on neurons specifically targeted in HD cannot be determined. Thus, a chemical induction and focal transgenic model might not capture the actual events resulting in neurodegeneration in HD. Furthermore, in these monkeys lentiviruses were only administered in the brain, and the disease could not be passes to the next generation by genetic inheritance. This rationale suggests the importance of developing germline HD transgenic monkeys.

There are several important criteria for creating a successful germline of transgenic monkeys, which include (1) integration of the transgene into the host monkey genome, (2) expression of the transgene and bio-activity in the specific targets, (3) germ line transmission to the next generation and (4) expression of the transgene in the next generation. One critical advantage of a germline transgenic model is the possibility of maintaining a unique phenotype by preserving the

genome through assisted reproductive techniques such as gamete preservation. Thus colonies of transgenic monkeys could be reproduced by traditional breeding, and the unique genotype and phenotype could be preserved based on Mendelian law. As a result, monkeys with a similar transgenic background could be used for advanced experiments, limiting individual differences. For these reasons, a germline transgenic monkey model would be superior to a chemical induction or focal transgenic model.

However, there are still some limitations and challenges existing with a transgenic monkey model. First of all, due to the lack of knowledge on non-human primate transgenesis, only one transgenic non-human primate model for human disease has been developed (Chan, 2004; Yang *et al.*, 2008a). Secondly, limited resources of non-human primates present a challenge due to the necessity of gametes for transgenesis (Chan *et al.*, 2001). In addition, the labor-intensive and time-consuming work as well as the long gestation period and life span are difficult for investigators (Chan, 2004). Therefore, to date, the number of germline transgenic monkey models is extremely limited.

The goals for this dissertation

Recent *in vivo* studies using different animal models, including mice, flies and other species have revealed important cellular and molecular mechanisms leading to HD. However, limitations remain due to the dissimilarity of the disease mechanism in humans compared to currently available animal models. Therefore, the primary goal of this dissertation was to generate a non-human primate model of HD based on the hypothesis that the development of HD in a non-human primate will be similar to that in human patients, which includes pathologic and transcriptional alterations. We anticipate an HD transgenic monkey model can capture the neurodegeneration observed in HD patients and that neurological symptoms will occur to a similar extent as in HD patients. In addition to developing HD transgenic monkeys, the secondary goal of this dissertation is to investigate the expression profile of miRNA in these transgenic monkeys based on the hypothesis that abnormal gene regulation occurs as a result of the developing neuropathology in HD transgenic monkeys. Since these monkeys were not

exposed to medical intervention, we expect to identify miRNA candidates that affect natural gene expression in HD. We hope to emulate the natural course of human HD in these transgenic monkeys. These studies will open the way to better understanding the underlying biology of HD and to the development of potential therapies for HD.

CHAPTER II

Establishing a Non-human Primate Model of Huntington's Disease

This chapter presents work published as: Yang SH, Cheng PH, Banta H, Piotrowska-Nitsche K, Yang JJ, Cheng EC, Snyder B, Larkin K, Liu J, Orkin J, Fang ZH, Smith Y, Bachevalier J, Zola SM, Li SH, Li XJ, Chan AW. 2008. Towards a transgenic model of Huntington's disease in a non-human primate. Nature 453:921-924. S.-H.Y. carried out all the experiments described in this chapter except for preparation of high titer lentiviruses and behavioral analysis; P.-H.C.,

construct design and evaluation; K.P.-N., monkey embryo manipulation; H.B., animal management; behavioural testing and all animal procedures; K.L., animal care and behavioural testing; E.C.H.C., molecular analysis; J.-J.Y., preparation of high titre lentiviruses; B.S., J.L. and Z.H.F., neuropathological analysis; J.O., surgical procedures and animal care; Y.S., neuropathological analysis; J.B., design of behavioural and cognitive testing; S.M.Z., experimental design and manuscript preparation; S.H.L. and X.J.-L., construct design, analysis and manuscript preparation; A.W.S.C., monkey embryo manipulation, viral gene transfer, experimental design, construct design, molecular analysis and manuscript preparation.

INTRODUCTION

HD is an autosomal-dominant genetic disorder caused by the expansion of CAG repeats in exon 1 of the *HTT* gene. The severity of HD is closely related to the number of CAG repeats and the size of the HTT fragments (Li and Li, 2006; Li and Li, 2004; Sharp *et al.*, 1995). With the development of transgenic technology, transgenic mice expressing mutant *HTT* have provided useful models for studying the *in vivo* pathogenesis of HD; however, there are clinical features and neuropathological changes that cannot be fully captured in HD mouse models. Therefore, it is important to develop an animal model with closer proximity to humans, which could emulate HD. Non-human primates are ideal for mimicking human neurodegenerative diseases because they are physiologically, anatomically and cognitively similar to humans. Our goal for this chapter is to generate a transgenic monkey model of HD, and evaluate if it is a better model than other available animal models of HD. With the design of the *HTT* transgene and development of an efficient gene transfer method, lentiviruses with mutant

HTT (LVU-*HTT*-84Q or LVU-*HTT*-147Q) were evaluated for gene transfer efficiency and biofunction of the transgenes in 293 FT cells and transgenic mice. In both 293 FT cells and transgenic mice, a high gene transfer rate was achieved. Additionally, overexpression of pLVU-*HTT*-84Q and pLVU-*HTT*-147Q resulted in pathological phenotypes in both cells and mice. To apply the mutant *HTT* lentiviruses to the non-human primate to generate HD transgenic monkeys, the results showed that HD monkeys can be generated and most importantly these animals developed hallmark neuropathology of HD, including the formation of nuclear inclusions and neuropil aggregates in the brains, and classical clinical features of HD, including dystonia and chorea. With this achievement, this transgenic HD monkey model may help elucidate the underlying biology of HD and lead to the development of novel and effective therapies for HD in the future.

MATERIALS AND METHODS

Lentiviral vector construction

Human *HTT* cDNA coding 244 and 307 amino acids, including exon 1 of the *HTT* gene with 84 and 147 CAG repeats (*HTT*-84Q and *HTT*-147Q), was inserted into a lentiviral vector (Gift from C. Lois) (Lois *et al.*, 2002), which was regulated by the human ubiquitin promoter (pLVU-*HTT*-84Q and pLVU-*HTT*-147Q). To increase the level of functional gene transcription, the woodchuck hepatitis virus post-transcriptional regulatory element (WRE) was located in the downstream of mutant *HTT*. To increase the titer of the lentiviruses, the human immunodeficiency virus–1 (HIV-1) flap element was located between the 5' long terminal repeat (LTR) and ubiquitin promoter. The 3' end is the self-inactivating LTR, which prevents the replication of the lentiviruses after integrating into the genome (Lois *et al.*, 2002) (Figure II-1). For the *GFP* lentiviral construct, the *HTT* gene was replaced with the *GFP* gene to generate pLVU-*GFP,* which is also regulated by the human ubiquitin promoter (Figure II-2).

Generation of high titer lentiviruses and infection of 293 FT cells

High titer lentiviruses were generated by co-transfection of lentiviral vectors coding for *HTT*-84Q, *HTT*-147Q and *GFP* (pLVU-*HTT*-84Q, pLVU-*HTT*-147Q and pLVU-*GFP*), pΔ8.9, and vesicular stomatitis virus glycoprotein vector (pVSV-G) (Invitrogen, Inc.) into 293 FT human embryonic kidney (HEK) packaging cells (Invitrogen). The lentiviruses were then concentrated by ultracentrifugation using the method described previously (Chan *et al.*, 2001; Pinkert, 2002). To infect the 239 FT cells using high titer lentiviruses, cells were cultured to 50 % confluency in Dulbecco's Modified Eagle's Medium (DMEM; Invitrogen) containing 10% heat-inactivated fetal bovine serum (Hyclone), 2mM L-Glutamine (Invitrogen) and 100U/mL Penicillin/ 100ug/mL Streptomycin (Invitrogen) followed by adding high titer lentiviruses with polybrene (final concentration: 8μg/mL) into culture medium. Medium with high titer lentiviruses was replaced by fresh medium after overnight culture.

Generation of transgenic mice via perivitelline space (PVS) lentiviral Injection

All procedures conducted in this study were approved by the IACUC at Emory University. Six- to eight-week female ICR/CD1 (Harlan) mice were super-ovulated by an intraperitoneal injection of 7.5 IU pregnant mares' serum gonadotropin (PMSG; Sigma) and followed by 7.5 IU human chorionic gonadotropin (hCG; Sigma) injection 46-50 hrs after PMSG injection. Mouse zygotes were recovered from super-ovulated ICR/CD1 females 18 hrs after hCG injection and mating with ICR/CD1 male mice (Hogan, 1994). The zygotes were cultured in KSOM medium (Chemicon) until lentiviral injection was performed. For PVS injection, a micropipette (Sutter) of 1–2 μm (inner diameter) was made by using P-97 Flaming / Brown Micropipette puller (Sutter) and then used for PVS-injection. Under the IX71 Inverted Microscope (Olympus), the micromanipulation of mouse embryo was processed, and about 100–200 picoliters of high titer lentiviruses with polybrene (final concentration: 5μg/μL) was injected into the PVS of mouse embryo at pronuclear stage (11-18 hrs post-insemination) (Figure II-3). Mouse

zygotes were then cultured in KSOM medium (Chemicon) *in vitro* or implanted into the oviducts of pseudopregnant ICR/CD1 females, and carried to term.

Collection and preparation of rhesus monkey oocytes

Female monkeys with regular menstrual cycles were used and super-ovulated by using exogenous hormone. The female monkeys were subjected once daily to Gonadotropin-releasing hormone (GnRH) antagonist, Antide (Sereno Inc.) and twice daily to r-hFSH (Sereno Inc.) for 8–9 consecutive days via subcutaneous injection. On the last 2 days of r-hFSH/Antide stimulation, animals also received twice daily injections of r-hLH (Sereno Inc.) via subcutaneous injection. On day 7 of hormone stimulation, ovarian development was examined using ultrasonography, and the monkeys received an injection of recombinant human chorionic gonadotrophin (r-hCG) if the follicles were larger than 3-4 mm in diameter.

Cumulus–oocyte complexes (COC) were collected from follicular aspiration around 37 hrs after r-hCG injection. By using laparoscopy, the suction needle with

continuous vacuum was punched into the abdominal cavity, and follicular fluid with COC was aspirated from follicles and collected in Tyrode's Lactate-Pyruvate-HEPES medium (TALP-HEPES) (Bavister *et al.*, 1983). COCs were treated with 1 mg/mL hyaluronidase (Sigma), and cumulus cells were stripped for the evaluation of maturation status (GV: existence of germinal vesicle; MI: disappearance of GV; or MII: extrusion of the first polar body). All oocytes were cultured *in vitro* in *in vitro* maturation (IVM) medium [Connaught Medical Research Laboratories medium (CMRL-1066) containing 10% heat-inactivated fetal bovine serum, 40μg/mL Sodium pyruvate, 150μg/mL Glutamine, 550μg/mL Calcium lactate, 100ng/ml Estradiol and 3ug/ml of Progesterone] at 37°C with 5% CO_2 and 5% O_2.

Collection and preparation of rhesus monkey semen

Male rhesus monkeys were trained and semen was collected via penile electro-ejaculation. Semen was kept at room temperature for 10 mins, and then washed three times using TLAP-HEPES. The sperm quality, such as concentration

and mobility, was evaluated and recorded, and the sperm was incubated in TLAP-HEPES medium at room temperature for at least 2 hrs until intracytoplasmic sperm injection (ICSI) was performed.

Gene delivery in mature rhesus monkey oocytes, ICSI, *in vitro* culture and embryo transfer

Metaphase-II-arrested oocytes were selected for PVS injection followed by ICSI (Figure II-4). A micropipette of 1–2 μm (inner diameter) was made by using P-97 Flaming / Brown Micropipette puller (Sutter) and used for PVS-injection, micromanipulation of monkey oocytes was processed under the IX71 Inverted Microscope (Olympus), and about 100–200 picoliters of high titer lentiviruses (LVU-*HTT*-84Q, LVU-*HTT*-147Q and LVU-*GFP*) with polybrene (final concentration: 5μg/μL) was injected into the PVS. After 1-2 hrs, ICSI was performed to fertilize the virus-injected oocytes. Sperm was aspirated by using an injection micropipette (Humagen) after breaking of the cell membrane in 7% polyvinylpyrrolidone (Humagen) medium. The lentivirus-injected oocyte was held using a holding

pipette, and a single sperm was injected into the cytoplasm through the zona pellucida. Fertilized oocytes were then transferred to Hamster Embryo Culture Medium (HECM-9) (Zheng *et al.*, 2001), and cultured *in vitro* at 37°C with 5% CO_2 and 5% O_2. After 48hrs when embryos had reached the 4-8 cell stage, a small opening was made at the zona pellucida of embryos selected for embryo transfer by a micropipptte driven by Piezo Impact Drive Unit (Prime. Tech Ltd). This procudure is commonly named “assisting hatching.” The selected embryos were transferred into the oviducts of a synchronized recipient female (1-2 days after ovulation) confirmed by the concentration of Estradiol and Progesterone. Ultrasonography and X-ray imaging were applied to determine pregnancy and the numbers of fetuses at 2-3 months after embryo transfer. For the remaining 4-8 cell stage embryos, fresh HECM-9 medium supplemented with 5% heat-inactivated fetal bovine serum was replaced every two days for developmental study.

Primary cell culture of various organs from HD transgenic monkeys

The tissues from miscarried monkeys were collected and washed thoroughly

using Dulbecco's Phosphate Buffered Saline (DPBS) with 100U/mL Penicillin/ 100ug/mL Streptomycin (Invitrogen). Tissues were cut into fine pieces in 0.05% Trypsin/EDTA (Invitrogen) using sterile scissors and digested for 10-15 mins at 37°C. Supernatant of the digested tissues was then transferred to a 10 cm culture dish with DMEM (Invitrogen) containing 10% heat-inactivated fetal bovine serum (Hyclone), 2mM L-Glutamine (Invitrogen) and 100U/mL Penicillin/ 100ug/mL Streptomycin (Invitrogen). The culture medium was changed every 3-4 days. When cell culture reached 95% confluency, they were passaged or frozen for future studies.

Genomic DNA extraction, PCR Analysis and determination of CAG repeat length

The mouse tail snip, approximately 0.5 cm, for genomic DNA extraction was cut from new pups 10-14 days after birth. The monkey tissues, such as umbilical cord, placental tissues and peripheral tissues, were collected from each monkey for genomic DNA extraction. Genomic DNA was extracted using the Wizard® Genomic

DNA Purification Kit (Promega), and DNA quality was determined by BioPhotometer (Eppendorf). To detect the foreign *HTT* gene, ubiquitin-F forward primer (5'-GAGGCGTCAGTTTCTTTGGTC-3') and HTT-R reverse primer (5'-GCTGGGTCACTCTGTCTCTG-3') was used to yield 818 and 1007 bp products (for *HTT*-84Q and *HTT*-147Q, respectively) after amplification of genomic DNA from the HD tissue. However, variation in the size of PCR products resulted because of variable numbers of CAG repeats. Genomic DNA (100 ng) was subjected to PCR with 1.65M Betaine (Sigma) at 96 ℃ for 5 mins first; 96 ℃ for 45 secs, 62 ℃ for 45 secs, 72 ℃ for 150 secs for 35 cycles and then 72℃ for 7 mins. To determine the number of CAG repeats in HD mice and monkeys, the PCR products were sequenced using HD exon 1 forward primer (5'-GGCGACCCTGGAAAAGCTGA-3'). To detect the GFP gene, GFP-F forward primer (5'-TTCAAGGACGACGGCAACTAC-3') and GFP-R reverse primer (5'-TAGTGGTTGTCGGGCAGCAG-3') were used for amplification at 94 ℃ for 5 mins first; 94 ℃ for 30 secs, 64 ℃ for 30 secs, 72 ℃ for 20 secs for 35 cycles and then 72℃ for 7 mins, yielding a product of 302 bp. DNA from wild-type mice was

used as the control.

RNA extraction, reverse transcription (RT), RT-PCR and real-time quantitative PCR (Q-PCR) Analysis

The brain tissue from the cortex and striatum of miscarried HD monkeys was used for RNA extraction using RNeasy Mini Kit (Qiagen). The extraction procedure was performed as recommended by the manufacturer. RNA quality was determined by BioPhotometer (Eppendorf). RT was performed using the High Capacity cDNA Reverse Transcription Kit (Applied Biosystems), and cDNA was used for RT-PCR and Q-PCR. To determine the RNA expression of mutant *HTT* via RT-PCR, two specific primers, HD 150Q forward primer (5'-GTTTTTGGCTTTTTTGTTAGACGA-3') and HD 150Q reverse primer (5'-TCAGCTTTTCCAGGGTCGCC-3'), were used for amplification at 94 ℃ for 5 mins first; 94 ℃ for 30 secs, 64 ℃ for 30 secs, 72 ℃ for 10 secs for 35 cycles and then 72℃ for 7 mins, yielding a product of 79 bp. To quantify the relative RNA expression levels, Q-PCR was performed using the cDNA. 2X Power SYBR®

Green PCR Master Mix (Applied Biosystems) was mixed with specific primers and cDNA, and subjected to the iQ5 real-time PCR detection system (Bio-Rad) for at 96 ℃ for 12 mins first; 96 ℃ for 15 secs, 60 ℃ for 30 secs for 50 cycles. 18S primers were used as an internal control to normalize expression levels. The sequences for the specific primers were the following:

HD Exon 1-F: ATGGCGACCCTGGAAAAGCT

HD Exon 1-R: TGCTGCTGGAAGGACTTGAG

rHAP1 F: GACACCAGCCGCCTACTTTG

rHAP1 R: TCTTTTTGACTGGCGGATGTAG

rHIP1 F: TAATAGAGGGGCTGCTTGTTGT

rHIP1 R: CAAATGATGAAACTGAAAAGACTG

rTBP F: CTTACGCTCAGGGCTTGGC

rTBP R: GCTGCCTTTGTTGCTCTTCCA

rCREBBP-F: AGCGAAACCAACAAACCATCCT

rCREBBP-R: TGGGGTCTATGGGATTTGGGT

18S F: CGGCTACCACATCCAAGGAA

18S R: CCTGTATTGTTATTTTTCGTCACTACCT

Southern blotting analysis

Eight micrograms of genomic DNA were digested overnight using *EcoR* I, which only cut once within the transgene. The digested genomic DNA was then separated by gel electrophoresis on a 0.8% agarose gel and transferred to Hybond-N nylon membranes (Amersham). To determine the number of integration events of the lentiviruses (LVU-*HTT*-84Q, LVU-*HTT*-147Q and LVU-*GFP*) in transgenic monkeys, a subtraction approach was used because all constructs have identical lentiviral backbones and the short fragment of *HTT* was not sufficient to distinguish between mutant and endogenous *HTT*. We hybridized two identical membranes with a [32P]-labeled probe that specifically binds to the *GFP* gene and to the flap sequence of the lentiviral vector. [32P]-hybridized membranes were then exposed to the phosphor screen followed by scanning using the Typhoon phosphorimager (GE). The number of integration events of the *GFP* gene and mutant *HTT* was calculated by subtracting the number of *GFP* integration

events from the total number of integration events determined by the flap probe. The number of transgenic mutant HTT gene integration events could then be estimated. Plasmid DNA (pLVU-*HTT*-84Q and pLVU-*GFP*) was used as a positive control; genomic DNA from a non-transgenic monkey was used as a negative control

Western blotting analysis

Total protein was extracted from different cell types and tissues by using the appropriate volume of 1X RIPA buffer (50mM Tris-HCl pH8.0, 150mM NaCl, 1mM EDTA pH 8.0, 1mM EGTA pH 8.0, 0.1% SDS, 0.5% deoxycholate, 1% Triton) with 1X protease inhibitor cocktail (Roche). The samples were lysed in a 1.5mL tube using a sonic dismembrator (Fisher) and then kept on ice for at least 30 mins. The samples inside 1.5 mL tubes were then centrifuged in 13,000 rpm speed for 10 mins, and the concentration of the supernatant was determined using the Bradford assay (Pierce). After measuring the protein concentration, equal amounts of protein extract with 1X loading dye (0.25 X Tris-HCl/SDS stacking gel buffer, pH

6.8, 2% SDS, 10% Glycerol, 0.1% 2-mercaptoethanol and 0.002% bromophenol blue) were boiled for 10 mins before loading into a polyacrylamide gel. After electrophoresis, proteins were transferred onto a PVDF membrane (Bio-Rad) using protein mini trans-blot cells (Bio-Rad) overnight at 4 ℃ followed by blocking in 5% skimmed milk for 2 hrs. The membrane was incubated with the primary antibodies, mouse monoclonal mEM48 (1:50 dilution), 1C2 (;1:2000 dilution) and γ-tubulin (Sigma; 1:2,000 dilution), for at least 2 hrs, followed by secondary peroxidase-conjugated antibodies (Jackson ImmunoResearch laboratories) for detecting proteins with an Amersham ECL kit (PerkinElmer).

Immunohistochemistry staining for 293 FT cells, mouse brain and monkey brain tissues

The infected 293 FT cells and primary culture cells from various tissues were cultured on cover slides and then fixed in 4% paraformaldehyde for 15 mins. After washing with DPBS, these fixed cells were then immunostained. Cell samples were incubated with the primary antibody, mEM48 (1:50) overnight at 4 ℃ followed

by incubation with the secondary antibody conjugated by Alexa Fluor® 488 or 594 (Invitrogen). The fluorescence images were examined by Olympus BX51 microscope and captured with MetaMorph software (Universal Imaging). For mouse brains, the transgenic mice was anesthetized using 2.5 % 2-2-2 Tribromoethanol (Sigma) dissolved in Tert/amyl alcohol (Sigma), and then were perfused using 4% paraformaldehyde. Post-mortem brain tissue from transgenic mice were fixed in 4% paraformaldehyde overnight at 4 ℃, transferred to 30% sucrose, stored at 4 ℃, embedded in Optimal Cutting Temperature (OCT) medium (Sakura) and cut at 50 μm, followed by DAB Immunohistochemistry staining. Post-mortem brain tissue of transgenic monkeys was fixed in 4% paraformaldehyde for 7-10 days at 4 ℃, and then transferred to 30% sucrose and stored at 4 ℃ until the brain tissues were saturated and sank down to the bottom of the container. Monkey brain tissue was embedded in OCT medium, cut at 50 μm, and used for DAB Immunohistochemistry staining. For DAB Immunohistochemistry, sections were incubated with 0.3% hydrogen peroxide for 15 mins, blocked for 1 hr at room temperature, and incubated with mEM48 (1:50) at 4 ℃ overnight. After

washing with DPBS, the brain sections were processed with avidin–biotin using the Vectastain Elite ABC kit (Vector Laboratories), and immediately stained with a 3, 3'-diaminobezidine (DAB; Vector Laboratories) for 30–40 secs or as required. Brain sections were mounted on the slides with mounting media (Sigma), and images were examined by Olympus BX51 microscope and captured by MetaMorph software (Universal Imaging). For 1C2 (1:4000 dilution) staining, the tissues were treated with formic acids (88%) for 10 mins before subjecting to the DAB immunohistochemistry staining.

Monitoring GFP expression in infants

To detect GFP expression, live HD monkey infants were placed under a Sky-blue II epifluorescent light (475 nm; Youlum), and images were captured using a digital camera equipped with an emission filter at an emission wavelength of 520 nm.

HD primate model rating scale

In order to determine the development of HD in nonhuman primate models, HD

primate model rating scale was designed and adapted from the Unified Huntington's Disease Rating Scale (1996; Andrich *et al.*, 2007a, 2007b) to evaluate the presence and severity of motor symptoms that classically accompany the disease. The scale is specific to motor activity, bradykinesia, rigidity, dystonia, chorea, diagnosis confidence level and functional assessment. A scoring system with 80 is the highest score of the most severe symptoms.

Statistical analysis

Chi-square analysis and SAS software for multiple comparisons were used to compare the development rate of embryos *in vitro*. Differences of $P < 0.05$ were considered statistically significant.

RESULT

Lentiviral vector construction and *in vitro* evaluation

Due to the limited number of monkeys and resources available, it is important to design an effective construct and gene transfer method for creating transgenic monkeys, specifically to achieve the overexpression of mutant *HTT* and the development of HD. Based on a hallmark study of HD in 1997 (Davies *et al.*, 1997), which showed exon 1 of *HTT* is sufficient to elicit the HD, we designed a mutant *HTT* construct with a human ubiquitin promoter to regulate the expression of mutant *HTT*. Therefore, exon 1 of the *HTT* gene with 84 or 147 CAG repeats under the control of the human ubiquitin promoter was developed (*HTT*-84Q and *HTT*-147Q) (Figure II-1). To achieve a high degree of gene transfer, we chose the lentiviral transgenesis approach because of our prior success (Lois *et al.*, 2002; Yang *et al.*, 2007). We inserted the transgene into the lentiviral vector (Gift from C. Lois)(Lois *et al.*, 2002) to generate pLVU-*HTT*-84Q and pLVU-*HTT*-147Q (Figure II-1). For the *GFP* construct, the *HTT* gene was replaced by the *GFP* gene to

generate pLVU-*GFP*, also regulated by the human ubiquitin promoter (Figure II-2). The functional expression of pLVU-*GFP* was confirmed in our prior study (Yang *et al.*, 2007). In order to achieve a high infection rate in 293 FT cells and mice, a high-titer virus (>10^9 CFU/mL) was produced. To confirm the biofunction of LVU-*HTT*-84Q and LVU-*HTT*-147Q *in vitro*, they were introduced into 293 FT cells, and crude protein was extracted for examination by Western blotting.

After lentiviral infection in 293 FT cells, extreme toxicity of mutant HTT with a truncated N-terminal region and expanded CAG repeats resulted in cell death. To confirm the expression of mutant HTT in 293 FT cells, Western blotting analysis was performed using mEM48 and 1C2, antibodies that specifically recognize the N-terminal region of mutant HTT and the expanded polyQ domain respectively. These antibodies were used to detect oligomeric HTT at different molecular weights in the stacking gel (>250 kD) and separating gel (< 250 kD). The antibody against γ-tubulin was used as an internal control to confirm equal amount of protein in each well. Mutant *HTT* was efficiently expressed in 293 FT cells and formed oligomeric HTT at high molecular weight (>250 kD) in the stacking gel via

the detection of mEM48 antibody. In the separating gel, 1C2 antibody detected expanded HTT at a lower molecular weight (< 250 kD) (Figure II-5).

In addition to Western blotting analysis, mEM48 antibody was used to determine the expression pattern of mutant HTT by immunocytochemistry. We observed a broad distribution of mutant HTT in cells expressing both LVU-*HTT*-147Q (Figure II-6) and LVU-*HTT*-84Q (Figure II-7), including inclusion bodies in the cytoplasm and nuclei.

The production of transgenic HD mice

To test the efficiency and biofunction of HD lentiviruses *in vivo*, the high-titer lentiviruses used in the 293 FT cell study were used to generate HD transgenic mice. We injected the lentiviruses into the PVS of embryos at the pronuclear stage followed by *in vitro* culture or embryo transfer into pseudopregnant females. First, we determined the impact of HD lentiviruses on the development of preimplantation mouse embryos. The rate of development to the 4-cell and blastocyst stage was significantly lower in both transgenic groups than in the

control group (P<0.05); whereas there was no difference in rate between the LVU-*HTT*-147Q and LVU-*HTT*-84Q groups (Table II-1).

Some of the injected embryos were transferred into surrogate females, and carried to term. At day 10-14 after birth, we snipped the tail for genotyping and determining the number of CAG repeats. By using specific primers that amplify the 3' terminus of the ubiquitin promoter and exon 1 with various CAG repeats, we confirmed the generation of nine (9/10; 90.00%) and six (6/9; 66.67%) transgenic founder mice using LVU-*HTT*-147Q and LVU-*HTT*-84Q lentiviruses (Figure II-8), respectively. Despite the use of these two specific lentiviral vectors, the exact length of the CAG repeats varied for each founder (Figure II-8; Table II-2).

Due to the ubiquitin promoter used to regulate mutant *HTT* expression, mutant HTT protein was expected to pervade all tissues, including the tail; therefore, a tail snip can be used to predict the expression pattern of mutant HTT without euthanizing the transgenic founders. Three antibodies, mEM48, 1C2, and γ-tubulin, were used for Western blotting analysis. In general, tail protein from the LVU-*HTT*-147Q (Figure II-9) or LVU-*HTT*-84Q (Figure II-10) transgenic founders

contained oligomeric HTT at high molecular weights, visualized by Western blotting in the stacking gel, but relatively less low molecular weight HTT, in the separating gel of a Western blotting. However, individual variations in the expression level of HTT were observed among founders.

Abnormal neuropathology in HD transgenic mice is an important indicator of our constructs' biofunction. Nuclear aggregation and intranuclear inclusions are two important features of HD neuropathology. Based on the immunohistochemistry staining using the mEM48 antibody, nuclear aggregation and inclusion bodies were observed in various brain regions, such as the cortex, striatum, cerebellum and hippocampus (Figure II-11). In addition to neuropathology, behavior was monitored to determine the extent of motor deficit in HD transgenic mice (Carter *et al.*, 1999; Lione *et al.*, 1999). Clasping is one important behavioral phenotype indicating a motor deficit in HD mice (Carter *et al.*, 1999; Lione *et al.*, 1999; Schilling *et al.*, 1999). At 5 months of age, our transgenic mice, LVU-*HTT*-147Q (9/9; 100.00%) or LVU-*HTT*-84Q (6/6; 100.00%) transgenic founders, displayed clasping behavior similar to N171-82Q mice, which have been well-characterized

(Schilling *et al.*, 1999) (Figure II-12).

The *in vitro* development rate of monkey embryos after lentivirus injection

Lentiviral transgenesis in monkeys is similar to that in mice, except lentiviruses were injected at different embryonic stages for each. In mice, we injected the lentiviruses into the PVS at the pronuclear stage; whereas we injected lentiviruses into the PVS at the MII stage of monkey oocytes followed by ICSI (Figure II-4). To establish an HD transgenic monkey, first we determined the rate of successful development in monkey embryos *in vitro* after lentivirus injection and ICSI. We injected the LVU-*GFP* and LVU-*HTT* lentiviruses at the same time and observed GFP expression after the 8-16 cell stage (Figure II-13). Embryos co-injected with LVU-*HTT*-84Q/LVU-*GFP* lentiviruses (n=130) showed comparable rates to the control group for reaching the blastocyst stage ($P>0.05$; n=450); however, the LVU-*HTT*-147Q (n=119) group had a significantly lower blastocyst rate compared to the other two groups ($P<0.05$; Figure II-14).

The generation of transgenic monkeys via lentiviral tansgenesis

We have generated a total of 17 monkeys, including four (4/4; 100%) LVU-*HTT*-147Q and nine (9/13; 69.23%) LVU-*HTT*-84Q transgenic monkeys (Table II-3). Among these 17 monkeys, twelve (No.1-No12) miscarried after approximately two-four months gestation. Nos. 1-4 were LVU-*HTT*-147Q transgenic monkeys, but carried different polyQ repeats. Three of these monkeys (Nos. 2-4) miscarried after four months gestation; whereas one (No. 1) miscarried after two months gestation. Nos. 4-18 were co-injected with the LVU-*GFP* and LVU-*HTT*-147Q or LVU-*HTT*-84Q lentiviruses and were all GFP positive (14/14; 100.00%). Among these fourteen GFP monkeys, nine of them (9/14) were double transgenic monkeys: No. 4 carried LVU-*GFP* and LVU-*HTT*-147Q and the others carried LVU-*GFP* and LVU-*HTT*-84Q (Table II-3).

There were five live-born infants, which included two sets of twins delivered by caesarean section and a singleton delivered naturally. We labeled these monkeys rHD-1, rHD-2, rHD-3, rHD-4 and rHD-5 (No. 14, 15, 16, 17 and 18, respectively) in the following studies. All five infants carried the LVU-*HTT*-84Q and LVU-*GFP*

transgenes, and the number of CAG repeats varied for each animal similar to the LVU-*HTT*-147Q transgenic monkey and HD transgenic mice (Figure II-15; Table II-2; Table II-3). Images of the HD transgenic monkeys, rHD-1 and rHD-2, were taken under fluorescent light in order to show the expression of GFP (Figure II-16). Unfortunately, rHD-2 was euthanized at one year old and rHD-3 was euthanized at one month because of severe neurological phenotypes. rHD-4 and rHD-5 were euthanized at one day after birth because of complications elicited by neurological abnormalities. At the time of writing, rHD-1 which carries twenty-nine CAG repeats in exon 1 of mutant *HTT* is fifteen months of age, and has not developed neurological symptoms.

The confirmation of transgene expression by DNA, RNA and protein analysis in HD transgenic monkeys

To confirm transgenic status and copy number in our monkeys, we extracted genomic DNA from available tissues for PCR and Southern blotting. By using primers that specifically amplify the 3' region of the ubiquitin promoter and *HTT*

fragment with various CAG repeats, four (4/4; 100%) LVU-*HTT*-147Q and nine (9/13; 69.23%) LVU-*HTT*-84Q monkeys were confirmed to be HD transgenic monkeys (Table II-3). For the pLVU-*GFP* and LVU-*HTT* co-injected group, all (14/14; 100.00%) monkeys were GFP positive. By sequencing the PCR products from these HD monkeys, we determined the exact CAG repeat length, and confirmed a variation ranging from 11 to 122 polyQ lengths (Table II-3).

For the 5 live-born monkeys, we used the DNA from placenta and umbilical cord for detection, and observed the positive bands in the PCR results of *HTT* and *GFP* sets (Figure II-15). For rHD-4 and rHD-5, we additionally determined the transgenic status in different tissues, and same PCR results from different organs in *HTT* and *GFP* sets were presented (Figure II-17).

To further verify the transgenic status and to determine the copy number of the transgene in each monkey, Southern blotting was performed using both GFP and flap probes as described in the Materials and Methods section. All live-born infants have multiple integration sites as indicated by the GFP probe. rHD-1 and rHD-2 had one copy of mutant *HTT* while rHD-3, rHD-4 and rHD-5 had two, two and four

copies of mutant *HTT* , respectively (Figure II-18). Multiple integration sites of *HTT* and *GFP* were also present in several miscarried monkeys (Table II-3); however, some fetuses had severe post-mortem damage resulting in poor DNA quality, and Southern blotting analysis was not possible.

The primary organ of interest for HD is the brain because of the specificity of neuropathological changes in HD patients (Vonsattel *et al.*, 1985). Therefore, we examined RNA expression profiles from various brain regions of euthanized monkeys, rHD-4 and rHD-5. To detect the RNA expression of mutant *HTT*, specific primers that amplified the junction of the ubiquitin promoter and the *HTT* translation start site were used because they could distinguish mutant and endogenous *HTT*. Mutant *HTT* RNA was detected in the cortex and striatum of rHD-4 and rHD-5 using RT-PCR (Figure II-19).

To measure the RNA expression levels of the mutant *HTT* and endogenous *HTT*, we conducted Q-PCR using primers (HD Exon 1-F & HD Exon 1-R) that detect the exon 1 region of the *HTT* gene, where mutant and endogenous *HTT* share the identical sequence. We observed higher levels of *HTT* RNA in the cortex

and striatum of rHD-4 and rHD-5, compared to those of wild-type monkeys (Figure II-20). In addition, the RNA expression levels of four HD related genes, HTT-associated protein 1 (*rHAP1*), HTT-interacting protein 1 (*rHIP1*), Transcription binding protein (*rTBP*) and cAMP response element-binding protein (CREB)-binding protein (*rCREBBP*), were evaluated. Higher RNA expression levels of these four genes were observed in the cortex and striatum of HD monkeys compared to those of wild-type monkeys by Q-PCR (Figure II-21).

Due to the limited access to tissue from the living monkeys, we collected the placental tissue from all infants to confirm the expression of HTT at a protein level by Western blotting. Oligomeric HTT at high molecular mass (>250 kDa), located in the upper portion of a gradient polyacrylamide gel, was observed in all placental tissues (Figure II-22). The intensity of HTT protein was stronger for rHD-3, rHD-4 and rHD-5 compared to rHD-1 and rHD-2. However, more oligomeric HTT was expressed in rHD-2 than rHD-1 (Figure II-22).

Since we used the ubiquitin promoter to regulate the expression of mutant *HTT*, ubiquitous expression of mutant HTT was expected in all tissues. Peripheral and

brain tissues from rHD-4 and rHD-5 were collected for Western blotting, including skin, heart, kidney, muscle, lung, liver, stomach and different regions of brain. Similar to the results from the Western blotting analysis using placental tissues, oligomeric mutant HTT accumulated in the peripheral tissues and various brain regions of HD transgenic monkeys (Figure II-23). Although the expression level of mutant HTT varied among peripheral tissue, it was fairly homogenously expressed in different brain regions (Figure II-23).

The evaluation of pathological and behavioral phenotypes in HD transgenic monkeys

We have established primary cell culture lines of different tissues collected from rHD-4 and rHD-5. To confirm the expression of mutant HTT in primary culture cells, immunostaining using mEM48 antibody was performed. Similar to our findings in infected 293 FT cells, nuclear aggregation and inclusion bodies developed in the nuclei of various primary culture cells (Figure II-24).

Regarding the pathological analysis in various brain regions,

immunohistochemistry with mEM48 and 1C2 antibodies revealed widespread expression of transgenic HTT throughout the brain with no substantial differences between regions. Mutant HTT aggregates and nuclear inclusions were observed in the striatum and cortex of rHD-4 and rHD-5 (Figure II-25). At a higher magnification (Figure II-25), mutant HTT accumulated in the nuclei and formed small neuropil aggregates that did not seem to be inside the cell body. Both antibodies revealed neuropil aggregates arranged in an array manner (Figure II-25).

As there is no standard rating scale for HD in monkeys, especially for infants, our evaluation was based on the unified Huntington's disease rating scale, which we modified for use in infant monkeys. Our preliminary assessment using the Huntington's disease primate model rating scale, in which 80 reflects the most severe phenotype, rHD-1 had a score of '0' at 2, 6 and 12 months, whereas rHD-2 had the scores 12, 26 and 52, respectively (Figure II-27). rHD-3 had the score 60 at only one month of age when we euthanized .

Discussion

Huntington's disease is an inherited autosomal-dominant neurodegenerative disease in humans. Unfortunately, there is no effective therapy for HD. Several animal models have been created for modeling human HD, such as *C. elegans*, *Drosophila*, and mice (Jung and Bonini, 2007; Schilling *et al.*, 1999; Wang *et al.*, 2006). These animal models are important for *in vivo* studies, and provide critical insight and new discoveries for HD research, especially HD transgenic mouse models. Although HD mouse models are available and have been used in clinical research, limitations remain due to the relatively primitive CNS in mice compared to humans. Since non-human primates are closely related to humans, we expect a transgenic non-human primate model of HD to lead to additional insight and therapies.

The first step to establishing an HD non-human primate model is to design a DNA transgene construct. Before applying to non-human primates, the biofunction of the transgene must be confirmed at both the cell and mouse level. In addition, a

high gene transfer rate is also important to determine the probability of successfully producing a transgenic non-human primate due to limited accessibility to non-human primates (Chan, 2004). Based on our prior success in rodents, we decided to use lentiviral gene transfer technology for non-human primates (Yang *et al.*, 2007).

Despite the advantages of using non-human primates for animal models of human disease (Chan, 2004), one of the limitations is their longer development growth rate compared to rodents. Therefore, a DNA construct leading to early onset of HD may be desirable for this study. Two important factors impacting the severity of HD are the size of the HTT fragment and the number of CAG repeats (Li and Li, 2006; Li and Li, 2004; Walker, 2007a). In principal, a larger HTT fragment and fewer CAG repeats result in a less severe HD phenotype in mice. Based on previous studies in rodents, *HTT* exon 1 with expanded polyQ leads to a progressive neurological phenotype (Mangiarini *et al.*, 1996; Schilling *et al.*, 2007). Additionally, the ubiquitin promoter is precise and effective, causing expression of the transgene in all cells *in vitro* and in *vivo* (Lois *et al.*, 2002; Yang *et al.*, 2007;

Yang *et al.*, 2008a). Based on the above criteria, we designed two gene constructs, pLVU-*HTT*-84Q and pLVU-*HTT*-147Q, for this study (Figure II-1). These two constructs consisted of exon 1 of *HTT* with 84 (244 amino acids) or 147 (307 amino acids) CAG repeats located at the N-terminus under the control of the human ubiquitin promoter. We expected both constructs to be sufficient to elicit a progressive neurological phenotype in a short time period in non-human primates.

In order to achieve a high gene transfer rate, high-titer lentiviruses (~ 10^9 CFU/mL) of these two constructs were produced and used in this study. To confirm the biofunction of the two constructs *in vitro*, we introduced each lentivirus into 293 FT cells. During the course of cell culture and lentiviral transduction, we observed numerous dead cells, suggesting toxicity of the mutant *HTT* transgenes. N-terminal HTT with expanded polyQ has already shown to be toxic, resulting in neuronal cell death in HD patients and mice (Borrell-Pages *et al.*, 2006; Davies *et al.*, 1997). Therefore, the N-terminal HTT with expanded polyQ likely caused our transgene to be toxic, leading to cell death during the course of cell culture and lentiviral transduction.

The expression pattern of mutant HTT was determined via Western blotting and immunostaining (Figure II-5; Figure II-6; Figure II-7). Oligomeric HTT at several molecular weights observed in the Western blotting suggested the formation of aggregates similar to those found in brain tissue of HD patients and transgenic mice (Davies *et al.*, 1997; Mangiarini *et al.*, 1996; Trottier *et al.*, 1995). Mutant HTT was broadly distributed in the form of nuclear aggregates and cytoplasmic or nuclear inclusion bodies (Figure II-6; Figure II-7). Both aggregates and inclusion bodies are characteristic cellular features observed in HD patients and mice (Li and Li, 2006; Li and Li, 2004; Walker, 2007a). These results suggested that high titer lentiviruses could infect mammalian cells with high efficiency, resulting in the expression of mutant HTT *in vitro*. Most importantly, nuclear aggregates and inclusion bodies were observed, supporting the pathogenic nature of the mutant *HTT* constructs.

Our next step was to determine if the two mutant *HTT* constructs led to abnormal neuropathology *in vivo*. To confirm the biofunction of the mutant *HTT* constructs *in vivo*, we generated HD transgenic mice using the same lentiviruses.

High-titer lentiviruses were injected into the PVS of the mouse embryo at the pronuclear stage to create transgenic mice. By observing the preimplantation embryos *in vitro*, we found both *HTT* groups had a lower development rate at the 4-cell and blastocyte stages (Table II-1). This result might be imputed to the onset of mutant HTT expression. Embryos infected via lentiviral transgenesis may start to express the mutant *HTT* transgenes during the maternal/zygotic transition, which happens between 2-cell to 4-cell stage in mice (Hogan, 1994). At this stage, the mouse embryos started to express zygotic genes, including mutant *HTT*, instead of using maternal transcripts; therefore, a lower development rate at the 4-cell stage was observed in this study. Continuous accumulation of mutant HTT may inhibit the development rate at the blastocyst stage in this study. Therefore, mutant *HTT* constructs may be toxic for *in vitro* development of embryos, which was also observed in infected 293 FT cells with mutant *HTT* in this study.

In addition to determining the biofunction of mutant HTT *in vivo*, the lentiviral transgenic efficiency in mammals was also investigated. Based on the PCR result, nine (9/10; 90.00%) and six (6/9; 66.67%) transgenic founder mice were generated

via LVU-*HTT*-147Q and LVU-*HTT*-84Q, respectively (Figure II-8). The transgenic rate in this study was much higher than other gene transfer methods, such as pronuclear microinjection, sperm vector or electroporation (Melo *et al.*, 2007; Niemann and Kues, 2007; Wall and Seidel, 1992). Thus, lentiviral transgenesis was our method of choice for generating HD transgenic non-human primates.

The number of CAG repeats varied in different transgenic founders (Figure II-8; Table II-2), even though the same lentiviruses were used to infect the embryos. Instability of CAG repeats has been reported in several studies (Goellner *et al.*, 1997; Kovtun *et al.*, 2000; Wheeler *et al.*, 2007), resulting in polymorphism among HD patients and families. Variations of CAG repeats have also been observed in other HD transgenic mice studies (Kovtun *et al.*, 2000; Wheeler *et al.*, 1999; Wheeler *et al.*, 2007). Since several processes have been used to produce these HD transgenic mice, we do not know which step resulted in truncated CAG repeats. It might occur during plasmid extraction (Hashem *et al.*, 2002a; Hashem *et al.*, 2002b), virus preparation, virus infection, or cell duplication (Manley *et al.*, 1999; Wheeler *et al.*, 2007). The plasmid extraction may be the most likely candidate

because the bands of PCR products from the plasmid amplification were not sharp (Figure II-8) and the plasmid extraction step causing the instability of CAG repeats have been reported (Hashem *et al.*, 2002a; Hashem *et al.*, 2002b). A combination of several factors may decrease the stability of CAG repeats (Cleary *et al.*, 2002; Kovtun *et al.*, 2007; Wheeler *et al.*, 2007), perhaps also resulting in CAG polymorphism in transgenic mice at different stages. This question has still not been fully addressed.

The advantage of using the ubiquitin promoter is its broad activity pattern, thus the expression of transgene can be determined in animals without euthanasia. This advantage is particularly beneficial when studying transgenic non-human primates that are rare and costly. Protein samples can be prepared from tail snips of transgenic founders for analysis. Western blotting analysis from LVU-*HTT*-147Q or LVU-*HTT*-84Q transgenic founders revealed the formation of oligomeric HTT at high molecular weight in the stacking gel, but relatively less in the separating gel (Figure II-9; Figure II-10). In fact, the aggregation profile of HTT based on tail protein was similar to the brain aggregation profile of HD patients and mice (Davies

et al., 1997; Schilling *et al.*, 2007; Wang *et al.*, 2008). This similarity suggested that our mutant *HTT* constructs affect the entire body *in vivo*, possibly impacting peripheral organs due to abnormal and misfolded HTT (DiFiglia *et al.*, 1995; Li and Li, 2006; Li and Li, 2004; Sharp *et al.*, 1995; Trottier *et al.*, 1995).

The primary organ of interest for HD is the brain because of the development of distinct neuropathological changes in HD patients (Vonsattel *et al.*, 1985). The formation of nuclear aggregates and intranuclear inclusions are two signature characteristics of HD. Therefore, it is important to determine whether these two signature characteristics occur in our HD transgenic mice. Based on immunostaining, misfolded mutant HTT formed nuclear aggregates and inclusion bodies in various brain regions, including the cortex, striatum, cerebellum and hippocampus of HD transgenic mice (Figure II-11). The neuropathology of our transgenic mice was comparable to prior reports on HD transgenic mice and HD patients (Davies *et al.*, 1997; Schilling *et al.*, 2007; Vonsattel *et al.*, 1985; Wang *et al.*, 2008). This suggested that our mutant *HTT* constructs could lead to neuropathological changes *in vivo* and that these abnormal aggregates may elicit

neuronal dysfunction in the brain.

Since we found abnormal pathological changes in the brains of HD transgenic mice, we expected these changes to elicit neuronal dysfunction and impact overall brain function, resulting in a behavioral phenotype. The size of these transgenic mice appeared smaller than that of non-transgenic mice in the same litter, suggesting weight loss or metabolic dysfunction. At five months, LVU-*HTT*-147Q or LVU-*HTT*-84Q transgenic founders displayed clasping (Figure II-12) similar to N171-82Q and R6/2 mice (Davies *et al.*, 1997; Schilling *et al.*, 1999). The abnormal neuronal function causes a motor deficit in HD patients and mice (Li and Li, 2006; Walker, 2007a, 2007b). Because the purpose of HD transgenic mice in this study was to determine the biofunction of our mutant *HTT* constructs *in vivo*, we only tested for a clasping phenotype, which is one behavior of dyskinesia in HD mouse model (Mangiarini *et al.*, 1996; van Dellen *et al.*, 2000). To determine detailed motor function in HD transgenic mice, rotarod testing, beam walking and footprint testing (Carter *et al.*, 1999) could be performed. Combined with the neuropathological changes, these phenotypes suggested that the biofunction of

our mutant *HTT* constructs were sufficient to elicit pathological and behavioral changes, which were observed in the HD patients and mice. This study supported the likelihood of developing a non-human primate model of HD using these lentiviruses.

Non-human primates may provide a better animal model of HD due to similar neuroanatomy and cognitive behavior to humans, strengthening the possibility of reproducing HD and developing therapeutic approaches and preventive strategies. Based on preliminary studies of HD using 293 FT cells and mice, we used the same mutant *HTT* constructs and lentiviral transgenesis to develop a HD transgenic monkey model. To generate a non-human primate model for HD, we first investigated the *in vitro* development rate of monkey embryos after lentivirus injection. Since we injected LVU-*GFP* with LVU-*HTT*, we observed weak GFP signal inside the blastomeres during the 8- to 16-cell stage followed by stronger GFP expression after the morula stage of monkey embryos (Figure II-13). In other words, embryos were successfully infected with LVU-*GFP* and started to express GFP during the 8-16 cell stage, which suggested that the onset of embryonic

transcription most likely began during the 8-16 cell stage in monkey embryos (Barnes and First, 1991; Brunet-Simon *et al.*, 2001). However, green fluorescence was also observed in the PVS during the 1- to 8-cell stages (Figure II-13), which may have resulted from the residue of lentiviral particles and transfected cell debris when making the high titer lentiviruses. Furthermore, the GFP signal increased during the morula and blastocyst stages and all blastocyst embryos showed strong green fluorescence (Figure II-13), suggesting a high efficiency of our lentiviral gene transfer system in monkey embryos.

As seen in the 293 FT cell and mouse lentiviral transgensis (Figure II-6, 7; Table II-1), LVU-*HTT*-147Q monkey embryos had a significantly lower development rate at blastocyst stage ($P<0.05$; Figure II-14), suggesting the potential toxicity of the mutant *HTT* transgene composed of a short HTT fragment and expanded polyQ (Borrell-Pages *et al.*, 2006; Davies *et al.*, 1997; Wang *et al.*, 2008). However, the LVU-*HTT*-84Q and wild-type control groups had comparable development rates ($P>0.05$) contrary to our mouse study (Table II-1; Figure II-14). This finding suggests that LVU-*HTT*-84Q has a less adverse impact on monkey

embryos than mouse embryos. Because different species have different sensitivities to lentiviruses (Zhao *et al.*, 2007), the impacts to embryos may be different as observed in our mouse and monkey embryos. This result suggests that the LVU-*HTT*-84Q construct is preferable for generating HD transgenic monkeys due to higher development rate *in vitro*.

A total of seventeen transgenic monkeys were created, including four (4/4; 100%) with LVU-*HTT*-147Q and nine (9/13; 69.23%) with LVU-*HTT*-84Q (Table II-3). Among these transgenic monkeys, twelve were miscarried and five reached full term. However, four of the five were euthanized between one day and one year of age due to the severity of HD symptoms. The low survival rate of transgenic monkeys might be due to toxicity from mutant N-terminal HTT containing elongated CAG repeats. Neuropathological analysis revealed mutant HTT nuclear aggregates and inclusion bodies in miscarried fetuses (Figure II-25), suggesting damage and dysfunction of neurons. Additionally, lentiviral transgenesis usually generates multiple copies of the transgene in transgenic animals (Yang *et al.*, 2007), and multiple integration patterns were also observed in the HD transgenic

monkeys in this study (Table II-3; Figure II-18). Because HD is an autosomal dominant disease, the increase in copy number suggests an increase in the dosage of mutant HTT, which increases the severity of the HD phenotype. These factors might explain the high percentage of miscarried fetuses and euthanized infants. It is not our goal to generate a HD monkey that cannot survive to puberty. Therefore, future experiments will implement an alternative *HTT* construct. One strategy is to use a larger N-terminal HTT fragment and a smaller number of CAG repeats to reduce toxicity. Additionally, an endogenous *HTT* promoter can replace the ubiquitin promoter in order to achieve a more specific expression pattern of mutant HTT. In order to reduce the number of integration events, less lentivirus can be delivered into an oocyte, thus minimizing the risk of mutant HTT dosage.

Since we observed a high gene transfer rate in HD transgenic mice (Figure II-8), we were interested in the transgenic efficiency in monkeys. Four (4/4; 100.00%) of LVU-*HTT*-147Q and nine (9/13; 69.23%) of LVU-*HTT*-84Q transgenic monkeys were created (Table II-3). When we co-injected LVU-*GFP* with LVU-*HTT*-147Q or LVU-*HTT*-84Q (No. 4 –No. 18), all of the transgenic monkeys (14/14; 100.00%)

expressed LVU-*GFP*, whereas ten were double transgenic monkeys (Table II-3) co-expressing mutant *HTT*. Therefore, LVU-*GFP* and LVU-*HTT*-147Q had higher gene transfer efficiencies than LVU-*HTT*-84Q. The titer, or concentration, of lentiviruses is highly related to the efficiency of the gene transfer. LVU-*GFP* had the highest titer at $5X10^9$ CFU/mL compared to $1X10^9$ CFU/mL for both the LVU-*HTT*-84Q and LVU-*HTT*-147Q. The high titer could explain why LVU-*GFP* had the best transgenic efficiency. However, since the HD is an autosomal dominant disease, high copy numbers of mutant *HTT* resulted from high efficiency of HTT lentiviruses are not desirable. Therefore, if we use lentiviral transgenesis to generate transgenic monkeys, we need to consider the adverse effect of high copy numbers, especially for HD. Some adjustments can be made to lentiviral transgeneis to overcome this effect, such as decreasing the volume for injection or the titer of the lentiviruses; however, these modifications may also decrease gene transfer efficiency. As a result, optimizing a high gene transfer rate and low copy numbers of gene integration will be an important challenge for the generation of transgenic animals using lentiviral transgenesis, especially for autosomal dominant

diseases. In summary, this highly efficient gene transfer method would be the best way to generate transgenic animals for which there is limited access to gametes, but potential limitations of lentiviral transgenesis and the nature of the disease need to be considered.

We confirmed the transgenic status of *HTT* and *GFP* in each animal by PCR, and determined the number of CAG repeats of HD monkeys by sequencing. Similar to transgenic mice, thirteen HD transgenic monkeys demonstrated instability of the number of CAG repeats ranging from 11 to 122, suggesting the instability of CAG repeats in HD transgenic monkeys which may also caused by the reasons discussed in HD mice. Southern blotting was used to determine the integration pattern and transgene copy number in the HD monkeys, which is especially important because HD is an autosomal dominant disease. First we confirmed the copy number of LVU-*GFP* integration sites. All five infants that reached full term (Figure II-18) and seven miscarried fetuses (Table II-3) had multiple LVU-*GFP* integration sites. Since high copy numbers of foreign transgenes may cause higher protein expression, we speculated that many

LVU-*GFP* integration sites might have caused the miscarriages. However, multiple integration sites of LVU-*GFP* might not be lethal. Based on a prior study (Yang *et al.*, 2007), mice can still survive with more than twenty copies of LVU-*GFP*, suggesting that the early death of these transgenic monkeys may have been caused by the other transgene, mutant *HTT*. To determine the copy number of mutant *HTT*, we used the subtraction method as described in Materials and Methods. In rHD-3, rHD-4 and rHD-5, at least two copies of mutant *HTT* were detected (Figure II-18; Table II-3; Table II-4). This result might explain the early development of severe symptoms in these monkeys. rHD-1 and rHD-2 each carried a single copy of mutant *HTT* (Figure II-18; Table II-3; Table II-4); however rHD-2 developed clinical features of HD at four months of age and gradually progressed until he was euthanized at one year; whereas rHD-1 has not developed any clinical signs to date (Table II-4). Since rHD-2 had more CAG repeats than rHD-1 (Figure II-15; Table II-3; Table II-4), the severity and early onset of the HD phenotype was likely due to the number of CAG repeats (Li and Li, 2006; Li and Li, 2004; Walker, 2007a), supporting the relationship between the CAG

repeats and the severity of HD Furthermore, the chromosomal loci where lentiviruses integrated could have impacts on the expression of transgenes, and influence normal function of cell due to randomly integration events. Since most animals had more than one lentiviral integration site (Table II-3), including LVU-*GFP* and LVU-*HTT*, the integration sites may be considered as reasons leading to various expressions and causing the miscarriage. Therefore, future studies should investigate these integration sites, which could be identified by a PCR-based method (Schroder *et al.*, 2002; Yang *et al.*, 2008b) because the chromosomal location of integration probably impacts on the phenotype of transgenic HD monkeys.

To examine the biofunction of mutant *HTT* in transgenic monkeys, we first determined the RNA expression of mutant *HTT* in the cortex and striatum due to development of distinctive neuropathological changes in the brain of HD patients (Vonsattel *et al.*, 1985). Since multiple copies of mutant *HTT* were detected in the HD transgenic monkeys of rHD-4 and rHD-5 (Figure II-18; Table II-3; Table II-4), we expected higher RNA and protein expression of mutant *HTT* in their brain

region. RT-PCR and Q-PCR were used to determine the expression of mutant *HTT* while higher expression of mutant *HTT* was found in transgenic monkeys compared to those of the wild-type monkeys (Figure II-19; Figure II-20), suggesting the transcription of mutant *HTT*. Compared to the copy numbers of mutant *HTT* in these two monkeys, the RNA expression levels were not directly correlated to the copy numbers of transgenic monkeys. Because lentiviruses integrate randomly in the genome, the expression of transgene may be influenced by the position effect (Clark *et al.*, 1994; Yee and Zaia, 2001). In addition, the copy numbers was not correlated to the expression levels of transgenes in the transgenic mouse study (Yang *et al.*, 2007), which also provides the possible explanations for the pattern of RNA expression above.

HTT is involved in several cellular gene regulatory pathways (Li and Li, 2006; Ryu *et al.*, 2006), thus abnormal gene regulation may occur in HD transgenic monkeys. Four important genes, *rHAP1* (Li *et al.*, 1995), *rHIP1* (Kalchman *et al.*, 1997), *rTBP* (Friedman *et al.*, 2008) and *rCREBBP* (Jung and Bonini, 2007), which have been studied in HD were chosen for this study. Based on Q-PCR, these

genes were expressed more in the cortex and striatum of rHD-4 and rHD-5 compared to those of wild-type monkeys (Figure II-21), suggesting abnormal regulation of these genes may result from overexpression of mutant *HTT*. Since mutant HTT is involved in different cellular gene regulatory pathways, we would expect HD transgenic monkeys to exhibit altered gene regulation in these pathways. In the next chapter, we will describe a high-throughput analysis for gene regulation of mutant HTT in HD monkeys.

Protein expression of mutant HTT was determined by Western blotting of the placenta in all infants that reached full-term (Figure II-22). In the upper portion of a gradient polyacrylamide gel, oligomeric HTT at high molecular mass (>250 kDa) was observed in all five monkeys, showing results comparable to those brains reported from HD patients and mice (Schilling *et al.*, 1999; Schilling *et al.*, 1995; Wang *et al.*, 2008). The expression of oligomergic HTT was more intense in rHD-3, rHD-4 and rHD-5 than in rHD-1 and rHD-2. This result was consistent with the Southern blot (Figure II-18) because more *HTT* copy numbers were expected to lead to the higher expression of oligomeric HTT. In fact, the early onset of a

phenotype in rHD-3, rHD-4 and rHD-5 may have been elicited by the high expression level of mutant HTT because high expression of N-terminal HTT with expanded polyQ leads to early death, suggesting the comparable result to the previous HD studies (Davies *et al.*, 1997; Schilling *et al.*, 1999).

HTT is selectively expressed in different tissues, especially within the brain (DiFiglia *et al.*, 1995; Li and Li, 2006; Li and Li, 2004; Sharp *et al.*, 1995; Trottier *et al.*, 1995). In this study, we used the human ubiquitin promoter to regulate mutant *HTT*. We were interested in investigating whether mutant HTT would retain its selective expression pattern despite the use of an ubiquitin promoter. Available post-mortem peripheral and brain tissue from rHD-4 and rHD-5 was collected for Western blotting analysis. Oligomeric mutant HTT at a high molecular weight was observed in peripheral tissue and various brain regions in rHD-4 and rHD-5 (Figure II-23). However, mutant HTT was not homogenously expressed in the peripheral tissues, but was expressed homogenously across various brain regions. The brain and muscle tissues had the highest expression level of oligomeric HTT (Figure II-23). These tissues showed aggregated patterns of mutant HTT comparable to

those in the brains of HD patient and mice (Schilling *et al.*, 1999; Schilling *et al.*, 1995; Wang *et al.*, 2008).The fact that mutant HTT misfords to form dimers, trimers and oligomers inside the cells (Walker, 2007a) suggested the misfolding of mutant HTT occurred in various tissues of HD transgenic monkeys, which may elicit the HD symptoms comparable to those of HD patients.

The mutant HTT expressed homogenously across various brain regions in rHD-4 and rHD-5, and this expression pattern were consistent with HD patients (Vonsattel *et al.*, 1985). The high level of mutant HTT in the brain may have caused to the neuropathological changes (Sharp *et al.*, 1995; Van Raamsdonk *et al.*, 2007b). In addition, oligomeric mutant HTT was also widespread in all peripheral tissue in HD monkeys, which also observed in HD patients (Sharp *et al.*, 1995). Because wild-type HTT plays a role in intracellular trafficking, transcription, intracellular signaling, trafficking, endocytosis and metabolism (Cowan and Raymond, 2006; Li and Li, 2004), overexpression of mutant HTT in other peripheral tissues may interfere with the normal function of various organs in HD monkeys, which may emulate the influence on peripheral tissues of HD patients.

In addition to determining the accumulation of oligomeric mutant HTT in the peripheral tissues, we were also interested in determining whether specific HD-related cellular pathology developed in these tissues. Primary cell culture from various tissues was established from the miscarried monkeys. We observed nuclear aggregates and the formation of nuclear inclusions, which are two signature characteristics of HD, in the primary cell culture using EM48 immunostaining (Figure II-24). The histopathology of primary cell culture was comparable to prior reports on HD transgenic mice and HD patients (Davies *et al.*, 1997; Schilling *et al.*, 2007; Vonsattel *et al.*, 1985; Wang *et al.*, 2008), suggesting the misfoded HTT were distributed in all peripheral tissues. Based on prior reports, aberrant expression of mutant HTT was detected ubiquitously and affected the gene expression pattern in peripheral tissue of HD patients and mice (Borovecki *et al.*, 2005; Luthi-Carter *et al.*, 2002a). Therefore, dysfunction of cells might occur in the peripheral tissues of HD transgenic monkeys.

The hallmark neuropathological features of HD are neuropil aggregates and intranuclear inclusions in neurons (Li and Li, 2006; Maat-Schieman *et al.*, 2007;

Walker, 2007a). In post-mortem brain tissue from rHD-4 and rHD-5, we observed widespread but homogenous expression of mutant HTT across different brain regions at low magnification (Figure II-25; top panel). At high magnification, we observed mutant HTT aggregates, nuclear inclusions and small aggregates outside of the cell body. Both antibodies illustrated an array of neuropil aggregates (Figure II-25; bottom panel), suggesting remnants of HTT aggregates localized in neuronal processes such as the axonal degeneration (Davies *et al.*, 1997; Lin *et al.*, 2001). These neuropil aggregates varied in size and are consistent with neuropil aggregates found in the brains of HD patients (DiFiglia *et al.*, 1997; Gutekunst *et al.*, 1999) and HD mice (Davies *et al.*, 1997; Schilling *et al.*, 1999; Wang *et al.*, 2008 200). These results further strongly support the contention that non-human primates could be an ideal model to mimic human neurodegenerative diseases.

Non-human primate models of HD are ideal due to complicated behavioral, cognitive, and social abilities, which are limited in other species (Chan, 2004). Several behavioral and physical conditions were observed in HD transgenic monkeys, including distinct chorea, dystonia, incoordination (imbalance),

swallowing difficulties, respiratory difficulties, weight loss, and motor impairment (Table II-4), which was comparable to clinical features of HD patients. We observed distinct chorea, rigidity, motor dysfunction and respiratory difficulties in rHD-3 at one month of age (Figure II-26; Table II-4). rHD-2 displayed motor dysfunction, involuntary movement and weight loss at four months of age and gradually progressed until he was euthanized at one year old. Based on our preliminary assessment using the Huntington's disease primate model rating scale, rHD-2 had higher scores compared to rHD-1 and wild-type monkeys (Figure II-27). rHD-3 had the score 60 at only one month of age. Based on our preliminary observations, the severity, frequency and onset of involuntary movements seemed to depend on the number of CAG repeats and integration sites, supporting the hypothesis that longer CAG repeats lead to more severe symptoms in HD. These behavioral abnormalities combined with a pathological phenotype supported that a non-human primate is a superior model than other species for HD.

In summary, in this chapter we have developed a transgenic non-human primate model of HD expressing mutant HTT with expanded polyQ. Hallmark

features of HD, including nuclear inclusions and neuropil aggregates, were observed in the brains of the HD transgenic monkeys. HD transgenic monkeys also developed unique clinical features of HD, including dystonia and chorea. Transgenic HD monkeys may be a unique model for understanding the underlying biology of HD and developing novel strategies for intervention and therapy. Moreover, our data suggests that it is feasible to generate valuable non-human primate models of HD for future applications in other human genetic diseases.

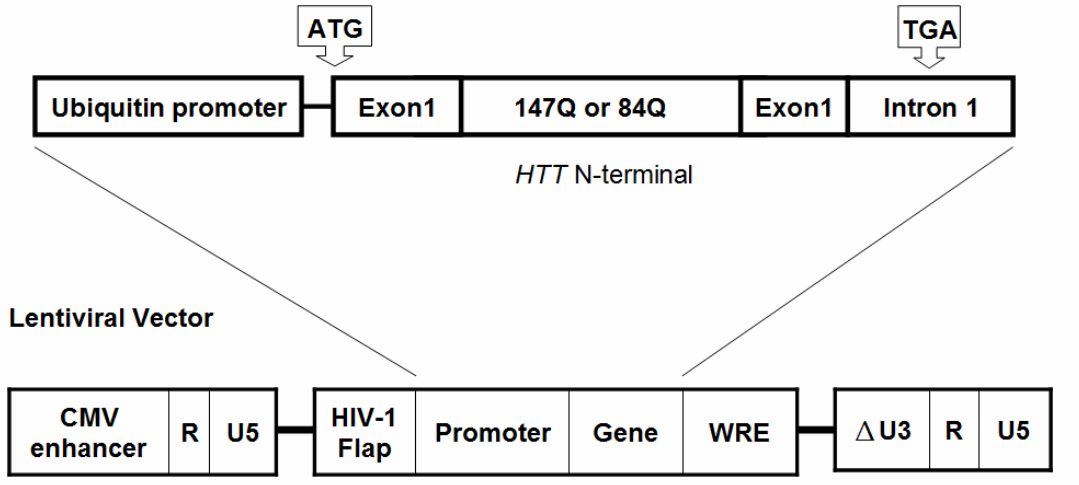

Figure II-1. **Schematic diagram of pLVU-*HTT*-84Q and pLVU-*HTT*-147Q.** The exon 1 region of *HTT* gene with 84 or 147 CAG repeats under the control of an ubiquitin promoter was constructed into a lentiviral vector backbone.

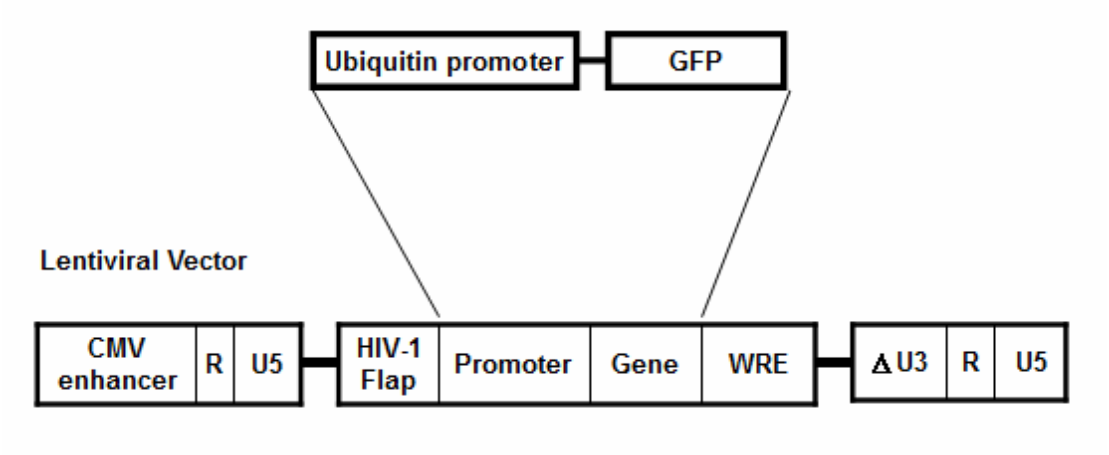

Figure II-2. Schematic diagram of pLVU-*GFP*. The *GFP* gene under the control of an ubiquitin promoter was constructed into a lentiviral vector backbone.

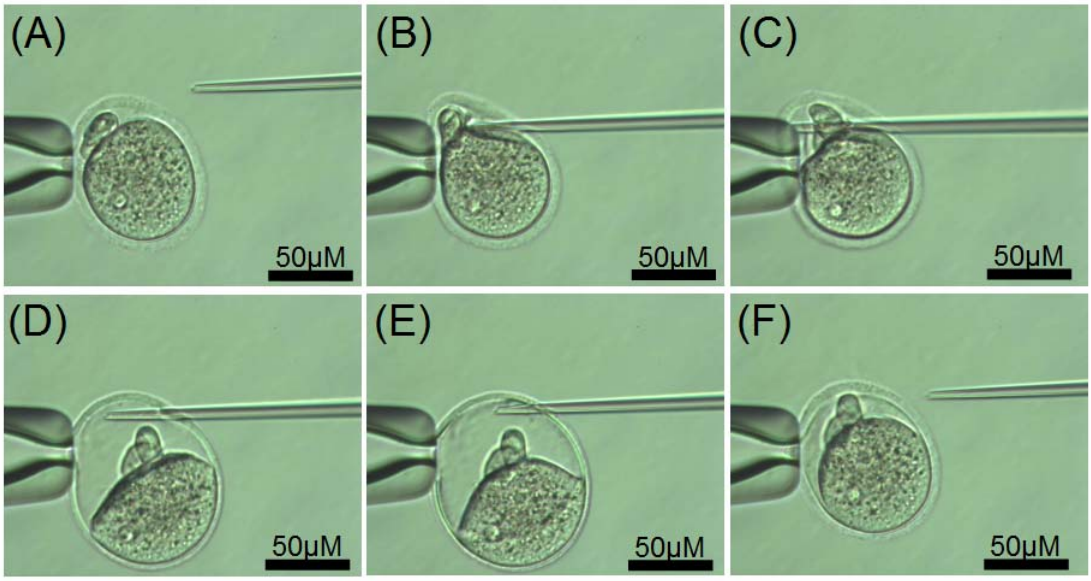

Figure II-3. Lentiviral transgenesis in the mouse embryo. (A)-(C) Insertion of micropipette with lentiviruses into PVS. (D)-(F) Injection of lentiviruses into the PVS of the mouse embryo. All pictures were taken under the transmitted light (Hoffman modulation contrast).

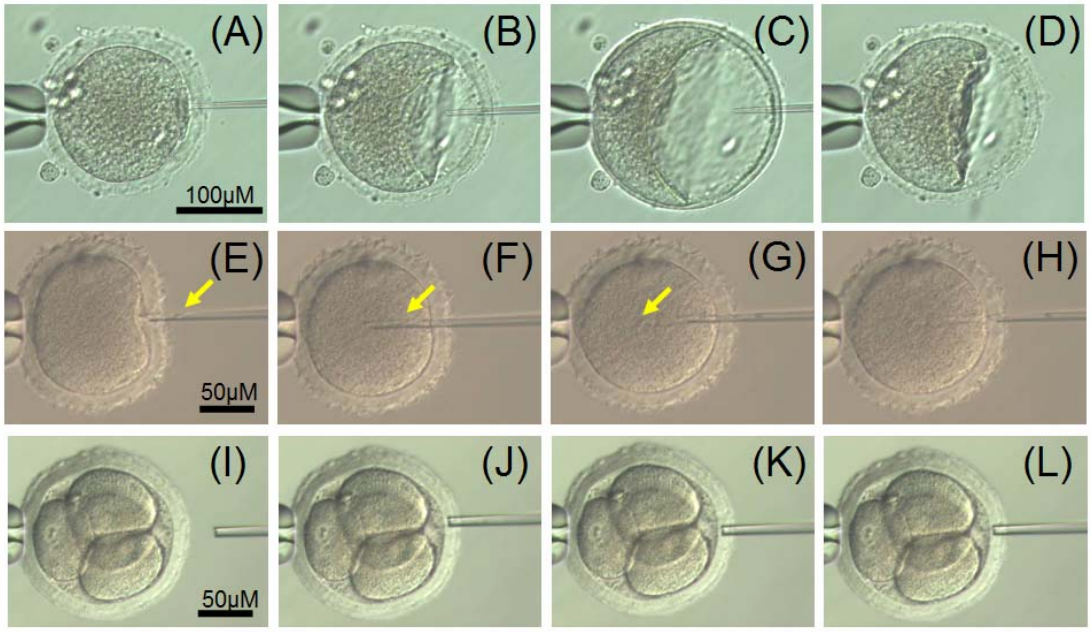

Figure II-4. Lentiviral transgenesis in the monkey oocyte. (A)-(D) Lentiviruses were injected into PVS of the monkey oocyte. (E)-(H) Single sperm (arrow) was injected into the cytoplasm through the zona pellucida to fertilize the oocyte. (I)-(L) The zona pellucida of the 4-cell embryo was punched and removed by using the micropipptte for assisting hatching. All pictures were taken under the transmitted light (Hoffman modulation contrast).

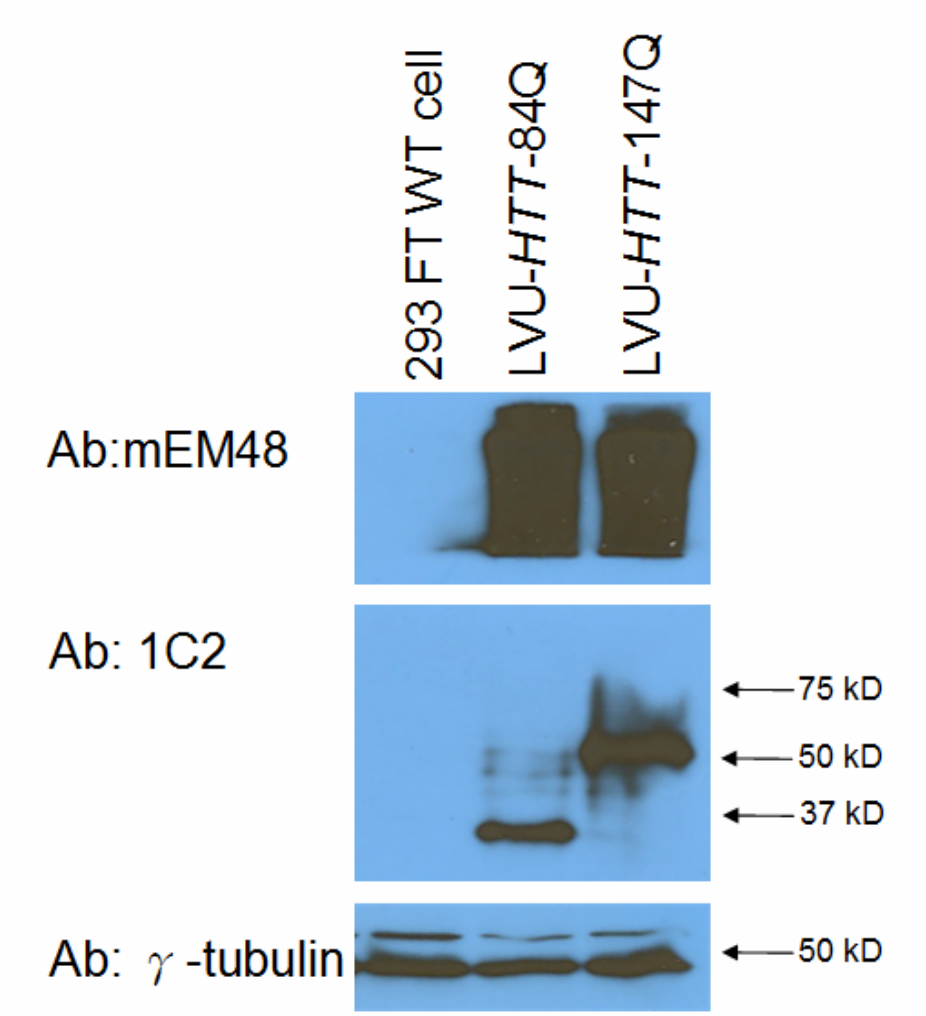

Figure II-5. Western blotting analysis of 293 FT cells infected with *HTT* lentiviruses. The upper panel was the stacking gel probed with mEM48 antibody showing the oligomeric HTT. The middle panel was the separating gel probed with 1C2 antibody showing the expression of mutant HTT at lower molecular weight. The lower panel was an internal control using γ-tubulin antibody. Wild-type 293 FT cells were used as a negative control.

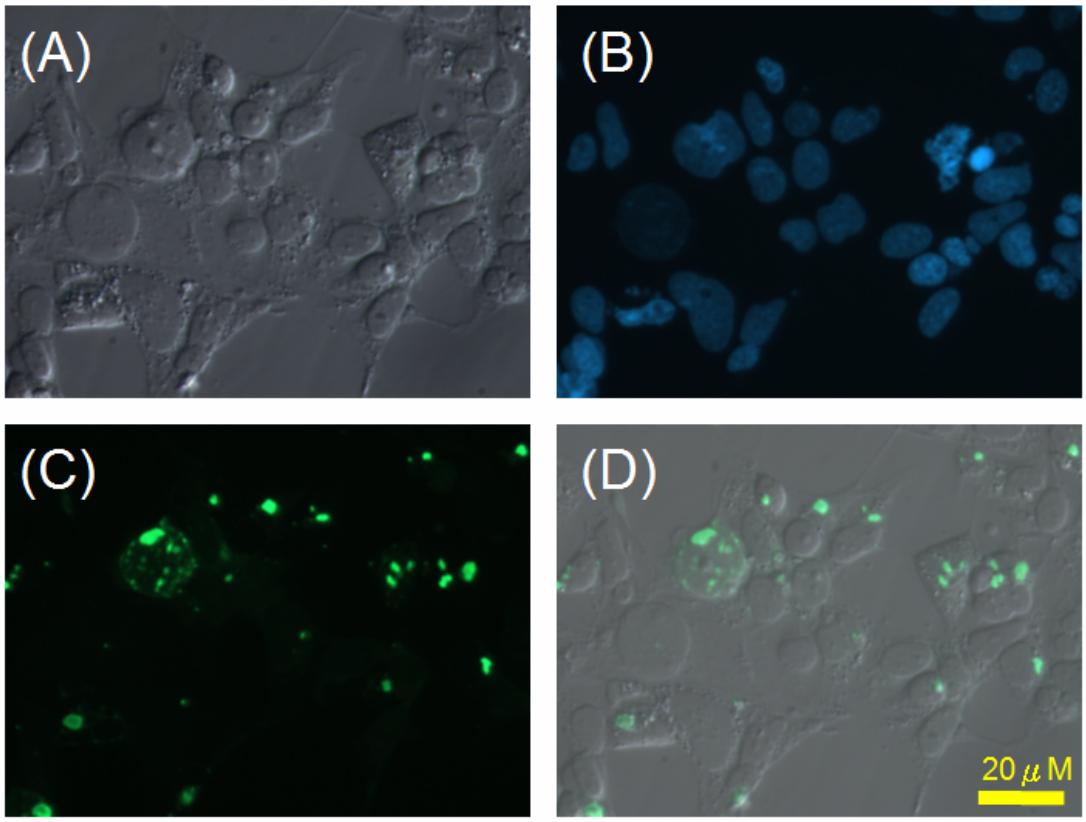

Figure II-6. Immunohistochemistry staining with mEM48 antibody in 293 FT cells infected with LVU-*HTT*-147Q. (A) Transmission light microcopy (Hoffman modulation contrast) showing the morphology of 239 FT cells. (B) Hoechst staining showing the positions of cell nuclei. (C) Immunofluorescent images using mEM48 antibody showing the expression of mutant HTT resulting in the nuclear aggregates and inclusion bodies. (D) Merged image from (A) and (C) showing the expression of mutant HTT forming the inclusion bodies in the cytoplasm or inside the nuclei.

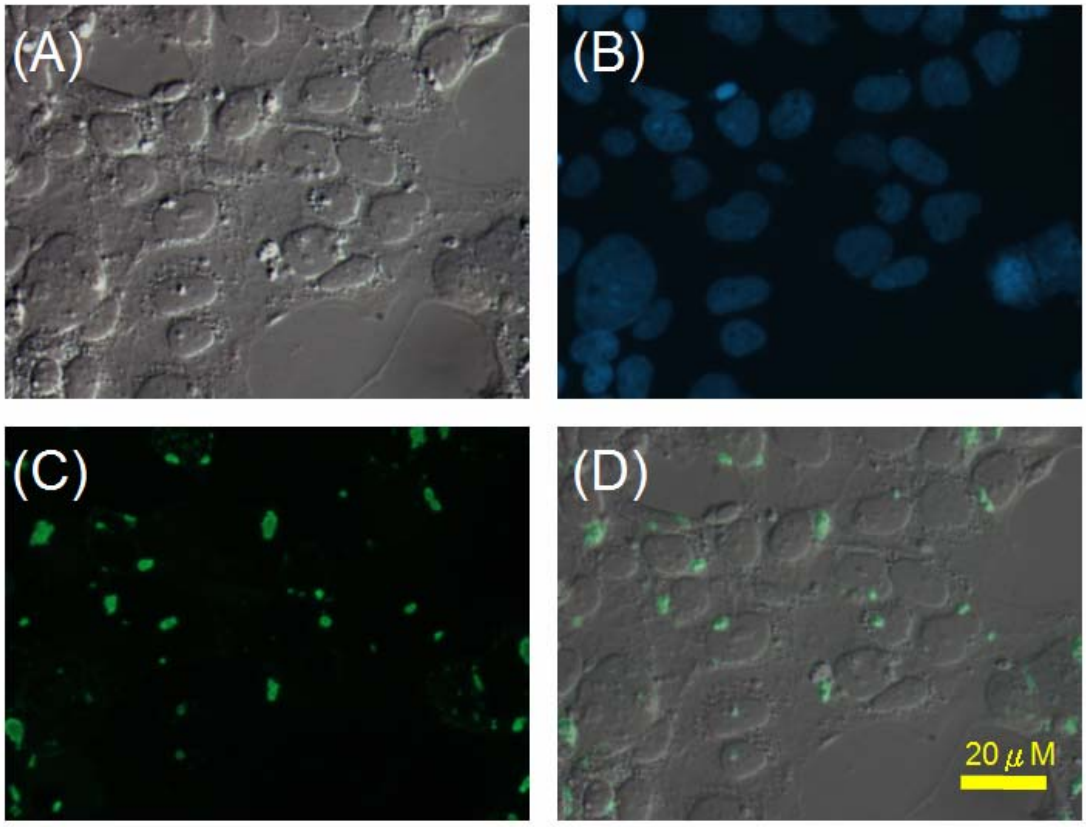

Figure II-7. Immunohistochemistry staining with mEM48 antibody in 293 FT cells infected LVU-*HTT*-84Q. (A) Transmission light microscopy (Hoffman modulation contrast) showed the morphology of 239 FT cells. (B) Hoechst staining showing the positions of cell nuclei. (C) Immunofluorescent images using mEM48 antibody showing the expression of mutant HTT resulting in the nuclear aggregates and inclusion bodies. (D) Merged image from (A) and (C) showing the expression of mutant HTT forming the inclusion bodies in the cytoplasm or inside the nuclei.

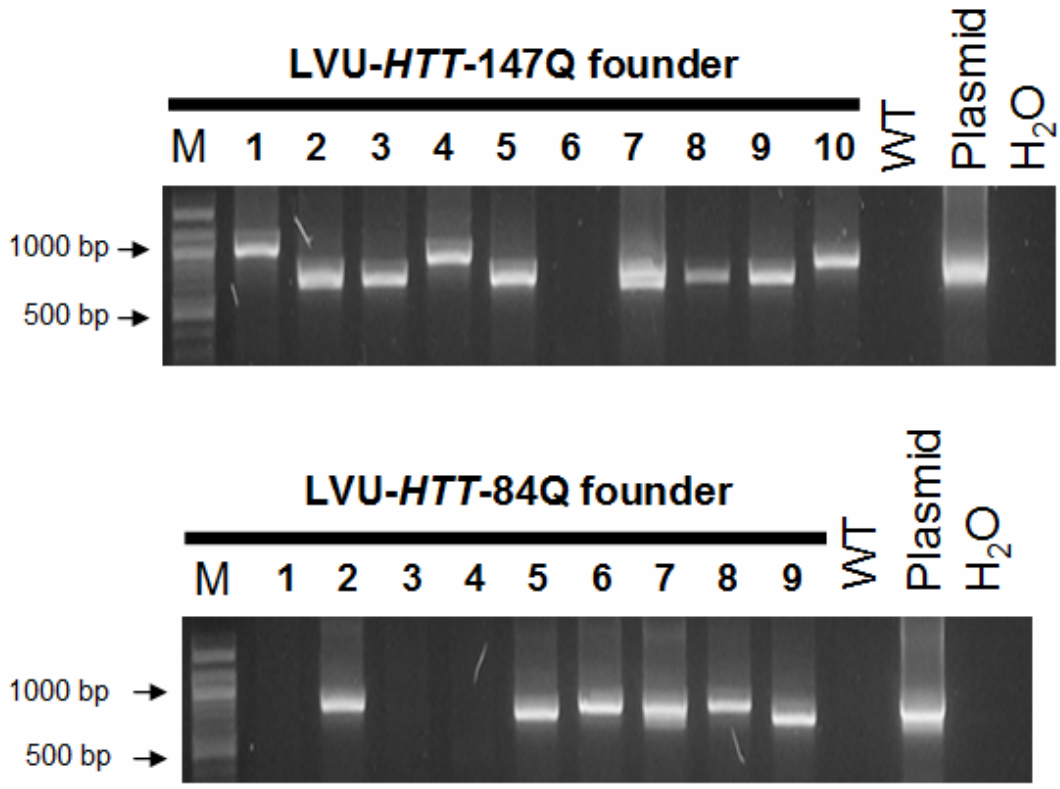

Figure II-8. PCR result for determining the transgenic status of transgenic founders. Top panel showed the PCR result of LVU-*HTT*-147Q founders, where nine out of ten (90.00%) were transgenic mice. The lower panel showed the PCR result of LVU-*HTT*-84Q founders, where six out of nine (66.67%) were transgenic mice.

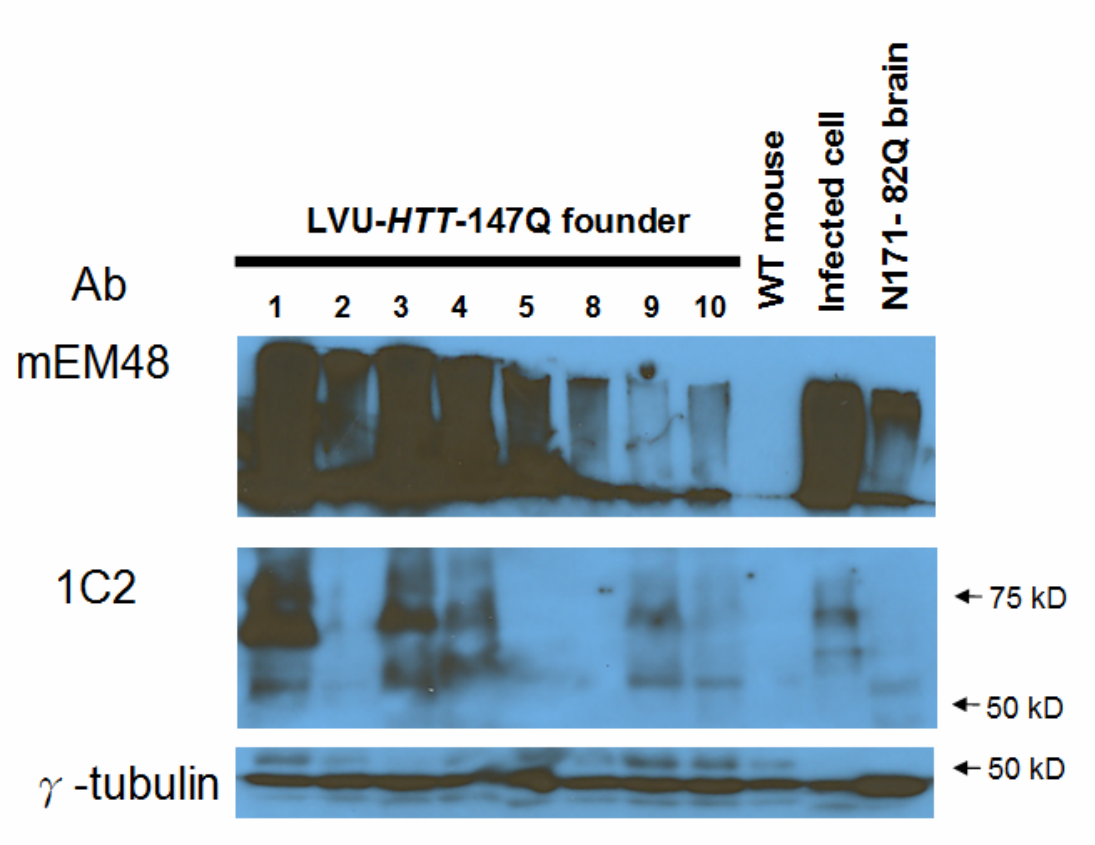

Figure II-9. The expression of mutant LVU-*HTT*-147Q in transgenic mice. Tail snips of HD mice revealed high-molecular weight oligomeric HTT in the stacking gel (mEM48; top panel), and soluble HTT was detected in the separating gel (1C2; middle panel). γ-tubulin was used as an internal control (bottom panel). The tail snip from a wild-type (WT) mouse was used as a negative control. The 293 FT cells infected with LVU-*HTT*-147Q and the brain tissue from a N171-82Q mouse were used as the positive control.

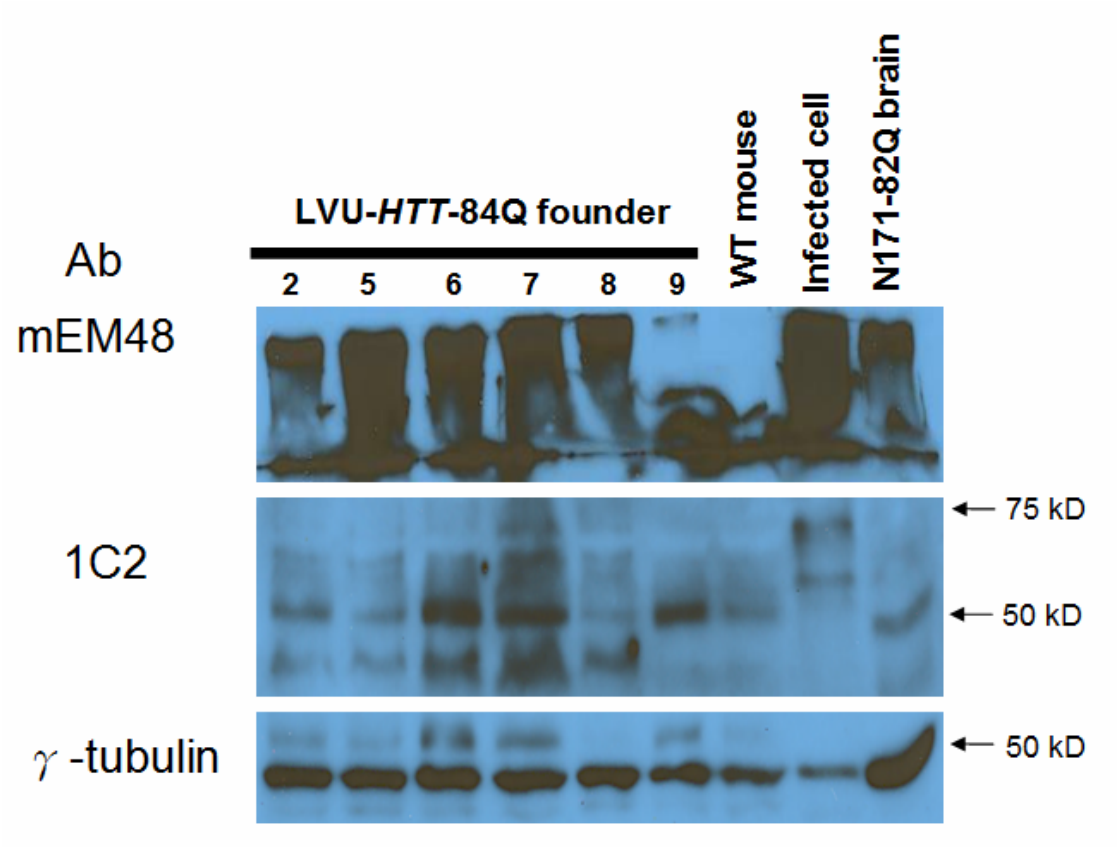

Figure II-10. The expression of mutant LVU-*HTT*-84Q in transgenic mice. Tail snip of HD mice revealed high-molecular weight oligomeric HTT in the stacking gel (mEM48; top panel), and soluble HTT was detected in the separating gel (1C2; middle panel). γ-tubulin was used as an internal control (bottom panel). The tail snip from a wild-type (WT) mouse was used as a negative control. The 293 FT cells infected with LVU-*HTT*-147Q and the brain tissue from a N171-82Q mouse were used as the positive control.

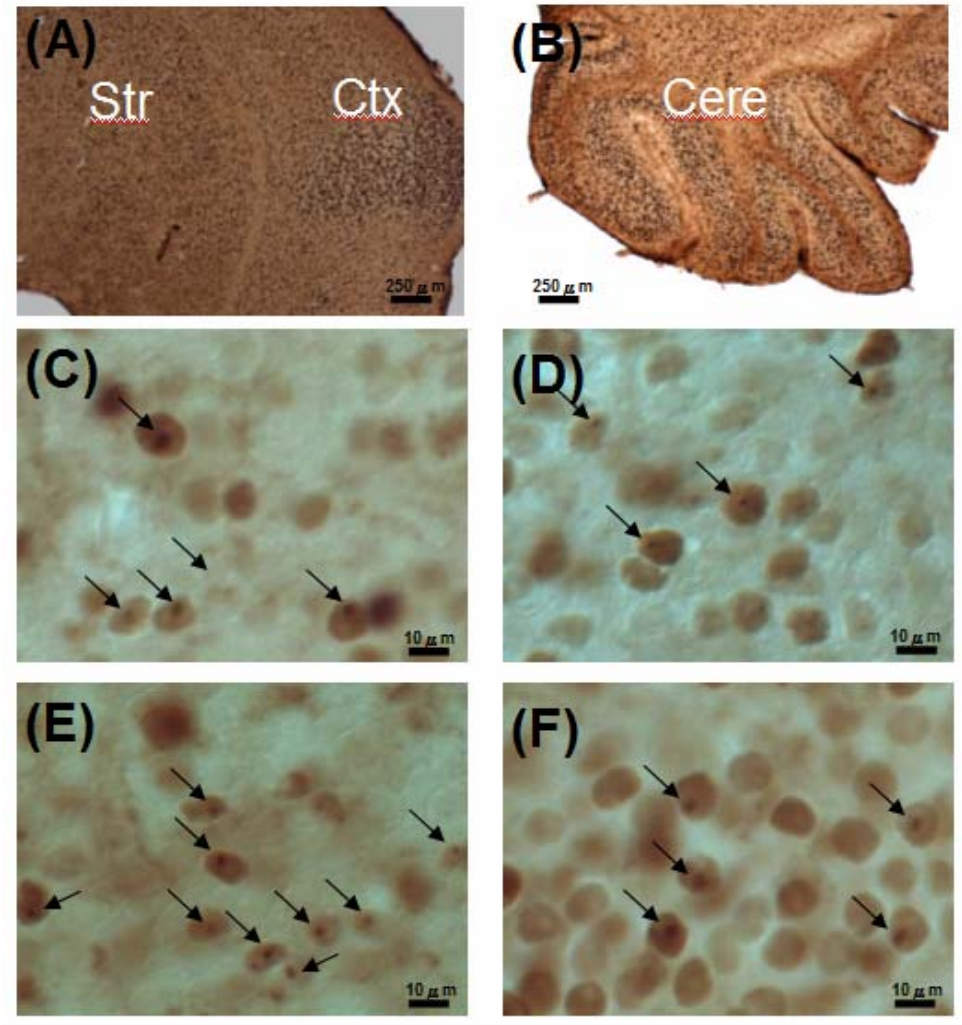

Figure II-11. Immunohistochemistry of LVU-*HTT*-84Q mouse brains. Brain sections collected at day ten after birth were immunostained with mEM48. (A, B) At low magnification showed an extensive expression of the mutant HTT in the (A) cortex (Ctx) and striatum (Str) and (B) cerebellum (Cere). (C)-(F) Nuclear aggregates and inclusion bodies (arrows) were revealed in the (C) cortex, (D) striatum, (E) cerebellum, and (F) hippocampus at high magnification.

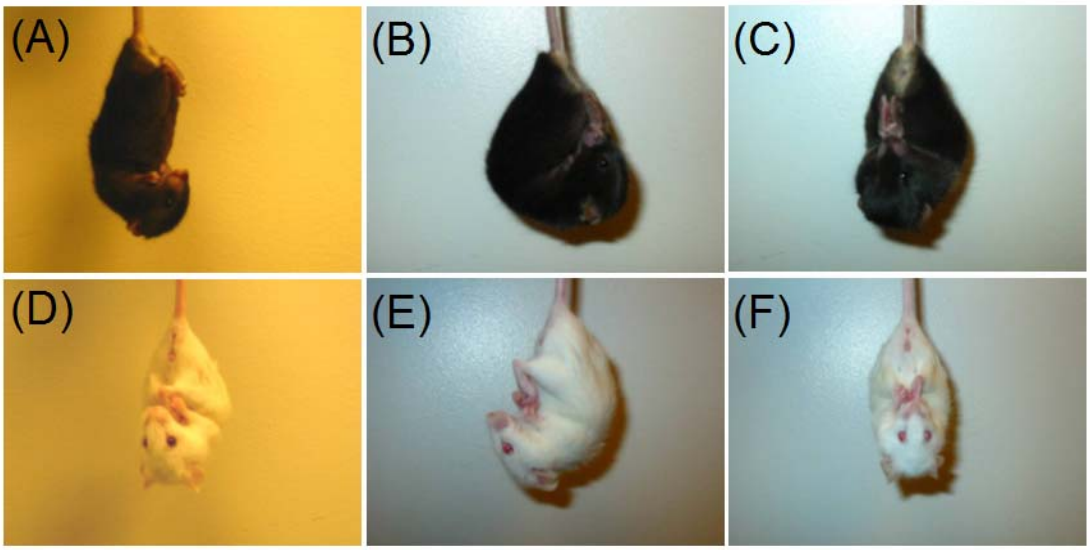

Figure II-12. The clasping behavioral phenotype of HD transgenic mice at 5 months of age. (A)-(C) A N171-82Q transgenic mouse which was well characterized in previous studies showed the clasping behavior at 5 months of age. (D)-(F) A LVU-*HTT*-84Q transgenic mouse at 5 months of age expressed the clasping behavior similar to the N171-82Q transgenic mouse in (A)-(C).

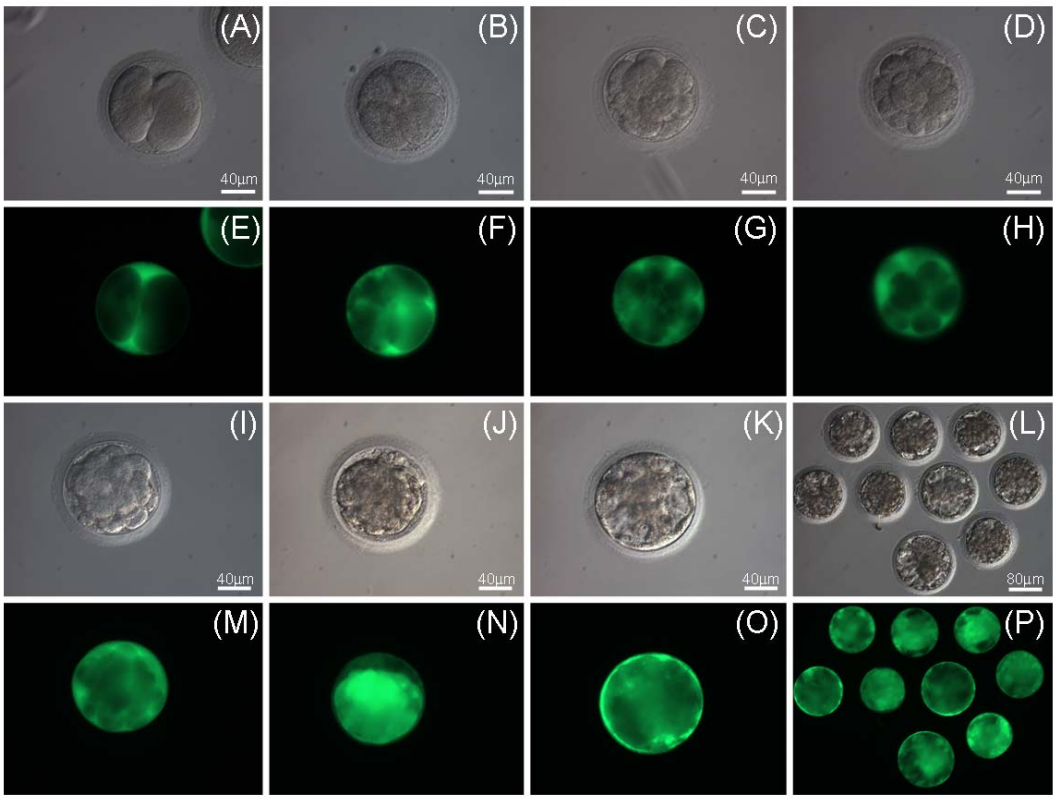

Figure II-13. Rhesus monkey embryos at different developmental stages after LVU-*GFP* and LVU-*HTT*-84Q injection. (A-D, I-L) were transmission light images (Hoffman modulation contrast) and (E-H, M-P) were fluorescent images. Embryos were at (A, E) 2-cell stage, (B, F) 4-cell stage, (C, G) 8-cell stage, (D, H) 8-16-cell stage, (I, M) 16-cell stage, (J, N) compact morula stage and (K, L, O, P) blastocyst stage.

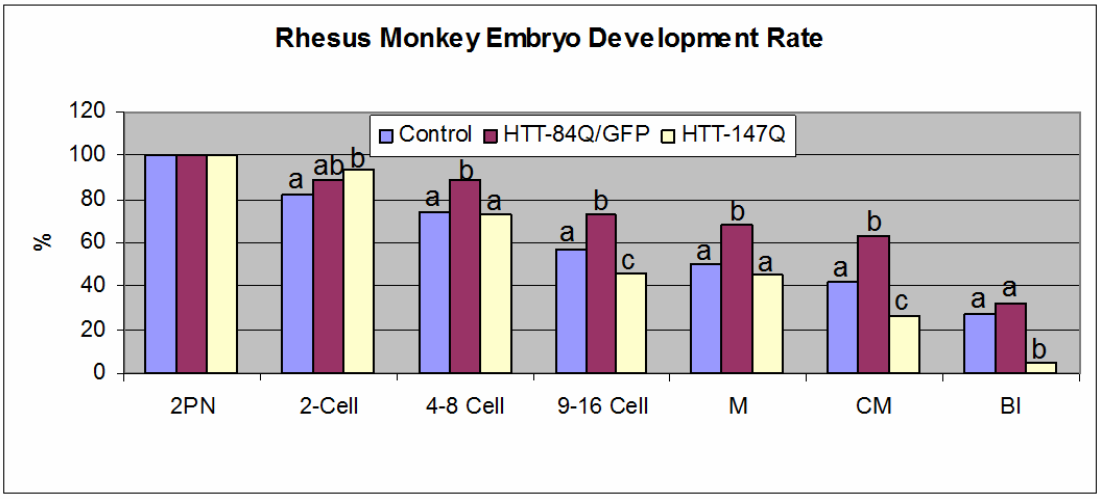

Figure II-14. The *in vitro* development rate of rhesus monkey embryos after lentivirus injection. Control group (Control; n=450) and LVU-*HTT*-84Q/LVU-*GFP* group (*HTT*-84Q/GFP; n=130) had comparable developmental rate; whereas LVU-*HTT*-147Q (*HTT*-147Q; n=119) had a much lower developmental rate. 2PN: 2 pronuclear stage; M: Morula stage; CM: Compacted morula stage; BI: Blastocyst stage. ^{abc} Values on the top of bars in the same stage without common superscript differ significantly ($P < 0.05$).

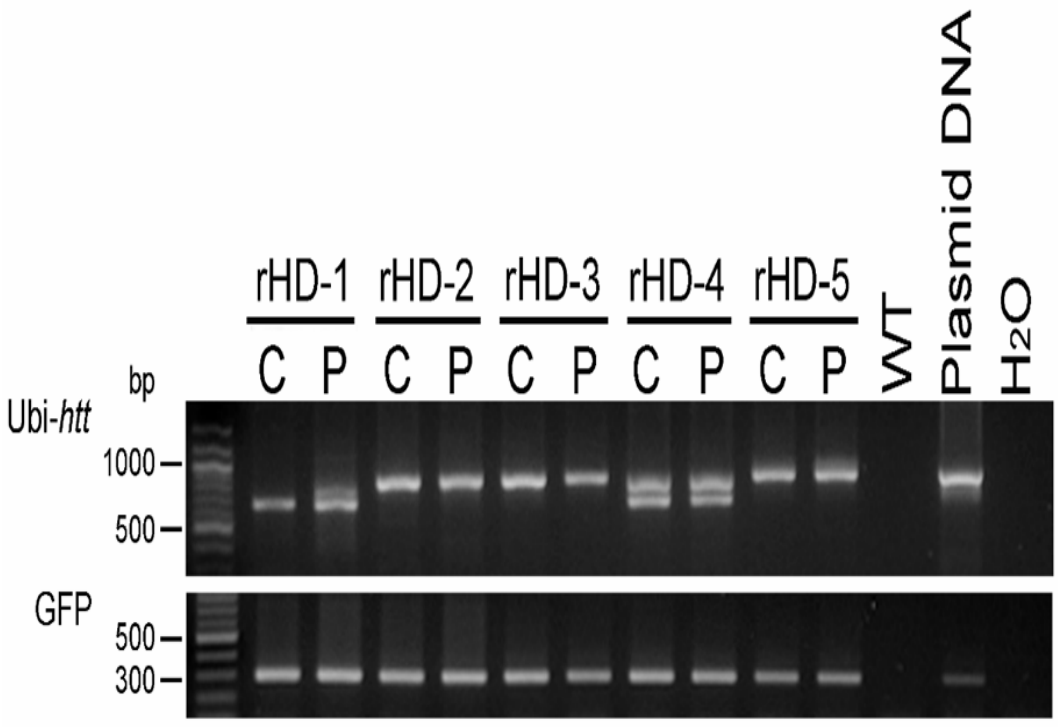

Figure II-15. The PCR result determining the transgenic status of five live-born monkeys. The presence of transgenes in HD monkeys was confirmed by PCR analysis using primer sets specific for mutant *HTT* (top panels) and for the *GFP* gene (bottom panels). The cord (C) and placental (P) tissues were subjected for PCR analysis.

Figure II-16. The HD transgenic monkeys rHD-1 (left) and rHD-2 (right). Transmission light image was presented in the left panel, and fluorescent image was presented in the right panel showing GFP expression in both HD monkeys.

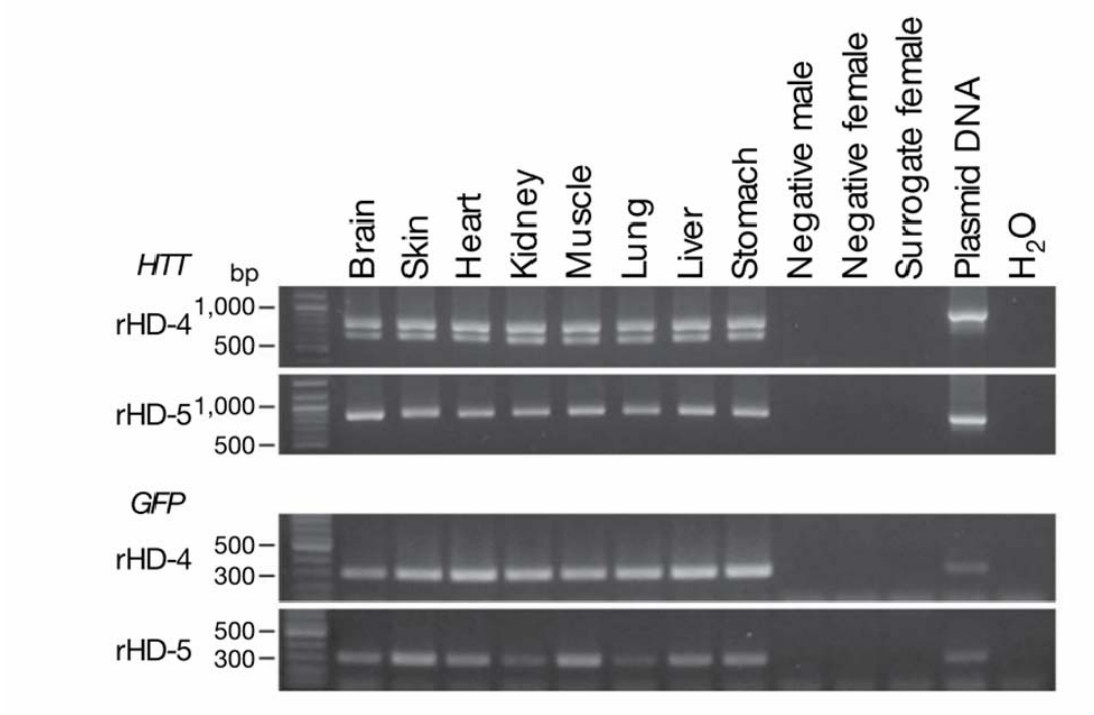

Figure II-17. The PCR result determining the transgenic status of different tissues from rHD-4 and rHD-5 monkeys. The presence of transgenes in rHD-4 and rHD-5 monkeys was confirmed by PCR analysis using primer sets specifically for mutant *HTT* (top panels) and for the *GFP* gene (bottom panels). The different peripheral tissues from rHD-4 and rHD-5 were subjected for PCR analysis.

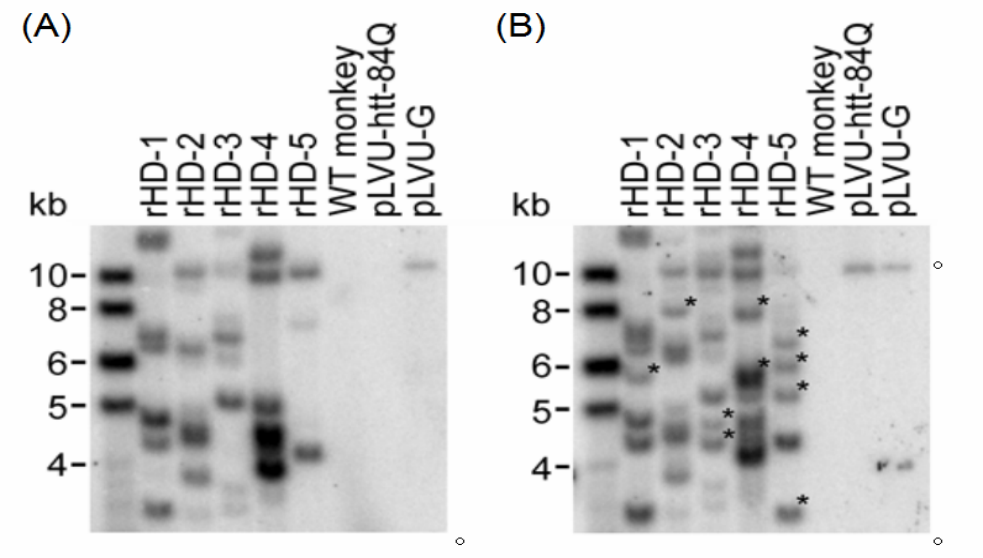

Figure II-18. Southern blotting analysis of placental tissues of HD transgenic monkeys. The number of integration events was determined by Southern blotting analysis using two probes that specifically recognized the flap sequence of the lentiviral vector (flap probe) and the *GFP* gene (*GFP* probe). Two separated but identical membranes were hybridized with *GFP* specific probe and flap specific probe, respectively. The number of integration events or the copy number of transgenic mutant *HTT* gene was determined by subtracting the total number of integration events of the *GFP* gene (A) from the total number of lentiviral integration events indicated by the flap probe (B). Transgenic mutant *HTT* integration events were indicated by the asterisk placed on the right side of the band (B).

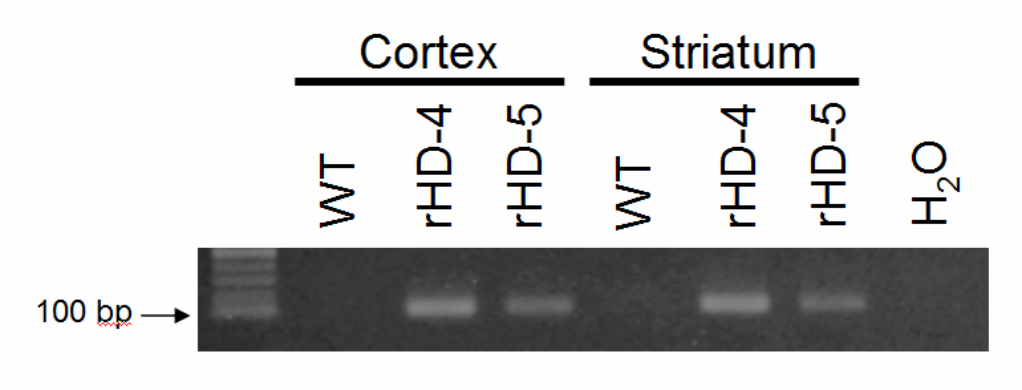

Figure II-19. The RNA expression of mutant *HTT* in the cortex and striatum of transgenic monkeys. RNA samples were extracted from the post-mortem brain tissues in rHD-4 and rHD-5, and tissues from wild-type (WT) monkey were used as the negative control. RT-PCR was performed, and specific primers were used to distinguish between mutant *HTT* and endogenous *HTT*.

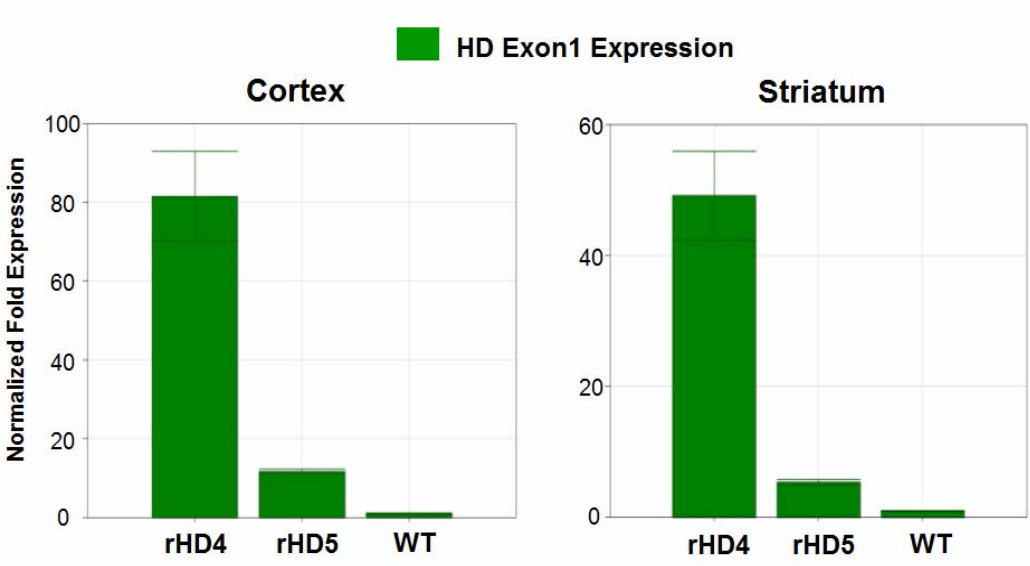

Figure II-20. The relative RNA expression level of *HTT* exon 1 in transgenic and wild-type (WT) monkeys. Q-PCR was performed to quantitate the RNA expression level of *HTT* exon 1 in cortex (left panel) and striatum (right panel). RNA samples were extracted from the postmortem brain tissues in rHD-4 and rHD-5, and tissues from wild-type monkeys (WT; n=2) were used as the negative control. 18S was the internal control to normalize the expression level.

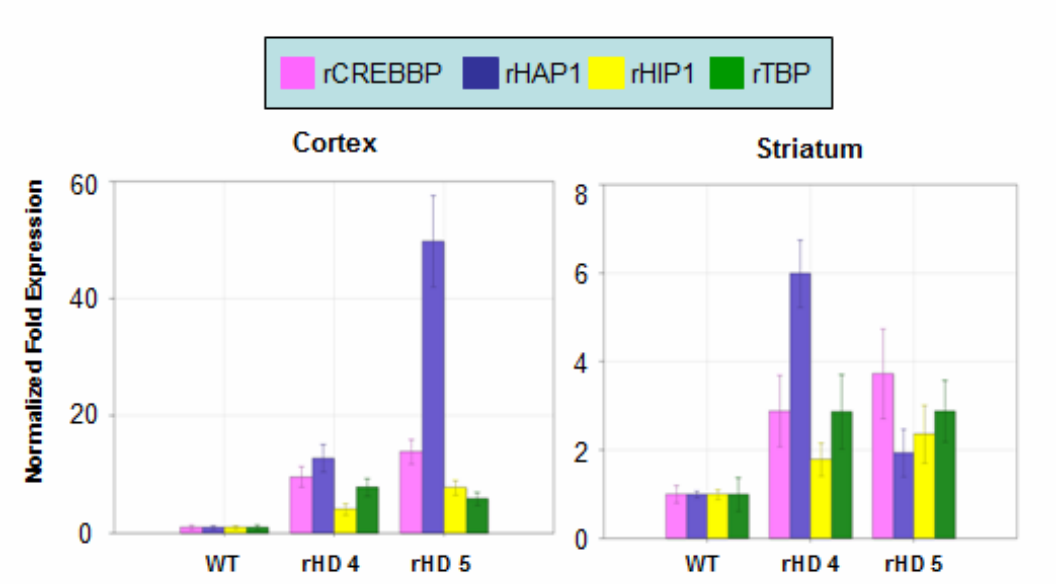

Figure II-21. The relative RNA expression level of four *HTT* related genes in transgenic and wild-type (WT) monkeys. Q-PCR was performed to quantitate the RNA expression level of *rCREBBP* (pink), *rHAP1* (blue), *rHIP1* (yellow) and *rTBP* (green) in cortex (left panel) and striatum (right panel). RNA samples were extracted from the postmortem brain tissues in rHD-4 and rHD-5, and tissues from wild-type monkeys (WT; n=2) were used as the negative control. 18S was the internal control to normalize the expression level from different individuals.

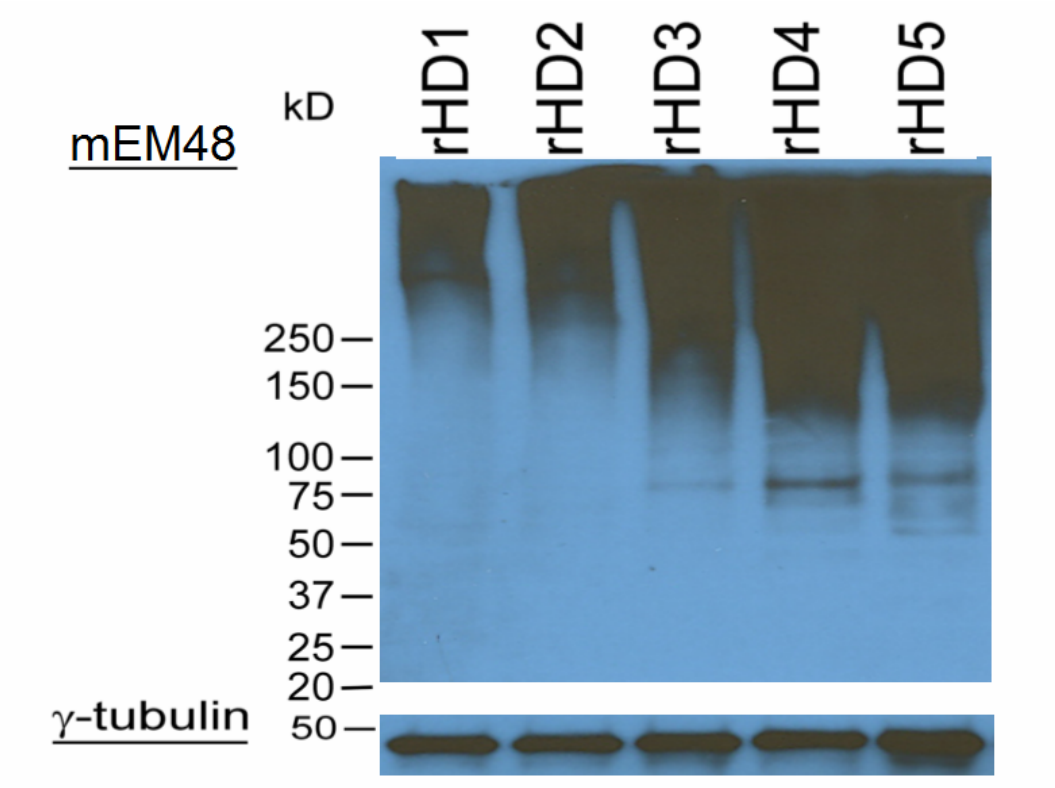

Figure II-22. Expression of mutant HTT in five live-born monkeys. Expression of the transgenic mutant HTT was confirmed by Western blotting analysis using the placental tissues. Immunostaining was performed using the mEM48 antibody (top panel) and the antibody against γ-tubulin (bottom panel).

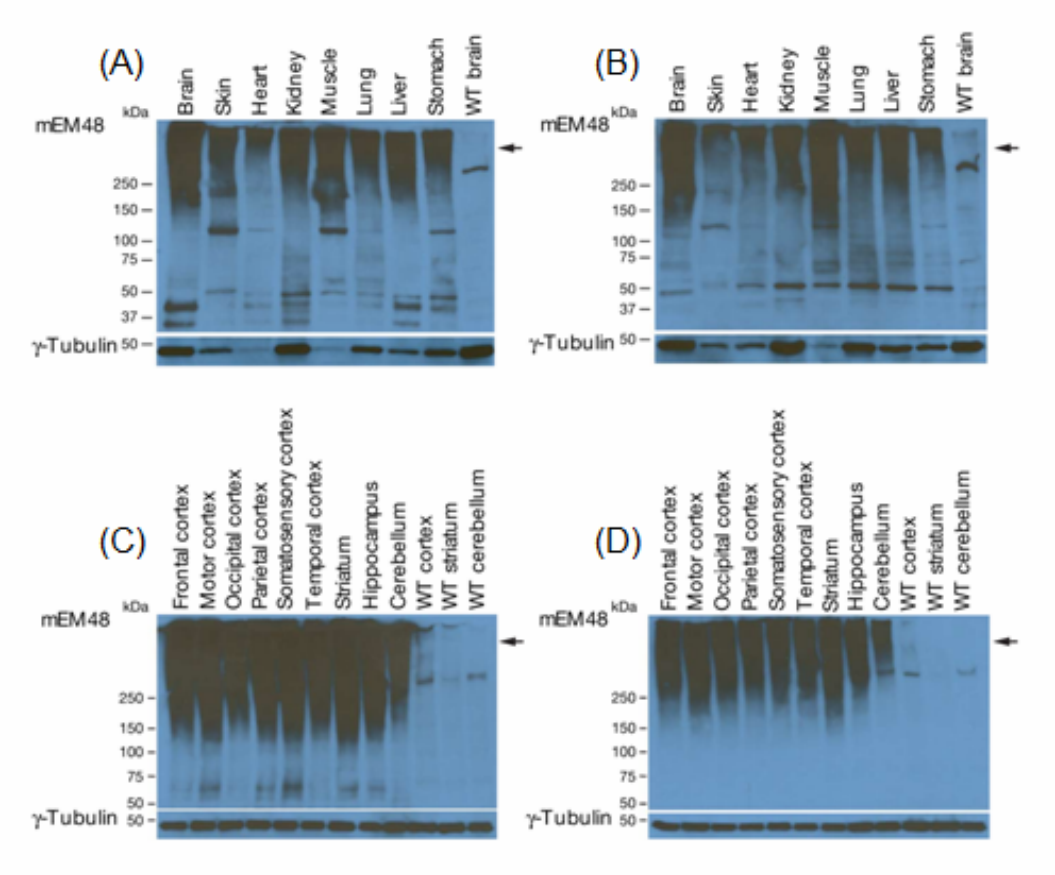

Figure II-23. Expression of mutant HTT in HD monkey peripheral tissues and brains. (A)-(D) mEM48 immunoblot of peripheral and brain tissues revealed high-molecular-mass oligomeric HTT (arrow) and soluble HTT products. The blot was also probed with an antibody to γ-tubulin as an internal control. Shown are immunoblots of peripheral tissues collected from monkey rHD-4 (A) and rHD-5 (B), and samples from different brain regions of monkey rHD-4 (C) and rHD-5 (D), with antibody to mEM48 (top panel) and γ-tubulin (bottom panel). WT, wild-type non-transgenic monkey

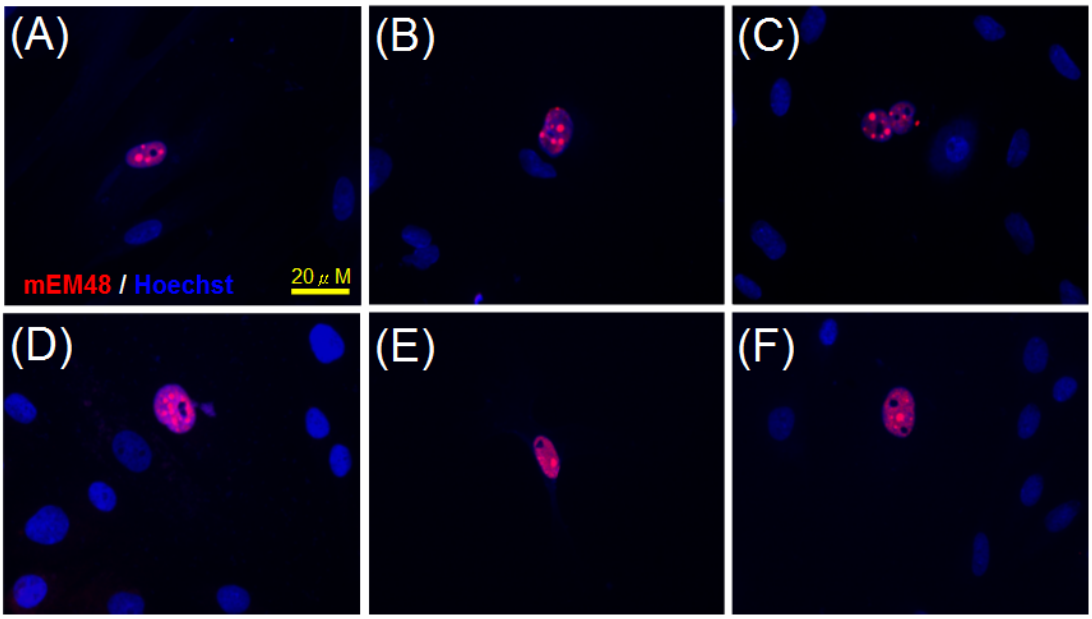

Figure II-24. Immunohistochemistry staining with mEM48 antibody in different primary culture cells from rHD-5 monkey. (A) Intestine, (B) kidney, (C) lung, (D) muscle, (E) skin, and (F) stomach samples were collected from the rHD-5 monkey for primary cultures. The mEM48 antibody (red) showed the expression of mutant HTT, and Hoechst staining (blue) showed the positions of cell nuclei. Merged images (A)-(F) showed the expression of mutant HTT forming the inclusion bodies inside the nuclei.

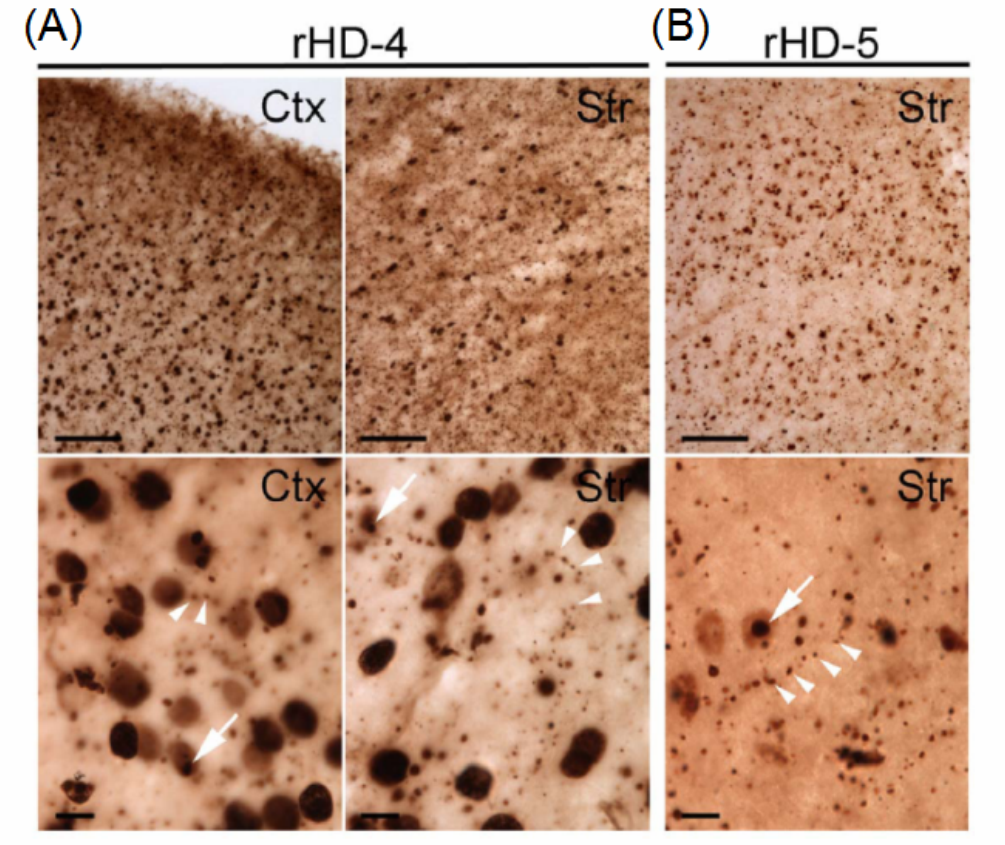

Figure II-25. Histopathology of HD monkey brain. (A), (B) Brain sections of rHD-4 (A) and rHD-5 (B) were immunostained with mEM48 and 1C2, respectively. Low magnification (upper panels; scale bars, 100 mm) showed the abundant distribution of transgenic mutant HTT in the cortex (Ctx) and striatum (Str). High magnification (bottom panels; scale bars, 10 mm) demonstrated that transgenic mutant HTT is distributed in neuronal nuclei and forms neuropil aggregates (arrowheads). Nuclear inclusions (arrows) were evident in sections stained with mEM48 or 1C2.

Figure II-26. Behavioral phenotype of the rHD-3 transgenic monkey. The whole body (A) of rHD-3 showed the severe chorea, neck rigidity, dystonia and body twist. The hands (B) and legs (C) of rHD-3 were severely twisted.

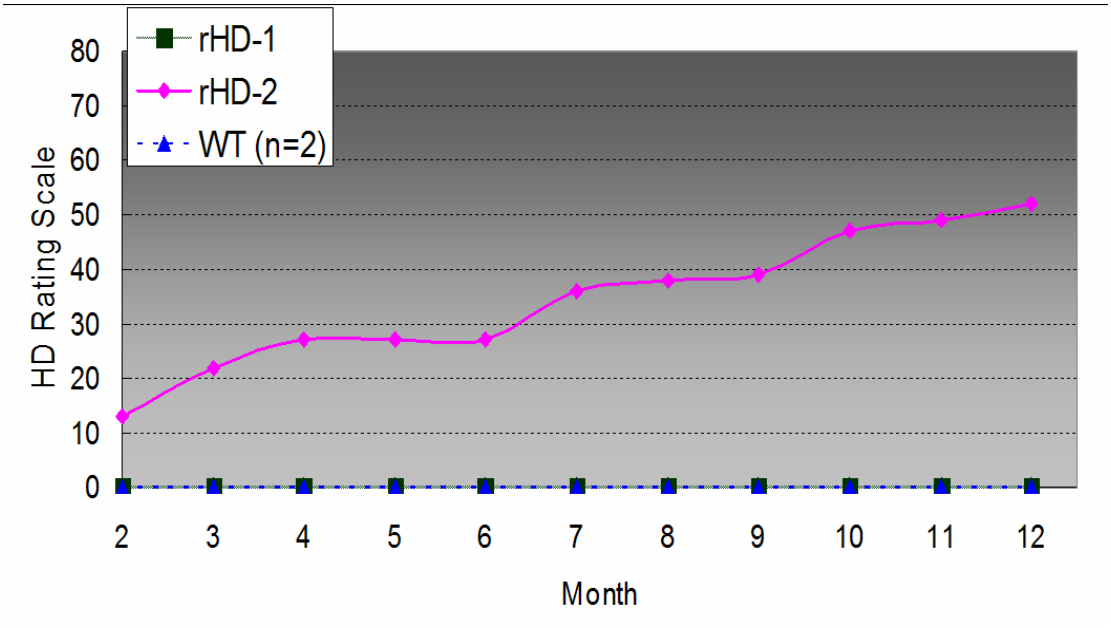

Figure II-27. HD primate model rating scale of rHD-1 and rHD-2. The HD primate model rating scale was modified from the Unified Huntington's Disease Rating Scale (UHDRS) for rating of HD progression. A scoring system with 80 is the highest score of the most severe symptoms.

Table II-1. The *in vitro* development rate of mouse embryos after the injection of LVU-*HTT*-147Q and LVU-*HTT*-84Q. Normal embryos without the injection of lentiviruses were used as the control. Chi-square analysis and SAS software for multiple comparisons were used to compare the development rate of embryos *in vitro*. Differences of P <0.05 was considered statistically significant.

Virus constructs	No. of surviving embryos after microinjection	No.(%) of embryos developed to				
		2-cell embryo	4-cell embryo	8-cell embryo	Morula embryo	Blastocyst embryo
LVU-*HTT*-147Q	43	43(100.00)	37(86.05)[a]	33(76.74)[a]	31(72.09)	11(25.58)[a]
LVU-*HTT*-84Q	35	35(100.00)	31(88.57)[a]	29(82.86)[ab]	27(77.14)	6(17.14)[a]
Normal	39	39(100.00)	39(100.00)[b]	37(94.87)[b]	33(84.62)	31(79.49)[b]

[ab] Values within the same columns without common superscript differ significantly (P < 0.05).

Table II-2. The number of CAG repeats in different transgenic founders

LVU-*HTT*-147Q transgenic founder	Ploy Q length
#1	137Q
#2	58Q, 42Q
#3	46Q
#4	104Q
#5	48Q
#7	64Q, 30Q
#8	39Q
#9	40Q
#10	80Q
LVU-*HTT*-84Q founder	**Ploy Q length**
#2	84Q
#5	60Q
#6	81Q
#7	82Q, 56Q
#8	83Q
#9	50Q

Table II-3. Summary of all transgenic monkeys. Same color within different rows represented the fetuses/infants delivered from the same surrogates.

Internal Code Code	Transgene	Aborted at	Poly Q length	*HTT Int. sites*	*GFP Int. sites*
No. 1	pLVU-*HTT*-147Q	~2M	47; 113	8	--
No. 2	pLVU-*HTT*-147Q	~4M	122	4	--
No. 3	pLVU-*HTT*-147Q	~4M	47; 77	6	--
No. 4	pLVU-*HTT*-147Q/GFP	~4M	11; 58	N.D.*	N.D.
No. 5	pLVU-*HTT*-84Q/*GFP*	~4M	72	2	10
No. 6	*GFP*	~4M	--	--	1
No. 7	pLVU-*HTT*-84Q/*GFP*	~4M	85	3	5
No. 8	*GFP*	~4M	--	--	N.D.
No. 9	*GFP*	~3M	--	--	3
No. 10	pLVU-*HTT*-84Q/*GFP*	~3M	30; 83	2	5
No. 11	pLVU-*HTT*-84Q/*GFP*	~4M	87	1	9
No. 12	*GFP*	~4M	--	--	6
No. 14	pLVU-*HTT*-84Q/*GFP*	Live-born	29	1	6
No. 15	pLVU-*HTT*-84Q/*GFP*	Live-born	83	1	5
No. 16	pLVU-*HTT*-84Q/*GFP*	Live-born	84	2	8
No. 17	pLVU-*HTT*-84Q/*GFP*	Live-born	27; 65	2	6
No. 18	pLVU-*HTT*-84Q/*GFP*	Live-born	88	4	3

N.D.: the sample could not be detected due to the poor quality of genomic DNA

Table II-4. Summary of five live-born transgenic monkeys

rHD	Sex	CAG repeats	*HTT* copy number	Expression of mutant HTT/GFP	Body weight ratio	Movement dysfunction				
						Onset/ frequency	Dystonia	Chorea	Swallowing difficulty	Respiratory difficulty
1	M	29	1	+/+	2.85*	–	–	–	–	–
2	M	83	1	+/+	2.16*	1 week/ sporadic	+	+	–	+
3	F	84	2	+/+	1.11†	2–3 days/ persistent	++++	++++	++++	++
4	F	27, 65	2	+/+	ND	At birth/ persistent	++	++	ND	++++
5	F	88	4	+/+	ND	At birth/ ND	ND	ND	ND	++++

* The ratio of body weight at 24 weeks after birth to birth weight.
† The ratio of body weight at 28 days after birth to birth weight.
F, female; M, male; ND, not determined.

CHAPTER III

Discovery of Novel MicroRNAs in a Non-Human Primate Model of Huntington's Disease

This chapter presents work to be submitted in the future with the inclusion of following authors: Shang-Hsun Yang, Keith Szulwach, Peng Jin, and Anthony W. S. Chan. S.-H.Y. carried out all the experiments described in this chapter. K.S., P.J., and A.W.S.C. aided in the design of experiments, interpretation of results, and preparation of this manuscript.

INTRODUCTION

HTT is involved in various cellular gene regulatory pathways whose mRNA expression profiles have been investigated in HD (Crocker *et al.*, 2006; Hebb *et al.*, 2004; Li and Li, 2006; Ryu *et al.*, 2006). Recent studies have focused on post-transcriptional gene regulation by non-coding RNAs, especially miRNAs, in metazoans. Several miRNAs have been identified that are involved in neuronal function and development (Lim *et al.*, 2005; Vo *et al.*, 2005; Yu *et al.*, 2008), which suggests the importance of miRNAs in gene regulation in the brain. miRNAs also play an important role in the pathogenesis of several neuronal diseases, such as Fragile X syndrome (Jin *et al.*, 2004; Li *et al.*, 2008; Qurashi *et al.*, 2007), Parkinson's and Alzheimer's Disease (Kim *et al.*, 2007; Lukiw, 2007). Therefore, it is possible that miRNA impacts neuropathogenesis in HD.

The miscarried and euthanized monkeys are a good model for studying gene regulation because they developed neuropathological changes without medical intervention. In addition, live-born HD monkeys with the same mutant *HTT* gene

displayed behavioral phenotypes, comparable to HD in human patients among all animal models. In this chapter, we used HD monkey brain tissues to identify miRNAs that may be involved in HD pathogenesis by using a high-throughput miRNA microarray. With the analysis of these experiments, there were four potential miRNA candidates, Hsa-mir-196a, Hsa-mir-451 and Hsa-mir-486 and Hsa-mir-429, and one target gene, CUGBP2, which may be correlated to HD. These results may identify novel candidates that regulate gene expression at the transcriptional or post-transcriptional level, and may be possible genetic markers for diagnosis or potential gene therapy targets in HD.

MATERIALS AND METHODS

miRNA expression profiling in HD monkey brains using low density miRNA microarray

The cortex from HD/GFP transgenic monkeys, No. 5 and No. 7, and GFP monkeys, No. 6 and No. 12, were used for total RNA extraction and further analysis. Cortex from different animals were subjected to TRIzol® Reagent (Invitrogen) to extract total RNAs, including miRNAs, as recommended by the manufacturer, and the RNAs quality were determined by BioPhotometer (Eppendorf). These samples were processed using a TaqMan® based low density expression profiling microarray for miRNA (Applied Biosystems). All procedures were provided by the manufacturer. Total RNAs were reverse transcribed with eight specific pools of RT primers [Multiplex (48-plex) RT for TaqMan® MicroRNA Assays; Applied Biosystems]. cDNA was then applied to a TaqMan® Human MicroRNA Array v1.0 (Early Access; Applied Biosystems) and real-time PCR was performed using a 7900HT Fast Real-Time PCR System (Applied Biosystems). In

total 365 different human miRNA assays were examined in addition to two small nucleolar RNAs (snoRNAs). Technical duplicates were conducted for each sample, and miRNA expression levels were evaluated by the ΔΔCt method. The results were subjected to *t*-test for statistical analysis, followed by identifying miRNA candidates.

Western blotting analysis and protein quantification

Total proteins from cortex of HD (Nos. 2, 3, 5, 7, 10, 11, 17 and 18) and wild-type (Nos. 6 and 12) monkeys were extracted and loaded into a polyacrylamide gel. After electrophoresis, the protein was transferred onto a PVDF membrane (Bio-Rad), and the membrane was incubated with the primary antibodies, mouse monoclonal mEM48 (1:50 dilution), CUGBP2 (Sigma; 1:1,000 dilution) and γ-tubulin (Sigma; 1:2,000 dilution), followed by secondary peroxidase-conjugated antibodies (Jackson ImmunoResearch laboratories) for detecting proteins with an Amersham ECL kit (PerkinElmer). To quantify the expression intensity and perform statistical analysis, the intensity of the

immunoreactive protein bands were determined using UVIDocMW software (Uvitec) and normalized with the expression of γ-tubulin, followed by *t*-test statistical analysis. The detailed protocol of Western blotting was described in chapter II.

RNA extraction, reverse transcription (RT), RT-PCR and real-time quantitative PCR (Q-PCR) Analysis

The cortex of HD (Nos. 2, 3, 5, 7, 10, 11, 17 and 18) and wild-type (Nos. 6 and 12) monkeys were used for total RNA extraction using RNeasy Mini Kit (Qiagen). All procedures were performed as recommended by the manufacturer. RNA quality was determined by BioPhotometer (Eppendorf). RT was performed by using High Capacity cDNA Reverse Transcription Kit (Applied Biosystems), and cDNA was then used for Q-PCR. 2X Power SYBR® Green PCR Master Mix (Applied Biosystems) was mixed with specific primers and cDNA, and then subjected to the iQ5 real-time PCR detection system (Bio-Rad) for 50 cycles at 96 ℃ for 12 mins first; 96 ℃ for 15 secs, 60 ℃ for 30 secs for 50 cycles. The sequences for the

specific primers were the following:

CUGBP2-F: CCAAAGAAGGGGATGAAAATGC

CUGBP2-R: CCGACTCAAAACTATGGGTATG

18S F: CGGCTACCACATCCAAGGAA

18S R: CCTGTATTGTTATTTTTCGTCACTACCT

Individual miRNA expression profiling

To detect the expression of individual miRNA, the TaqMan® Q-PCR method was used. Total RNA extracted from the cortex and blood lymphocytes using TRIzol® Reagent (Invitrigen) were used in this study. Cortex samples from GFP monkeys (control group; No. 6 and No. 12) and HD monkeys [HD group; No. 2, No. 3, No. 5, No. 7, No. 10, No. 11, No. 17 (rHD-4) and No. 18 (rHD-5)] were used for cortex expression profiling study (Table II-3). Blood samples from No. 14 (rHD-1), No. 15 (rHD-2) and age-matched wild-type monkeys were used for blood expression profiling study. The four miRNA candidates identified with the miRNA microarray were Hsa-miR-196a, Hsa-miR-429, Hsa-miR-451 and Hsa-miR-486.

Hsa-miR-383 showing smallest varitation served as the endogenous control. To perform the RT of mature miRNAs, 40ng RNA was subjected to RT using the High Capacity cDNA Reverse Transcription Kit (Applied Biosystems) and miRNA specific stem-loop RT primers (Applied Biosystems) to synthesize the first cDNA strands at 16 ℃ for 30 mins, 42 ℃ for 30 mins, 85 ℃ for 5 mins and then 4 ℃. To perform the PCR amplification and miRNA quantitation, a 10uL reaction consisting of 1X TaqMan® Gene Expression Master Mix (Applied Biosystems), 1× TaqMan® specific probes (Applied Biosystems), and 1.33uL cDNA was processed by the iQ5 real-time PCR detection system (Bio-Rad) at 95℃ for 12 mins; 95℃ for 15 secs, 60℃ for 60 secs for 50 cycles. The expression analysis was conducted using the iQ5 2.0 Standard Edition Optical System (Bio-Rad), and relative gene expression was calculated and plotted by comparing different samples.

In silico **analysis of miRNA candidates**

To analyze the basic function of the identified miRNA candidates, two websites were used for reference. These included miRBase

(http://microrna.sanger.ac.uk/), where we searched genomic information for each miRNA, and TargetScan (http://www.targetscan.org/), where we screened the predicted target genes.

Statistic analysis

t-test analysis via Excel software (Microsoft) was used to compare the mRNA and protein expression profiles. Differences of $P < 0.05$ were considered statistically significant.

RESULTS

miRNA expression profiling in age-matched HD monkey brains using low density miRNA microarray

To compare miRNA expression profiles, total RNA from the cortex of two groups of age-matched miscarried monkeys (four months gestation), HD/GFP (Nos. 5 and 7) and GFP (Nos. 6 and 12) monkeys, were used for low density miRNA microarray analysis. miRNAs with Ct values below 35 were considered authentic miRNA candidates that were most likely to be expressed at biologically relevant levels. miRNAs with Ct values above 35 were excluded. As a result, a total of 272 miRNAs were identified by the above threshold (Table III-1). To narrow down these miRNA candidates for further analysis, the miRNAs with the higher expression fold change (<0.5 and >1.5 folds) were tested by *t*-test stastical analysis. Four miRNAs significantly different between the two groups were selected (Figure III-1). Among these four miRNAs, Hsa-mir-196a, Hsa-mir-451 and Hsa-mir-486, were significantly up-regulated ($P<0.01$), while Hsa-mir-429 was significantly down-regulated ($P<0.05$) in the HD/GFP group (Figure III-1; Table

III-2). To further confirm the expression level of these four miRNA candidates, each one was analyzed using Q-PCR. The expression level of each miRNA was consistent with the results observed in the low density microarray study (Figure III-2). In brief, Hsa-mir-196a, Hsa-mir-451 and Hsa-mir-486 were more highly expressed in the HD/GFP group compared to GFP control group. However, the HD/GFP group displayed a lower expression level of Hsa-mir-429 than the control group.

Expression level of the miRNA candidates in cortex samples of HD transgenic monkeys

In order to confirm the expression level of the four miRNA candidates in our HD monkeys, six additional HD monkey brain samples (Nos. 2, 3, 10, 11, 17 and 18) were analyzed. The ages of these monkeys spanned from three months gestation to full-term (5.5 months gestation; Table II-3). First of all, oligomeric HTT was observed at a high molecular mass (>250 kDa) in the upper portion of a gradient polyacrylamide gel in all HD samples, but Nos. 10 and 11 had less oligomeric HTT

(Figure III-3). Since the brains of eight monkeys showed mutant HTT, we were interested in investigating the expression profiles of the miRNA candidates. Hsa-mir-196a was up-regulated in the cortex of all HD samples except No. 11 when compared to the control group (7/8; 87.5%; Figure III-4). Samples from Nos. 5 and 7 had the lowest expression of Hsa-mir-429 when compared to the other monkeys. All of the HD monkeys exhibited lower expression level of Hsa-mir-429 than those of the control group (8/8; 100.00%; Figure III-5). Regarding Hsa-mir-451 and Hsa-mir-486, the six additional HD samples did not appear higher expression than those of the control group, especially Hsa-mir-451, but Nos. 5 and 7 were much higher (Figure III-6; Figure III-7).

In silico analysis of miRNA candidates

To further analyze the basic characteristics of the miRNA candidates, two databases, miRBase and TargetScan, were used for identifying their mature sequences, chromosome locations and predicted target genes. Based on the miRBase database, Hsa-mir-196a, Hsa-mir-429, Hsa-mir-451 and Hsa-mir-486

are located on chromosome 17, 1, 17 and 8, respectively. The mature sequences of each miRNA are listed in Table III-2. To predict the target genes in the genome, we used the recently updated TargetScan website (April 2008). Since TargetScan does not provide a database for the rhesus monkey, the human database was used for this study based on the closer similarity between humans and rhesus monkeys. Hsa-mir-196a, Hsa-mir-429, Hsa-mir-451, and Hsa-mir-486 have 146, 181, 14, and 103 predicted target genes, respectively (Table III-2). Among these target genes, thirteen were affected by at least two of the four candidates (Table III-3). One of the most interesting target genes was the CUG triplet repeat RNA binding protein 2 (CUGBP2) gene, which was targeted by Hsa-mir-196a, Hsa-mir-451, and Hsa-mir-486 at the 3' untranslated region (3' UTR) (Table III-3; Figure III-8).

Expression of CUGBP2 in HD cells and animals

Since our *in silico* analysis of the four miRNA candidates predicted that one potential target gene, CUGBP2, is a target for three of the miRNA examined, we

wanted to demonstrate the CUGBP2 expression profiles in HD cells and animals. 293 FT cells expressing LVU-*HTT*-147Q or LVU-*HTT*-84Q, as described in Chapter II, were used for Western blotting analysis. A monoclonal antibody that specifically detects CUGBP2 was used to locate the target protein. γ-tubulin was used as the internal control. Based on Western blotting analysis, a more intense signal of CUGBP2 was observed in wild-type 293 FT cells; whereas 293 FT expressing LVU-*HTT*-147Q or LVU-*HTT*-84Q had relatively lower expression of CUGBP2 (Figure III-9). After normalization and quantification analysis, the expression of CUGBP2 in wild-type 293 FT cells was significantly higher than in HD transgenic cells (P <0.05). The expression of CUGBP2 in 293 FT cells expressing LVU-*HTT*-84Q was significantly higher than those expressing LVU-*HTT*-147Q (P <0.05) (Figure III-9).

To determine the expression of CUGBP2 in the brains of HD transgenic mice, we used crude protein extract from the cortex of N171-82Q transgenic mice, which were well-characterized in HD studies (Schilling *et al.*, 1999; Wang *et al.*, 2008), and wild-type mice with the same genetic background for Western blotting analysis.

A significantly lower expression of CUGBP2 was observed in the HD group (n=3) than the wild-type control group (n=3) (Figure III-10).

In order to determine the expression level of CUGBP2 in HD transgenic monkeys, eight HD monkey brain samples were analyzed. Since miRNA interacts with the target gene at the 3' UTR at the post-transcriptional level (Ambros, 2004; Bartel, 2004; He and Hannon, 2004; Kosik, 2006), we further determined the mRNA expression profile of CUGBP2 in the HD monkeys by Q-PCR. There was no significant difference (P=0.783) in the mRNA expression level of CUGBP2 between the HD group (n=8; Nos. 2, 3, 5, 7, 10, 11, 17 and 18 monkeys) and the control group (n=2; Nos. 6 and 12 monkeys) (Figure III-11). The protein level of CUGBP2 in the cortex was determined by Western blotting analysis, and significantly lower expression of CUGBP2 was found in the HD group (n=8) when compared to the control group (n=2) (P<0.01; Figure III-12).

Expression level of miRNA candidates in HD transgenic monkey blood

Peripheral blood from two HD monkeys was used to verify the expression of

the four candidate miRNAs since mutant HTT is also expressed in the peripheral blood, which may affect the gene regulation in blood. The blood samples from rHD-1 and rHD-2 (Table II-4) and three wild-type age-matched monkeys were collected at 8 months old. The expression levels of Hsa-mir-196a, Hsa-mir-451 and Hsa-mir-486 in rHD-2 were higher than in rHD-1 and the age matched control monkeys (Figure III-13). However, Hsa-mir-429 expression was not lower in rHD-2 than the wild-type age-matched control group (Figure III-13).

Discussion

Aberrant gene regulation caused by mutant HTT is one of the areas of interest in HD pathogenesis. Based on previous reports, mutant HTT interferes with various cellular and gene regulatory pathways leading to alteration of gene expression in HD animal models and patients, resulting in HD pathogenesis (Li and Li, 2006; Ryu *et al.*, 2006). Therefore, investigating gene expression profiles in our transgenic HD monkeys could help elucidate the underlying mechanism of HD.

Many gene regulation studies have focused on the relationship between mRNA expression level and phenotype. With the latest discovery of non-coding RNA, several studies have shown the influence of non-coding RNA on gene expression in mice and humans. The role of non-coding RNA in disease progression has also been demonstrated. Among non-coding RNA, miRNA is an important regulator of pathogenesis in several neuronal diseases, such as Fragile X syndrome (Jin *et al.*, 2004; Li *et al.*, 2008; Qurashi *et al.*, 2007), Parkinson's and Alzheimer's disease

(Cogswell *et al.*, 2008; Hebert *et al.*, 2008; Kim *et al.*, 2007; Lukiw, 2007). However, the role of miRNA in HD pathogenesis has not been fully elucidated. Several lines of evidence imply the role of miRNA in HD pathogenesis; for example, miRNAs express during the development of neuronal processes in brain (Lim *et al.*, 2005; Vo *et al.*, 2005; Yu *et al.*, 2008). Therefore, it is logical to investigate the impact of miRNA pathways on HD pathogenesis.

Genome-wide microarray analysis is a powerful tool to produce an enormous amount of data by monitoring the response of thousands of genes to different pathological states. Several genome-wide mRNA expression profiling studies in HD mice have demonstrated that overexpressing mutant HTT impacts the gene expression profile in multiple tissues (Chan *et al.*, 2002; Crocker *et al.*, 2006; Luthi-Carter *et al.*, 2002a; Luthi-Carter *et al.*, 2002b). In addition to mRNA microarray, miRNA microarray is a powerful tool to study gene regulation at the post-transcriptional level, which is also related to protein expression. Therefore, our goal in this chapter was to investigate the role of miRNA on HD pathogenesis.

Brain samples from miscarried monkeys are ideal for investigating the impact

of miRNA in HD. To compare miRNA expression profiles, total RNAs from the cortex of two HD/GFP and two age-matched GFP monkeys were used for low density miRNA microarray. Based on the low density miRNA microarray data, 272 miRNAs were identified, with more than 90% (247/272; 90.81%) of these only exhibiting slight changes (0.5-1.5 fold) between the HD/GFP and control groups (Table III-1). There were 25 miRNA with large differences between the two groups. Variations due to biological and technical duplicates were considered and analyzed to eliminate false positives. Statistical analysis was used to narrow the number of potential miRNA candidates. A total of four miRNA candidates were selected. Three of the four miRNA, Hsa-mir-196a, Hsa-mir-451 and Hsa-mir-486, were up-regulated significantly ($P<0.01$) in the HD/GFP monkeys, while Hsa-mir-429 was significantly down-regulated ($P<0.05$; Figure III-1). In order to confirm the microarray for the four miRNA candidates, individual miRNA assays were performed on each miRNA candidate to determine their expression level in both groups (Figure III-2). Based on these resuts, the four miRNA were considered potential biomarkers for HD.

To confirm the role of the four miRNA candidates, the cortex of six additional HD monkey brain samples from miscarried HD monkeys were analyzed by Q-PCR. Hsa-mir-196a was up-regulated in all HD monkeys, except No. 11, when compared to the control group (Figure III-4). The relatively low expression level of mutant HTT in No. 11 (Figure III-3) may have resulted in limited induction of Hsa-mir-196a, making it similar to the control group. However, No. 10 also expressed a lower level of mutant HTT (Figure III-3) and the expression of Hsa-mir-196a was not reduced. Therefore, individual differences in integration/expression patterns of *HTT* may have affected Has-mir-196a expression. Additionally, No. 11 had more than 2 Ct differences in the internal control, Hsa-mir-383, compared to other samples. Since we used the same amount of RNA for RT and Q-PCR, we expected no distinct differences between samples, suggesting No. 11 may have a unique pattern and that Hsa-mir-383 may not be a good internal control for this monkey.

Based on previous reports, Hsa-mir-196a is expressed from Homeobox (HOX) gene clusters in mammals and also targets back to HOX clusters, such as HOXB8,

HOXC8, HOXD8 and HOXA7 (Yekta *et al.*, 2004). In addition, Hsa-mir-196a is related to gene expression of annexin A1 in cancer (Luthra *et al.*, 2008). Therefore, it is possible that Hsa-mir-196a is influenced more by these target genes than *HTT*. Perhaps preferential control by these genes resulted in a distinct expression profile in No. 11. However, Hsa-mir-196a was up-regulated in the cortex of other HD monkeys (7/8; 87.50%), suggesting it may be a good marker for post-transcriptional regulation of HD pathogenesis. However, a larger sample size, including from human brains, should be examined, and functional assays have to be addressed to validate Hsa-mir-196a as a good marker for HD.

The cortex from all HD monkeys exhibited a lower level of Hsa-mir-429 than that of the control monkeys (Figure III-5). However, variations were observed among HD samples. Nos. 5 and 7, which were used for miRNA microarray, had the lowest expression level. Nos. 3 and 10 had relatively higher expression of Hsa-miR-429 than the other HD samples (Figure III-5). Individual differences and differences in integration/expression patterns may explain these discrepancies. Hsa-mir-429 was first reported in 2005 (Xie *et al.*, 2005) and has only been

detected in ovarian carcinoma (Nam *et al.*, 2008) and epithelial-mesenchymal transition (Katoh and Katoh, 2008). Therefore, this miRNA would be a novel candidate for functional studies in HD research. Overall, the expression level of Hsa-mir-429 was higher in the control group than in the HD group (8/8; 100.00%). The expression profile of the additional six miscarried HD monkeys was consistent with the low density microarray data, suggesting Hsa-mir-429 may be a potential marker of HD.

Hsa-mir-451 and Hsa-mir-486 were first reported in 2007 (Landgraf *et al.*, 2007). Although Hsa-mir-451 and Hsa-mir-486 were highly expressed in the two samples used for miRNA microarray analysis, all the samples from miscarried HD monkeys had relatively low expression levels compared to the control group (Figure III-6; Figure III-7). Due to the potential individual differences, more samples must be examined to explain this result. Additionally, these two miRNAs have been described in oncogenesis and erythropoiesis (Bruchova *et al.*, 2007; Masaki *et al.*, 2007; Merkerova *et al.*, 2008; Zhu *et al.*, 2008), but their roles in HD remains unknown. These two miRNAs may be more related to general developmental

processes than to HD specifically. As a result, these miRNAs may respond to other developmental factors leading to varying results. Therefore, more advanced experiments, such as functional assays and additional sample screening, have to be conducted using more samples in order to conclude the influence of these two miRNAs on HD.

Two comprehensive miRNA databases were used to further understand the characteristics of the four miRNA candidates (Table III-2). The two databases are miRBase (http://microrna.sanger.ac.uk/) and TargetScan (http://www.targetscan.org/). miRBase provides basic information, such as chromosome location, mature sequence, stem loop and database link; whereas TargetScan predicts miRNA targets based on the 3' UTR region of the target genes. We have identified numerous genes that could potentially be influenced by the four miRNA candidates, and some of these genes have already been shown to be involved in HD. Among these predicted targets, thirteen were affected by at least two of the four miRNA candidates (Table III-3). This finding suggested that the four miRNA candidates may be involved in the same miRNA pathways, which may

influence the regulatory networks contributing to HD pathogenesis.

The most interesting target was the CUGBP2 gene (Figure III-8), which was a predicted target of Hsa-mir-196a, Hsa-mir-451 and Hsa-mir-486 (Table III-3; Figure III-8). The CUGBP2 gene has been studied extensively, and plays a critical role in colon cancer, breast cancer, cell cycle regulation and apoptosis (Mukhopadhyay *et al.*, 2003; Natarajan *et al.*, 2008; Subramaniam *et al.*, 2008). However, no study had yet correlated this gene to HD. Since HD is one of the CAG triplet repeat diseases which carrying the aberrant transcripts of CUG repeats, it was reasonable to speculate CUGBP2 may bind to the CUG transcripts of *HTT* in HD.

Because Hsa-mir-196a, Hsa-mir-451 and Hsa-mir-486 are all up-regulated in the miRNA microarray study, CUGBP2 protein is expected to be reduced in HD. We have shown a significant reduction of CUGBP2 in 293 FT cells overexpressing the mutant *HTT* gene, even in cells with different numbers of CAG repeats within the mutant *HTT* gene (Figure III-9). 293 FT cells that overexpressed mutant *HTT* with 147 CAG repeats had a much lower level of CUGBP2 compared to 293 FT cells that overexpressed mutant *HTT* with 84 CAG repeats. Since the number of

CAG repeats is correlated to the severity of the disease (Li and Li, 2006; Walker, 2007a), CUGBP2 may be a good indicator for the progression of HD.

The N171-82Q HD transgenic mouse is a well-characterized mouse model of HD (Schilling *et al.*, 1999; Wang *et al.*, 2008). Therefore we used this model to determine the relationship between the expression level of CUGBP2 and HD. Compared to wild-type control mice, the expression level of CUGBP2 in the cortex of HD mice was significantly lower than that of the control group (Figure III-10), similar to cells overexpressing mutant *HTT*. This result demonstrated the reduction of CUGBP2 protein in the brain of HD mice *in vivo*, which may have resulted from altered miRNA expression.

We performed an in-depth study on the expression pattern of CUGBP2 because our primary interest was to determine if CUGBP2 is a biomarker for HD progression in HD monkeys. This analysis included determining mRNA and protein expression profiles of CUGBP2. miRNA suppresses translation by interacting with 3' UTR of the target gene at the post-transcriptional level (Ambros, 2004; Bartel, 2004; He and Hannon, 2004; Kosik, 2006); therefore, the mRNA expression level

of CUGBP2 may not be affected in HD. Our results showed no difference in the mRNA expression level of CUGBP2 between the HD and control groups (Figure III-11). However, the amount of CUGBP2 protein was significantly reduced in HD monkey cortex compared to that of the control monkeys based on Western blotting analysis (Figure III-12). This finding suggested the down-regulation of CUGBP2 protein might occur at post-transcription level, which is the primary mechanism of miRNA to suppress target genes. The suppression at the protein, but not mRNA, level suggests miRNA may be involved in HD pathogenesis. Future studies investigating the role of miRNA and CUGBP2 in HD pathogenesis should be addressed.

Our goal is to identify novel genetic markers for pre-symptomatic diagnosis, and miRNA are potential candidates because of their regulatory role in disease progression. Peripheral blood from live HD monkeys was used to determine the expression level of the four miRNA candidates outside the CNS. rHD-1, which has not shown a behavioral phenotype, and rHD-2, which displayed difficulty in movement coordination and involuntary movement (Table II-4), were used as the

HD experimental group in this study. rHD-2 had higher expression levels of three of the four miRNA candidates, Hsa-mir-196a, Hsa-mir-451 and Hsa-mir-486, when compared to rHD-1 and three control monkeys. rHD-1 may have had a different expression pattern than rHD-2 (Figure III-13) because rHD-1 is pre-symptomatic. In fact, the peripheral expression levels of these miRNA may be related to specific stages of HD, thus pre-symptomatic monkeys may have similar expression patterns as control monkeys. However, since we just have limited sample size for this study, more biological samples need to be confirmed the expression profiles. Additionally, blood samples from HD patients would be considered for screening since we would like to apply these expression profiles in human HD patient study.

Furthermore, we have to concern about whether or not Hsa-mir-383 is a good internal control for miRNA analysis using peripheral blood because the original Ct values of Hsa-mir-383 varied between different sample sets. On the other hand, Hsa-mir-383 may not be consistently expressed in the blood of different individuals, despite similar expression profiles in low density miRNA microarray study. Therefore, selecting another miRNA for the internal control, which has a consistent

expression level between peripheral blood samples, would be important for screening miRNA expression in blood samples.

In summary, we have identified four miRNA candidates that displayed distinct expression patterns in HD and wild-type monkeys by low-density miRNA microarray. Three of the four miRNA, Hsa-mir-196a, Hsa-mir-451 and Hsa-mir-486, were up-regulated in the HD monkey brain and Hsa-mir-429 was down-regulated. These four miRNAs were then analyzed in more detail using Q-PCR in the cortex of these HD monkeys and the miscarried HD fetuses. Consistent expression profiles were found in Hsa-mir-196a and Hsa-mir-429, but not in Hsa-mir-451 and Hsa-mir-486, when compared to the low density microarray data. By searching in two online databases, we identified CUGBP2 as a potential target gene for three of the miRNA candidates. The expression of CUGBP2 was decreased in cells overexpressing mutant *HTT* and in the brains of HD mice and monkeys. Finally, blood samples from live animals were used to determine the expression patterns of the four miRNAs in the peripheral blood. rHD-2, which exhibited a severe behavioral phenotype, displayed up-regulation patterns of three miRNAs,

Hsa-mir-196a, Hsa-mir-451 and Hsa-mir-486, similar to the low density microarray data. These results were novel studies of miRNA in HD, and suggest new clues in identifying candidates, such as Hsa-mir-196a, Hsa-mir-429 and CUGBP2, which may regulate gene expression at the transcriptional or post-transcriptional level. This procedure may also lead to novel genetic markers for pre-symptomatic diagnosis or even for potential gene therapy in the future.

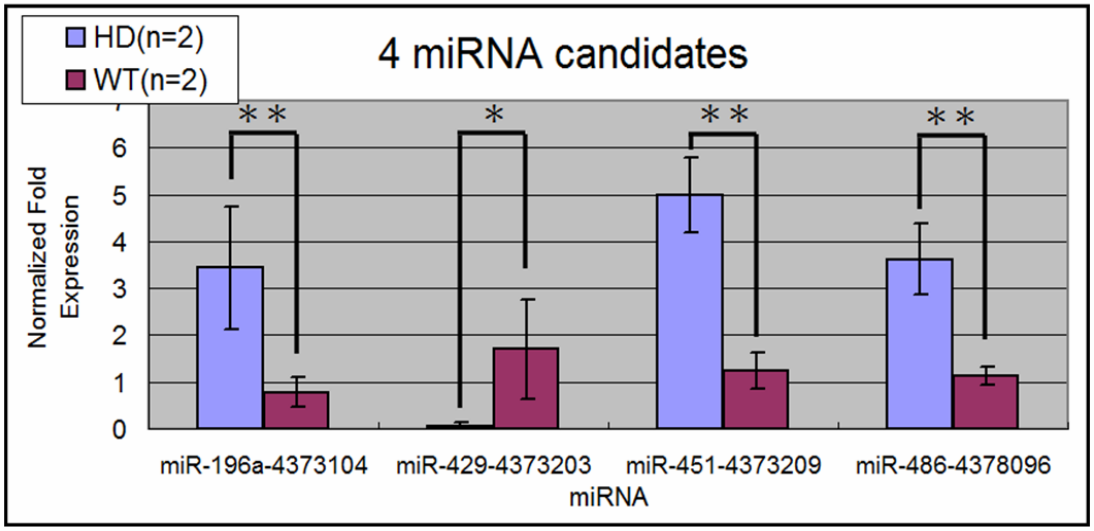

Figure III-1. Four miRNA candidates identified from low density microarray of miRNA via the comparison between HD/GFP (HD) and GFP (WT) groups. Hsa-mir-196a, Hsa-mir-451 and Hsa-mir-486, were up-regulated in the HD/GFP monkeys; whereas the Hsa-mir-429 was down-regulated in the HD/GFP monkeys. ** $P<0.01$; * $P<0.05$

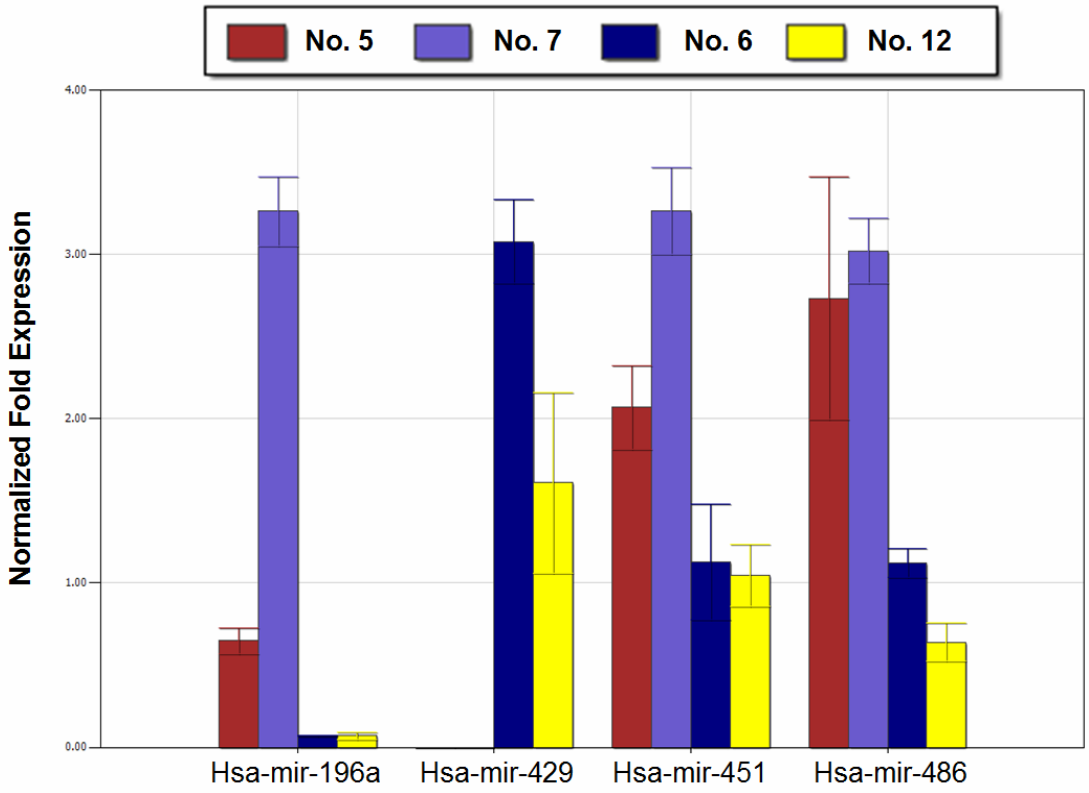

Figure III-2. The confirmation of four miRNA candidates in original RNA samples via the TaqMan® Q-PCR. No. 5 and No. 7 were the RNA samples from the cortex of HD/GFP transgenic monkeys; No.6 and No. 12 were the RNA samples from the cortex of GFP transgenic monkeys. Hsa-mir-196a, Hsa-mir-451 and Hsa-mir-486 were up-regulated in the No. 5 and No. 7 monkeys; whereas the Hsa-mir-429 was up-regulated in the No. 6 and No. 12 monkeys.

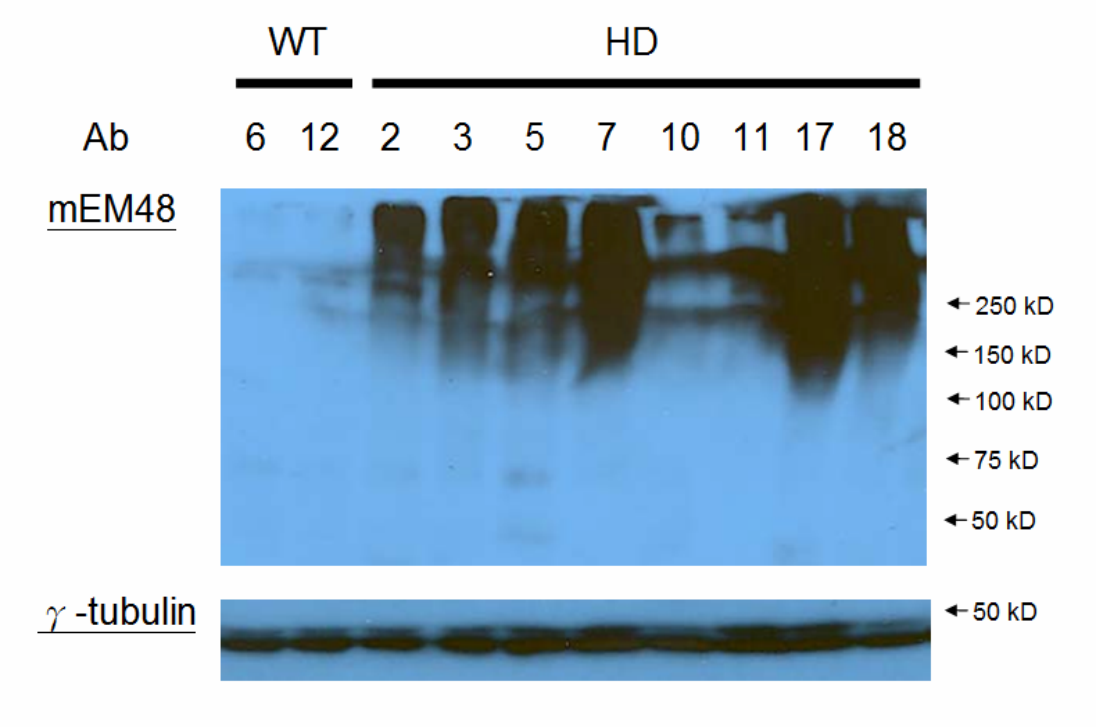

Figure III-3. Expression profiles of mutant HTT in the brains of HD monkeys used for miRNA analysis. No.6 and No.12 were the control monkeys carrying the *GFP* transgenes; the other samples (No. 2, No. 3, No. 5, No. 7, No. 10, No. 11, No. 17 and No. 18) were from HD monkeys, showing the oligomeric HTT at high molecular mass (>250 kDa) in the upper portion of a gradient polyacrylamide gel.

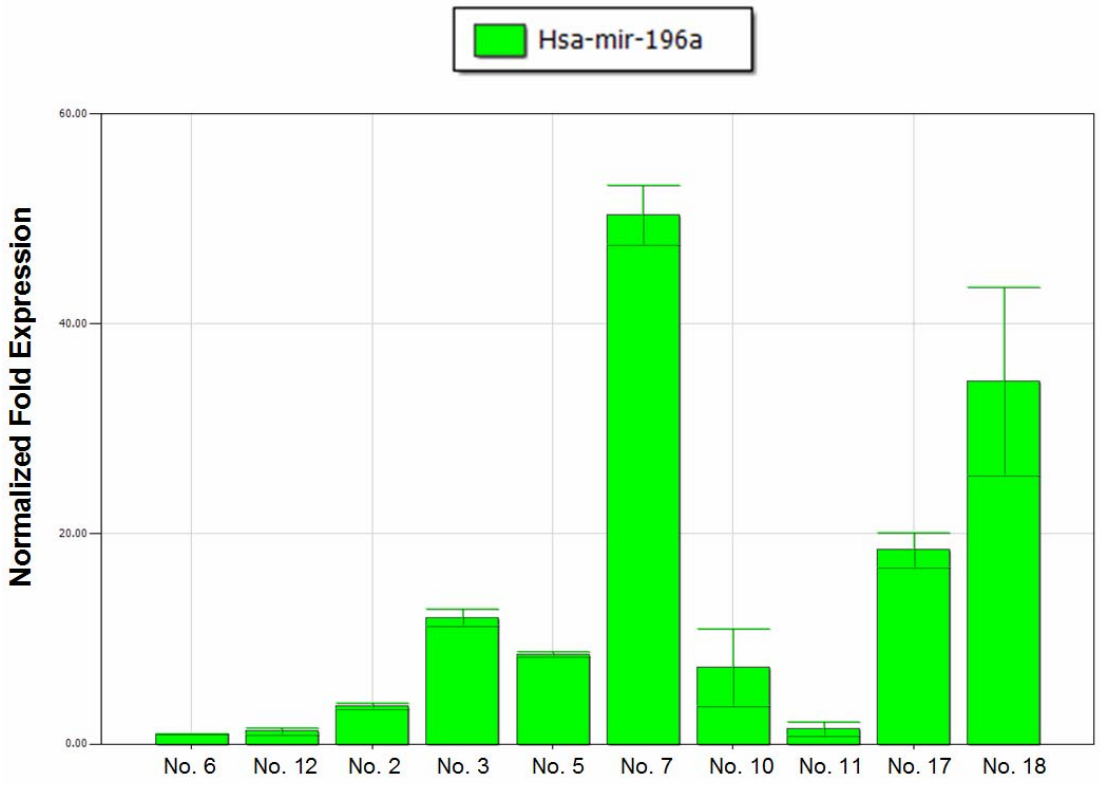

Figure III-4. The miRNA expression profiling of Hsa-mir-196a in different HD monkeys. No.6 and No.12 were the control monkeys carrying the *GFP* transgenes; the other samples were from HD monkeys. Normalized fold expressions were referenced to the expression level of No. 6. Except the No. 11, the Hsa-mir-196a was up-regulated in the HD samples compared to the control group.

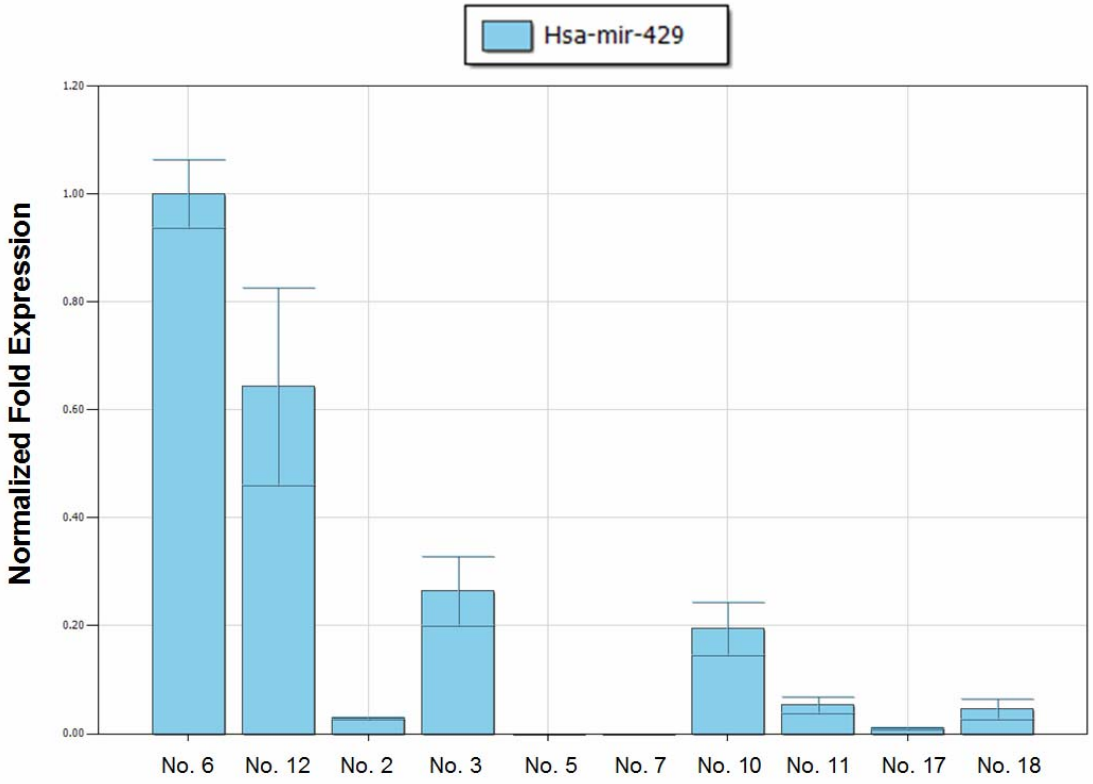

Figure III-5. The miRNA expression profiling of Hsa-mir-429 in different HD monkeys. No.6 and No.12 were the control monkeys carrying the *GFP* transgenes; the other samples were from HD monkeys. Normalized fold expressions were referenced to the expression level of No. 6. No.5 and No. 7 were detected weakly via the Q-PCR. The expression level of Hsa-mir-429 in HD group was lower than that of control group.

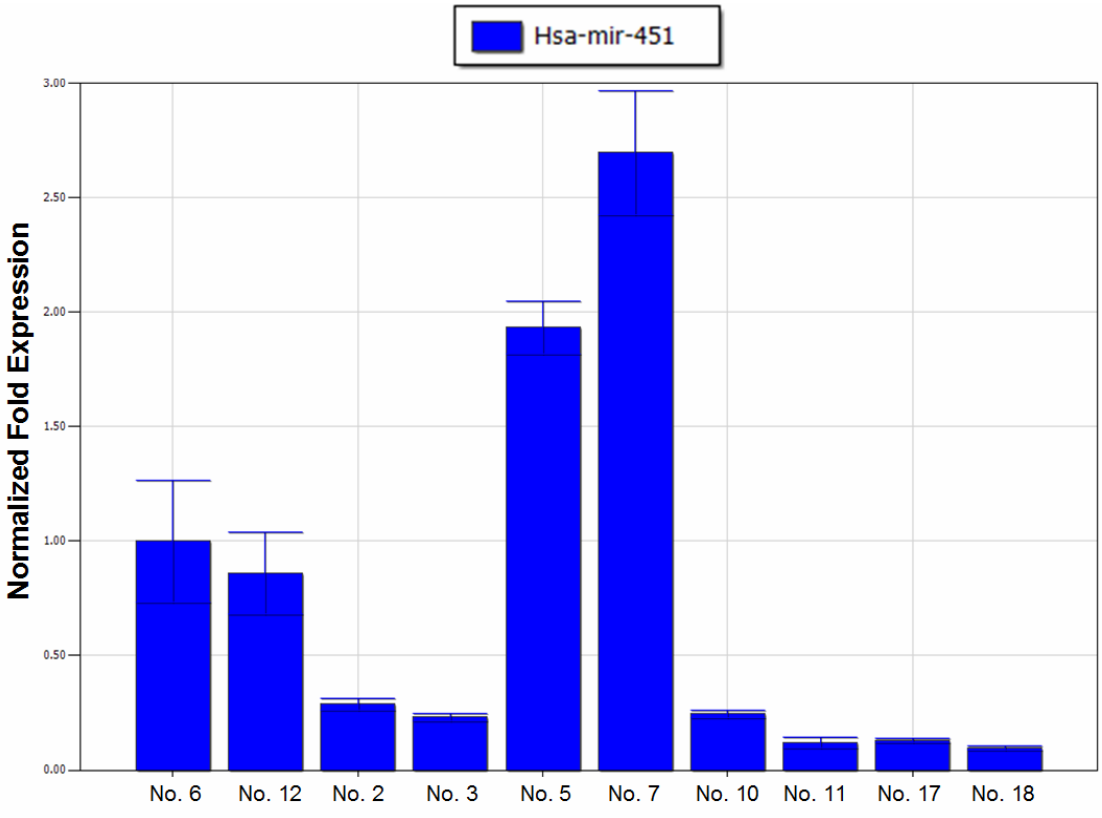

Figure III-6. The miRNA expression profiling of Hsa-mir-451 in different HD monkeys. No.6 and No.12 were the control monkeys carrying the *GFP* transgenes; the other samples were from HD monkeys. Normalized fold expressions were referenced to the expression level of No. 6.

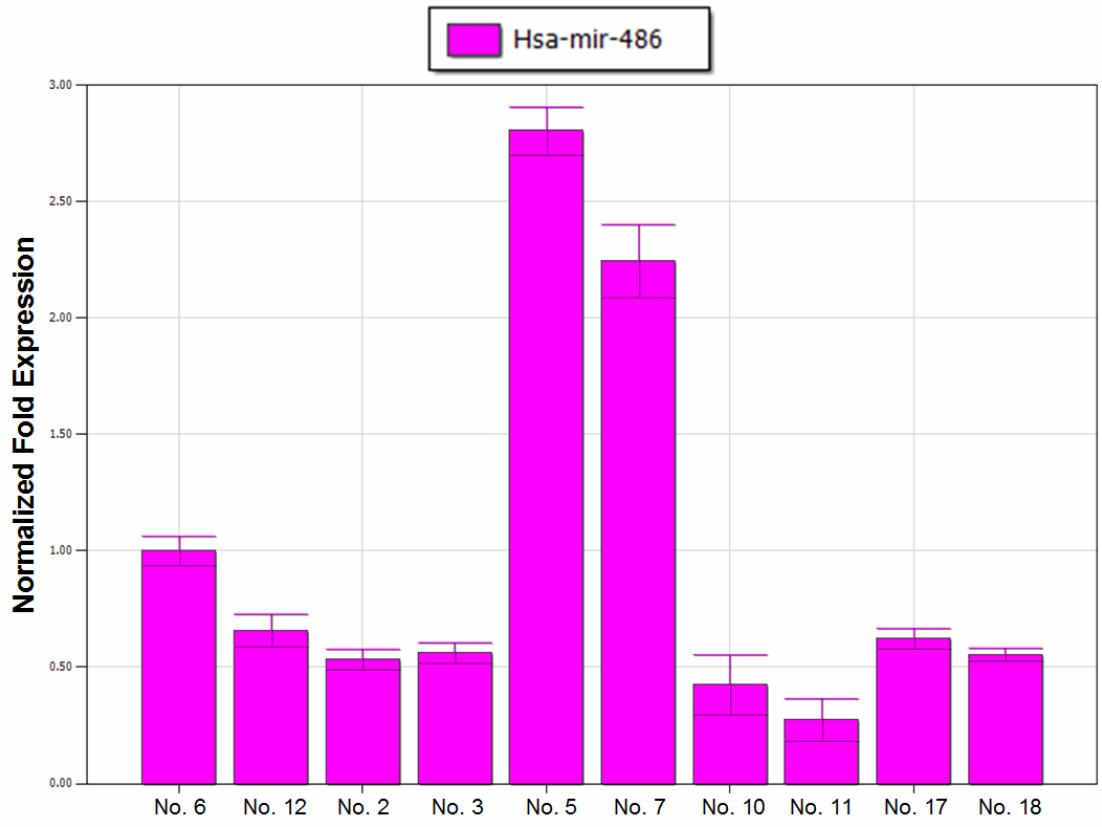

Figure III-7. The miRNA expression profiling of Hsa-mir-486 in different HD monkeys. No.6 and No.12 were the control fetuses carrying the *GFP* transgenes; the other samples were from HD monkeys. Normalized fold expressions were referenced to the expression level of No. 6.

Figure III-8. The miRNA targets in 3' untranslation region (UTR) of CUG triplet repeat RNA binding protein 2 (CUGBP2). These data were downloaded and modified from TargetScan website (http://www.targetscan.org/). Squares showed the target positions of 3 miRNA candidates chosen by the low density miRNA microarray in CUGBP2 3'-UTR region

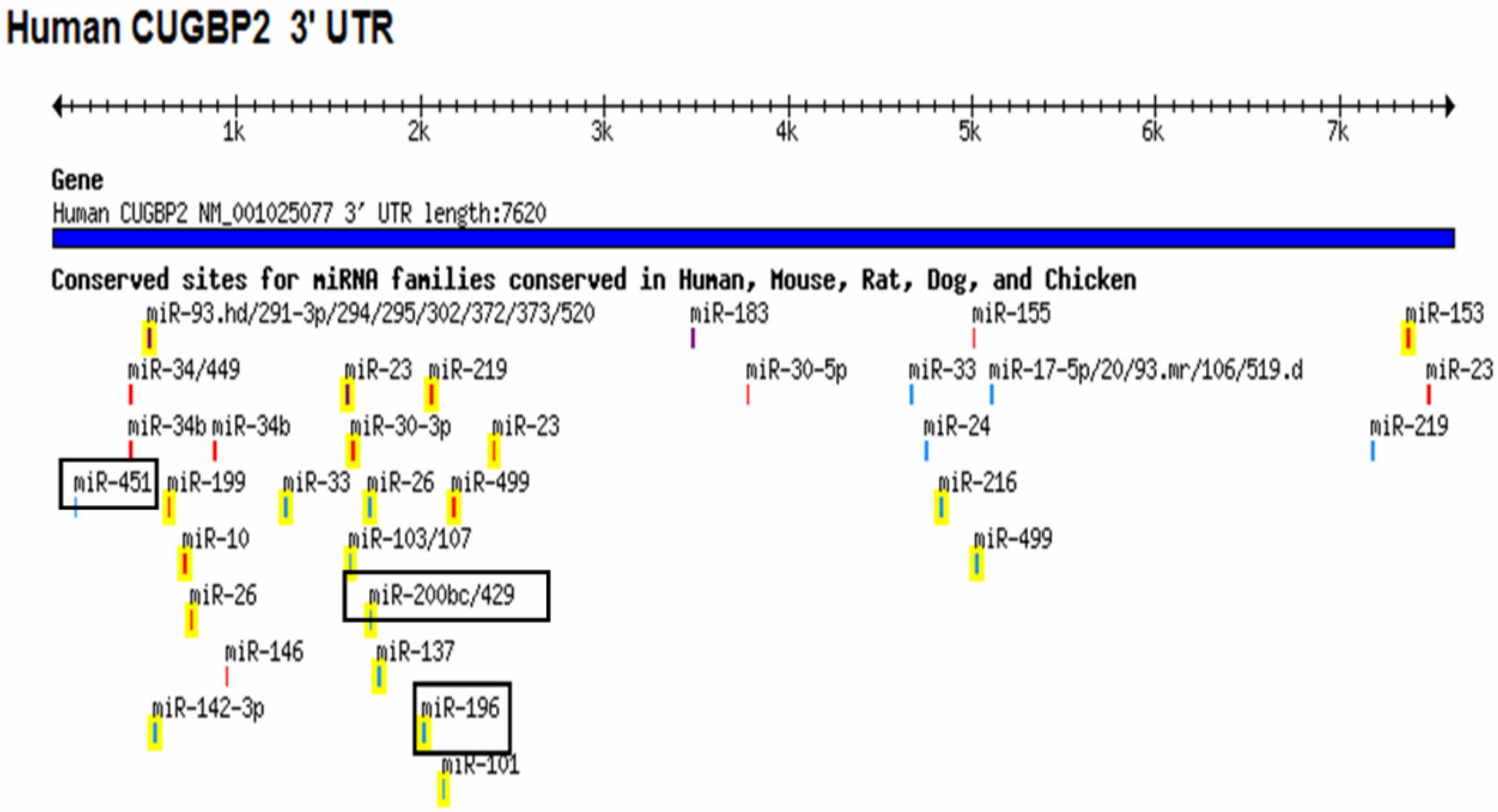

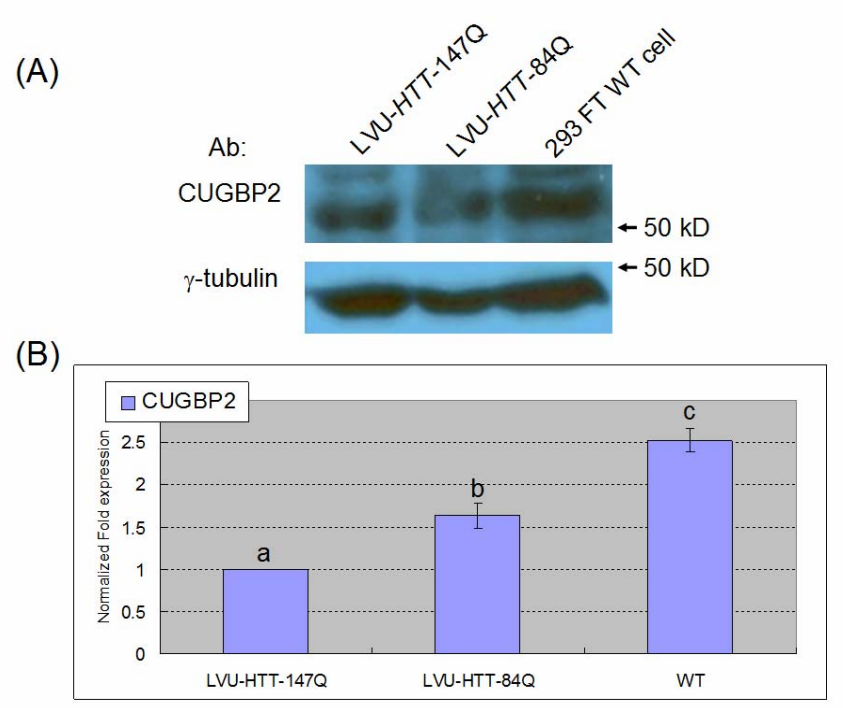

Figure III-9. Expression profiles of CUGBP2 in the different HD 293 FT cells. 293 FT cells infected LVU-*HTT*-147Q and LVU-*HTT*-84Q were used for Western blotting analysis while wild-type 293 cells was used as control. Three batches of experiments were performed. (A) Expression of the CUGBP2 was detected by Western blotting analysis. Immunostaining was performed using the CUGBP2 antibody (top panel) and the antibody against γ-tubulin (bottom panel). (B) The intensity of immunoreactive protein bands were determined by using UVIDocMW software (Uvitec), and then subjected to statistical analysis. ^{abc} Values on the top of different bars without common superscript differ significantly ($P < 0.05$).

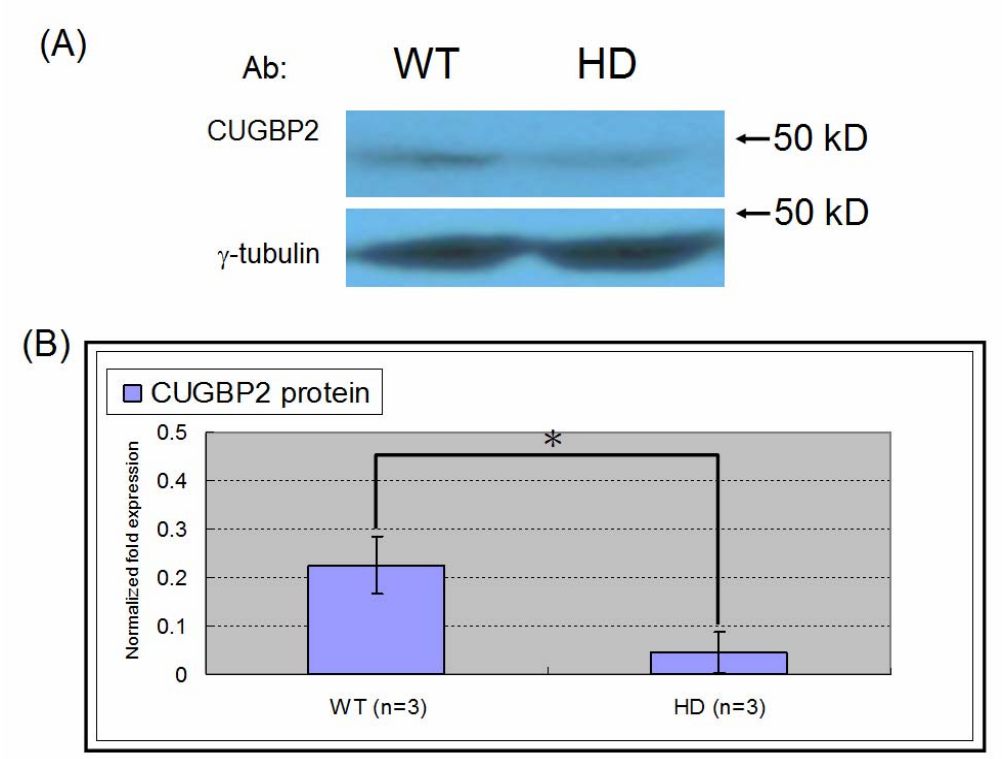

Figure III-10. Expression profiles of CUGBP2 in the cortex of N171-82Q HD transgenic mice. Three wild-type (WT) and three N171-82Q (HD) mice were subjected for Western blotting analysis. (A) Expression of the CUGBP2 was detected by Western blotting analysis. Immunostaining was performed using the CUGBP2 antibody (top panel) and the antibody against γ-tubulin (bottom panel). (B) The intensity of immunoreactive protein bands were determined by using UVIDocMW software (Uvitec), and then subjected to statistical analysis. * represented the significant difference (P<0.05) of expression levels between WT and HD groups.

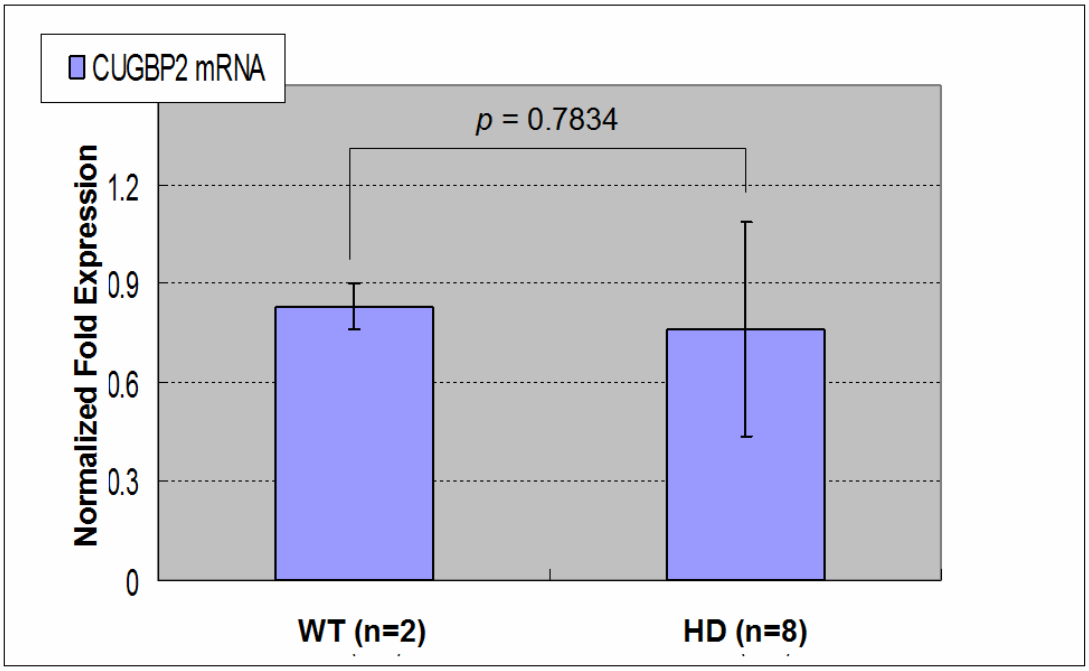

Figure III-11. mRNA expression profiles of CUGBP2 in the cortex of HD transgenic monkeys. Wild-type samples (WT) were the control monkeys carrying the *GFP* transgene from No.6 and No.12; the other HD samples were from HD monkeys (No. 2, No. 3, No. 5, No. 7, No. 10, No. 11, No. 17 and No. 18). There was no significant difference ($P>0.05$) of mRNA expression levels between WT and HD groups.

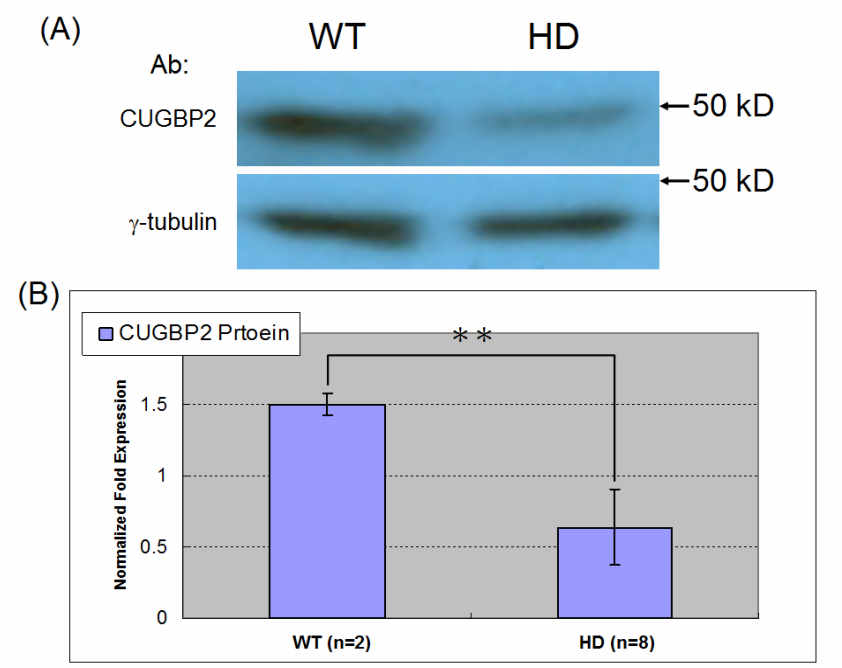

Figure III-12. Expression profiles of CUGBP2 in the cortex of HD transgenic monkeys. Wild-type samples (WT) were the control monkeys carrying the *GFP* transgene from No.6 and No.12; the other HD samples were from HD monkeys (No. 2, No. 3, No. 5, No. 7, No. 10, No. 11, No. 17 and No. 18). (A) Expression of the CUGBP2 was detected by Western blotting analysis. Immunostaining was performed using the CUGBP2 antibody (top panel) and the antibody against γ-tubulin (bottom panel). (B) The intensity of immunoreactive protein bands were determined by using UVIDocMW software (Uvitec), and then subjected to statistical analysis. ** represented the significant difference (P<0.01) of expression levels between WT and HD groups.

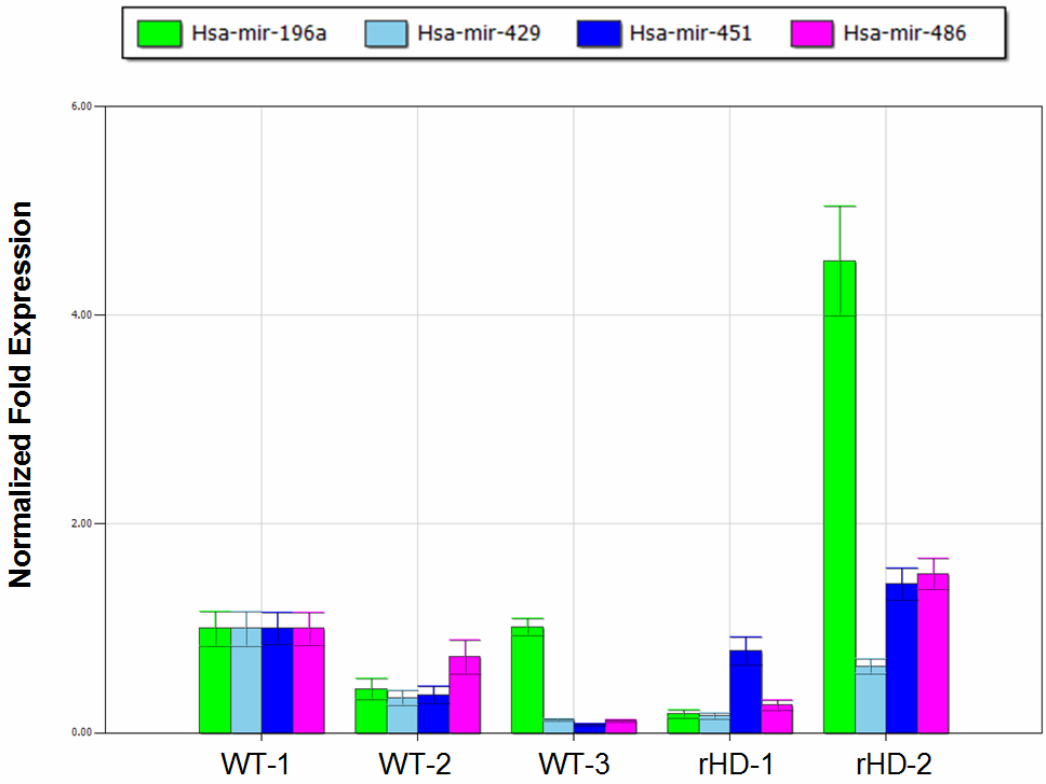

Figure III-13. The expression profiles of four miRNA candidates in the blood samples of different HD monkeys at eight months old. rHD-1 and rHD-2 were the HD samples; WT-1, WT-2 and WT-3 were three age-matched control. Normalized fold expressions were referenced to the expression level of WT-1.

Table III-1. The summary of of miRNAs with different folds expression detected from the low density miRNA microarray.

Expression fold change[1]	No. of miRNAs detected[2]
0-0.5	2
0.5-1	136
1-1.5	111
1.5-2	12
>2	11
Total	272

[1] Expression fold change was determined by the expression level of HD/GFP group (n=2) divided by the expression levels of control group (n=2).

[2] The miRNAs with Ct value lower than 35 were considered for the number of miRNAs detected via this microarray system.

Table III-2. Four candidates of miRNA selected from the low density miRNA microarray.

miRNA	Fold change[1]	Chromosome[2]	Mature sequence[2]	No. of predicted target genes in human[3]
Hsa-mir-196a	4.37	17	uagguaguuucauguuguuggg	146
Hsa-mir-429	0.04	1	uaauacugucugguaaaaccgu	181
Hsa-mir-451	4.02	17	aaaccguuaccauuacugaguu	14
Hsa-mir-486	3.19	8	uccuguacugagcugccccgag	103

[1] Reference was the tissues from GFP monkeys

[2] Data were from miRBase (http://microrna.sanger.ac.uk/)

[3] Predicted no. was from the TargetScan website (http://www.targetscan.org/)

Table III-3. The predicted target genes affected by at least two miRNA candidates chosen from the low density miRNA microarray study.

Target gene	Gene name	Involved miRNAs
CUGBP2	CUG triplet repeat, RNA binding protein 2	mir-196a; mir-451; mir-486
ELAVL2	ELAV (embryonic lethal, abnormal vision, Drosophila)-like 2 (Hu antigen B)	mir-429; mir-486
NRK	Nik related kinase	mir-196a; mir-486
OSR1	odd-skipped related 1 (Drosophila)	mir-429; mir-451
PTEN	phosphatase and tensin homolog (mutated in multiple advanced cancers 1)	mir-429; mir-486
PTPN12	protein tyrosine phosphatase, non-receptor type 12	mir-429; mir-486
PUM2	pumilio homolog 2 (Drosophila)	mir-429; mir-486
SCHIP1	schwannomin interacting protein 1	mir-196a; mir-429
SMCR7L	Smith-Magenis syndrome chromosome region, candidate 7-like	mir-196a; mir-429
SRF	serum response factor (c-fos serum response element-binding transcription factor)	mir-429; mir-486
THRAP1	thyroid hormone receptor associated protein 1	mir-196a; mir-429
TSC22D2	TSC22 domain family, member 2	mir-429; mir-486
ZFYVE20	zinc finger, FYVE domain containing 20	mir-429; mir-486

These data was organized from TargetScan website (http://www.targetscan.org/).

CHAPTER IV

General Conclusion

Non-human primates are ideal for modeling human neurodegenerative diseases because they are the closest relatives to humans. However, little work has been reported in establishing transgenic non-human primate models of human diseases. The goal of my thesis was to establish a non-human primate model for HD, an autosomal dominant neurodegenerative disorder characterized by motor impairment and cognitive deterioration. In addition, I addressed the possibility of using miRNA expression profiles to identify candidates and target genes highly related to HD in our HD transgenic monkey model. These studies support the use of HD monkeys, which displayed similar neuropathological and behavioral abnormalities to human patients, to mimic human HD. Furthermore, we identified several changes in miRNA expression in our transgenic HD monkeys, which may provide insight on novel genetic markers for pre-symptomatic diagnosis and potential gene therapy in HD.

Since monkeys are a limited and valuable resource, we needed to design DNA constructs, which could exhibit the biofunctions *in vitro* and *in vivo*, and also developed a highly efficient gene transfer method for this study. In chapter II, we

constructed mutant *HTT* transgenes with exon 1 and expanded CAG repeats into lentiviral vector. The transgenes were delivered to 293 FT cells and mice via lentiviral transgenesis. Based on Western blotting and immunohistochemistry, the HD transgene had a high gene transfer efficiency in both cell and mouse models. In the transgenic mouse study, mutant *HTT* elicited pathological and behavioral phenotypes. Therefore, we used the same constructs and methodology to create HD transgenic monkeys. With the generation of HD transgenic non-human primates, we analyzed these monkeys in DNA, RNA and protein levels. This analysis revealed the hallmark features of HD in the brain, including nuclear inclusions and neuropil aggregates. Additionally, the transgenic monkeys showed key clinical features of HD, including dystonia and chorea.

In chapter III, we investigated miRNA expression profiles in HD monkeys using a high-throughput miRNA microarray. These transgenic monkeys may provide natural gene expression profiles for HD because they displayed behavioral and pathological phenotypes comparable to human patients and have no history of medical intervention. As a result, we identified four potential miRNAs that showed

significant differences in HD and control groups. Hsa-mir-196a, Hsa-mir-451 and Hsa-mir-486 were up-regulated and Hsa-mir-429 was down-regulated in HD/GFP group compared to control monkeys. By searching in two online databases, CUGBP2 was a predicted target gene that is influenced by three of the four miRNAs. Based on the expression profile of CUGBP2 in 293 FT cells carrying mutant *HTT*, HD mice and monkeys, the protein expression of CUGBP2 was reduced compared to the wild-type control. Furthermore, blood samples from live monkeys were used to determine the expression patterns of the four miRNAs. The HD monkey with severe behavioral phenotypes also displayed up-regulated patterns of Hsa-mir-196a, Hsa-mir-451 and Hsa-mir-486, which were also shown in the low density microarray data

In conclusion, establishing a HD transgenic monkey would provide the opportunity for a wide range of behavioral and cognitive assessments similar to those used for human patients. Future longitudinal studies in these monkeys, such as blood samples and non-invasive imaging, may further confirm the process of HD and correlate pathological changes with behavioral symptoms. These studies

may lead to the discovery of novel factors which lead to symptoms of HD. Additionally, investigating gene regulation in these monkeys, which have not received medical intervention, would provide natural and novel mechanisms for understanding the causes of HD. One day, these genes and target genes may be beneficial for pre-symptomatic diagnosis and gene therapy. Therefore, establishing an effective non-human primate transgenic HD model is invaluable for understanding disease pathogenesis and for developing early diagnostic and treatment strategies.

REFERENCES

1993. A novel gene containing a trinucleotide repeat that is expanded and unstable on Huntington's disease chromosomes. The Huntington's Disease Collaborative Research Group. Cell 72:971-983.

1996. Unified Huntington's Disease Rating Scale: reliability and consistency. Huntington Study Group. Mov Disord 11:136-142.

Ambros V. 2004. The functions of animal microRNAs. Nature 431:350-355.

Andrich J, Saft C, Ostholt N, Muller T. 2007a. Assessment of simple movements and progression of Huntington's disease. J Neurol Neurosurg Psychiatry 78:405-407.

Andrich J, Saft C, Ostholt N, Muller T. 2007b. Complex movement behaviour and progression of Huntington's disease. Neurosci Lett 416:272-274.

Bae BI, Xu H, Igarashi S, Fujimuro M, Agrawal N, Taya Y, Hayward SD, Moran TH, Montell C, Ross CA, Snyder SH, Sawa A. 2005. p53 mediates cellular dysfunction and behavioral abnormalities in Huntington's disease. Neuron 47:29-41.

Barnes FL, First NL. 1991. Embryonic transcription in in vitro cultured bovine embryos. Mol Reprod Dev 29:117-123.

Bartel DP. 2004. MicroRNAs: genomics, biogenesis, mechanism, and function. Cell 116:281-297.

Bavister BD, Leibfried ML, Lieberman G. 1983. Development of preimplantation embryos of the golden hamster in a defined culture medium. Biol Reprod 28:235-247.

Bilen J, Liu N, Burnett BG, Pittman RN, Bonini NM. 2006. MicroRNA pathways modulate polyglutamine-induced neurodegeneration. Mol Cell 24:157-163.

Borovecki F, Lovrecic L, Zhou J, Jeong H, Then F, Rosas HD, Hersch SM, Hogarth P, Bouzou B, Jensen RV, Krainc D. 2005. Genome-wide expression profiling of human blood reveals biomarkers for Huntington's disease. Proc Natl Acad Sci U S A 102:11023-11028.

Borrell-Pages M, Zala D, Humbert S, Saudou F. 2006. Huntington's disease: from huntingtin function and dysfunction to therapeutic strategies. Cell Mol Life Sci 63:2642-2660.

Bruce AW, Donaldson IJ, Wood IC, Yerbury SA, Sadowski MI, Chapman M, Gottgens B, Buckley NJ. 2004. Genome-wide analysis of repressor element 1 silencing

transcription factor/neuron-restrictive silencing factor (REST/NRSF) target genes. Proc Natl Acad Sci U S A 101:10458-10463.

Bruchova H, Yoon D, Agarwal AM, Mendell J, Prchal JT. 2007. Regulated expression of microRNAs in normal and polycythemia vera erythropoiesis. Exp Hematol 35:1657-1667.

Brunet-Simon A, Henrion G, Renard JP, Duranthon V. 2001. Onset of zygotic transcription and maternal transcript legacy in the rabbit embryo. Mol Reprod Dev 58:127-136.

Burns LH, Pakzaban P, Deacon TW, Brownell AL, Tatter SB, Jenkins BG, Isacson O. 1995. Selective putaminal excitotoxic lesions in non-human primates model the movement disorder of Huntington disease. Neuroscience 64:1007-1017.

Carter RJ, Lione LA, Humby T, Mangiarini L, Mahal A, Bates GP, Dunnett SB, Morton AJ. 1999. Characterization of progressive motor deficits in mice transgenic for the human Huntington's disease mutation. J Neurosci 19:3248-3257.

Cha JH, Kosinski CM, Kerner JA, Alsdorf SA, Mangiarini L, Davies SW, Penney JB, Bates GP, Young AB. 1998. Altered brain neurotransmitter receptors in transgenic mice expressing a portion of an abnormal human huntington disease gene. Proc

Natl Acad Sci U S A 95:6480-6485.

Chan AW. 2004. Transgenic nonhuman primates for neurodegenerative diseases. Reprod Biol Endocrinol 2:39.

Chan AW, Chong KY, Martinovich C, Simerly C, Schatten G. 2001. Transgenic monkeys produced by retroviral gene transfer into mature oocytes. Science 291:309-312.

Chan EY, Luthi-Carter R, Strand A, Solano SM, Hanson SA, DeJohn MM, Kooperberg C, Chase KO, DiFiglia M, Young AB, Leavitt BR, Cha JH, Aronin N, Hayden MR, Olson JM. 2002. Increased huntingtin protein length reduces the number of polyglutamine-induced gene expression changes in mouse models of Huntington's disease. Hum Mol Genet 11:1939-1951.

Chen-Plotkin AS, Sadri-Vakili G, Yohrling GJ, Braveman MW, Benn CL, Glajch KE, DiRocco DP, Farrell LA, Krainc D, Gines S, MacDonald ME, Cha JH. 2006. Decreased association of the transcription factor Sp1 with genes downregulated in Huntington's disease. Neurobiol Dis 22:233-241.

Clark AJ, Bissinger P, Bullock DW, Damak S, Wallace R, Whitelaw CB, Yull F. 1994. Chromosomal position effects and the modulation of transgene expression. Reprod

Fertil Dev 6:589-598.

Cleary JD, Nichol K, Wang YH, Pearson CE. 2002. Evidence of cis-acting factors in replication-mediated trinucleotide repeat instability in primate cells. Nat Genet 31:37-46.

Cogswell JP, Ward J, Taylor IA, Waters M, Shi Y, Cannon B, Kelnar K, Kemppainen J, Brown D, Chen C, Prinjha RK, Richardson JC, Saunders AM, Roses AD, Richards CA. 2008. Identification of miRNA changes in Alzheimer's disease brain and CSF yields putative biomarkers and insights into disease pathways. J Alzheimers Dis 14:27-41.

Conaco C, Otto S, Han JJ, Mandel G. 2006. Reciprocal actions of REST and a microRNA promote neuronal identity. Proc Natl Acad Sci U S A 103:2422-2427.

Cowan CM, Raymond LA. 2006. Selective neuronal degeneration in Huntington's disease. Curr Top Dev Biol 75:25-71.

Crocker SF, Costain WJ, Robertson HA. 2006. DNA microarray analysis of striatal gene expression in symptomatic transgenic Huntington's mice (R6/2) reveals neuroinflammation and insulin associations. Brain Res 1088:176-186.

Davies SW, Turmaine M, Cozens BA, DiFiglia M, Sharp AH, Ross CA, Scherzinger E, Wanker EE, Mangiarini L, Bates GP. 1997. Formation of neuronal intranuclear inclusions underlies the neurological dysfunction in mice transgenic for the HD mutation. Cell 90:537-548.

DiFiglia M, Sapp E, Chase K, Schwarz C, Meloni A, Young C, Martin E, Vonsattel JP, Carraway R, Reeves SA, et al. 1995. Huntingtin is a cytoplasmic protein associated with vesicles in human and rat brain neurons. Neuron 14:1075-1081.

DiFiglia M, Sapp E, Chase KO, Davies SW, Bates GP, Vonsattel JP, Aronin N. 1997. Aggregation of huntingtin in neuronal intranuclear inclusions and dystrophic neurites in brain. Science 277:1990-1993.

Dompierre JP, Godin JD, Charrin BC, Cordelieres FP, King SJ, Humbert S, Saudou F. 2007. Histone deacetylase 6 inhibition compensates for the transport deficit in Huntington's disease by increasing tubulin acetylation. J Neurosci 27:3571-3583.

Dunah AW, Jeong H, Griffin A, Kim YM, Standaert DG, Hersch SM, Mouradian MM, Young AB, Tanese N, Krainc D. 2002. Sp1 and TAFII130 transcriptional activity disrupted in early Huntington's disease. Science 296:2238-2243.

Estrada Sanchez AM, Mejia-Toiber J, Massieu L. 2008. Excitotoxic neuronal death and the pathogenesis of Huntington's disease. Arch Med Res 39:265-276.

Fernandes HB, Baimbridge KG, Church J, Hayden MR, Raymond LA. 2007. Mitochondrial sensitivity and altered calcium handling underlie enhanced NMDA-induced apoptosis in YAC128 model of Huntington's disease. J Neurosci 27:13614-13623.

Friedman MJ, Wang CE, Li XJ, Li S. 2008. Polyglutamine expansion reduces the association of TATA-binding protein with DNA and induces DNA binding-independent neurotoxicity. J Biol Chem 283:8283-8290.

Gafni J, Ellerby LM. 2002. Calpain activation in Huntington's disease. J Neurosci 22:4842-4849.

Gauthier LR, Charrin BC, Borrell-Pages M, Dompierre JP, Rangone H, Cordelieres FP, De Mey J, MacDonald ME, Lessmann V, Humbert S, Saudou F. 2004. Huntingtin controls neurotrophic support and survival of neurons by enhancing BDNF vesicular transport along microtubules. Cell 118:127-138.

Giorgini F, Moller T, Kwan W, Zwilling D, Wacker JL, Hong S, Tsai LC, Cheah CS,

Schwarcz R, Guidetti P, Muchowski PJ. 2008. Histone deacetylase inhibition modulates kynurenine pathway activation in yeast, microglia, and mice expressing a mutant huntingtin fragment. J Biol Chem 283:7390-7400.

Goellner GM, Tester D, Thibodeau S, Almqvist E, Goldberg YP, Hayden MR, McMurray CT. 1997. Different mechanisms underlie DNA instability in Huntington disease and colorectal cancer. Am J Hum Genet 60:879-890.

Graham RK, Deng Y, Slow EJ, Haigh B, Bissada N, Lu G, Pearson J, Shehadeh J, Bertram L, Murphy Z, Warby SC, Doty CN, Roy S, Wellington CL, Leavitt BR, Raymond LA, Nicholson DW, Hayden MR. 2006. Cleavage at the caspase-6 site is required for neuronal dysfunction and degeneration due to mutant huntingtin. Cell 125:1179-1191.

Gunawardena S, Her LS, Brusch RG, Laymon RA, Niesman IR, Gordesky-Gold B, Sintasath L, Bonini NM, Goldstein LS. 2003. Disruption of axonal transport by loss of huntingtin or expression of pathogenic polyQ proteins in Drosophila. Neuron 40:25-40.

Gusella JF, Wexler NS, Conneally PM, Naylor SL, Anderson MA, Tanzi RE, Watkins PC,

Ottina K, Wallace MR, Sakaguchi AY, et al. 1983. A polymorphic DNA marker genetically linked to Huntington's disease. Nature 306:234-238.

Gutekunst CA, Li SH, Yi H, Mulroy JS, Kuemmerle S, Jones R, Rye D, Ferrante RJ, Hersch SM, Li XJ. 1999. Nuclear and neuropil aggregates in Huntington's disease: relationship to neuropathology. J Neurosci 19:2522-2534.

Hashem VI, Klysik EA, Rosche WA, Sinden RR. 2002a. Instability of repeated DNAs during transformation in Escherichia coli. Mutat Res 502:39-46.

Hashem VI, Rosche WA, Sinden RR. 2002b. Genetic assays for measuring rates of (CAG).(CTG) repeat instability in Escherichia coli. Mutat Res 502:25-37.

He L, Hannon GJ. 2004. MicroRNAs: small RNAs with a big role in gene regulation. Nat Rev Genet 5:522-531.

Hebb AL, Robertson HA, Denovan-Wright EM. 2004. Striatal phosphodiesterase mRNA and protein levels are reduced in Huntington's disease transgenic mice prior to the onset of motor symptoms. Neuroscience 123:967-981.

Hebert SS, Horre K, Nicolai L, Papadopoulou AS, Mandemakers W, Silahtaroglu AN, Kauppinen S, Delacourte A, De Strooper B. 2008. Loss of microRNA cluster

miR-29a/b-1 in sporadic Alzheimer's disease correlates with increased BACE1/beta-secretase expression. Proc Natl Acad Sci U S A 105:6415-6420.

Heng MY, Tallaksen-Greene SJ, Detloff PJ, Albin RL. 2007. Longitudinal evaluation of the Hdh(CAG)150 knock-in murine model of Huntington's disease. J Neurosci 27:8989-8998.

Hodgson JG, Agopyan N, Gutekunst CA, Leavitt BR, LePiane F, Singaraja R, Smith DJ, Bissada N, McCutcheon K, Nasir J, Jamot L, Li XJ, Stevens ME, Rosemond E, Roder JC, Phillips AG, Rubin EM, Hersch SM, Hayden MR. 1999. A YAC mouse model for Huntington's disease with full-length mutant huntingtin, cytoplasmic toxicity, and selective striatal neurodegeneration. Neuron 23:181-192.

Hogan B. 1994. Manipulating the mouse embryo : a laboratory manual, 2nd ed. Plainview, N.Y.: Cold Spring Harbor Laboratory Press. xvii, 497 p. p.

Huang CC, Faber PW, Persichetti F, Mittal V, Vonsattel JP, MacDonald ME, Gusella JF. 1998. Amyloid formation by mutant huntingtin: threshold, progressivity and recruitment of normal polyglutamine proteins. Somat Cell Mol Genet 24:217-233.

Jin P, Zarnescu DC, Ceman S, Nakamoto M, Mowrey J, Jongens TA, Nelson DL, Moses K,

Warren ST. 2004. Biochemical and genetic interaction between the fragile X mental retardation protein and the microRNA pathway. Nat Neurosci 7:113-117.

Johnson MA, Rajan V, Miller CE, Wightman RM. 2006a. Dopamine release is severely compromised in the R6/2 mouse model of Huntington's disease. J Neurochem 97:737-746.

Johnson R, Gamblin RJ, Ooi L, Bruce AW, Donaldson IJ, Westhead DR, Wood IC, Jackson RM, Buckley NJ. 2006b. Identification of the REST regulon reveals extensive transposable element-mediated binding site duplication. Nucleic Acids Res 34:3862-3877.

Johnson R, Zuccato C, Belyaev ND, Guest DJ, Cattaneo E, Buckley NJ. 2008. A microRNA-based gene dysregulation pathway in Huntington's disease. Neurobiol Dis 29:438-445.

Jung J, Bonini N. 2007. CREB-binding protein modulates repeat instability in a Drosophila model for polyQ disease. Science 315:1857-1859.

Kalchman MA, Koide HB, McCutcheon K, Graham RK, Nichol K, Nishiyama K, Kazemi-Esfarjani P, Lynn FC, Wellington C, Metzler M, Goldberg YP, Kanazawa I,

Gietz RD, Hayden MR. 1997. HIP1, a human homologue of S. cerevisiae Sla2p, interacts with membrane-associated huntingtin in the brain. Nat Genet 16:44-53.

Katoh Y, Katoh M. 2008. Hedgehog signaling, epithelial-to-mesenchymal transition and miRNA (review). Int J Mol Med 22:271-275.

Kim J, Inoue K, Ishii J, Vanti WB, Voronov SV, Murchison E, Hannon G, Abeliovich A. 2007. A MicroRNA feedback circuit in midbrain dopamine neurons. Science 317:1220-1224.

Kim YJ, Sapp E, Cuiffo BG, Sobin L, Yoder J, Kegel KB, Qin ZH, Detloff P, Aronin N, DiFiglia M. 2006. Lysosomal proteases are involved in generation of N-terminal huntingtin fragments. Neurobiol Dis 22:346-356.

Kim YJ, Yi Y, Sapp E, Wang Y, Cuiffo B, Kegel KB, Qin ZH, Aronin N, DiFiglia M. 2001. Caspase 3-cleaved N-terminal fragments of wild-type and mutant huntingtin are present in normal and Huntington's disease brains, associate with membranes, and undergo calpain-dependent proteolysis. Proc Natl Acad Sci U S A 98:12784-12789.

Kosik KS. 2006. The neuronal microRNA system. Nat Rev Neurosci 7:911-920.

Kovtun IV, Liu Y, Bjoras M, Klungland A, Wilson SH, McMurray CT. 2007. OGG1 initiates age-dependent CAG trinucleotide expansion in somatic cells. Nature 447:447-452.

Kovtun IV, Therneau TM, McMurray CT. 2000. Gender of the embryo contributes to CAG instability in transgenic mice containing a Huntington's disease gene. Hum Mol Genet 9:2767-2775.

Kung VW, Hassam R, Morton AJ, Jones S. 2007. Dopamine-dependent long term potentiation in the dorsal striatum is reduced in the R6/2 mouse model of Huntington's disease. Neuroscience 146:1571-1580.

Landgraf P, Rusu M, Sheridan R, Sewer A, Iovino N, Aravin A, Pfeffer S, Rice A, Kamphorst AO, Landthaler M, Lin C, Socci ND, Hermida L, Fulci V, Chiaretti S, Foa R, Schliwka J, Fuchs U, Novosel A, Muller RU, Schermer B, Bissels U, Inman J, Phan Q, Chien M, Weir DB, Choksi R, De Vita G, Frezzetti D, Trompeter HI, Hornung V, Teng G, Hartmann G, Palkovits M, Di Lauro R, Wernet P, Macino G, Rogler CE, Nagle JW, Ju J, Papavasiliou FN, Benzing T, Lichter P, Tam W, Brownstein MJ, Bosio A, Borkhardt A, Russo JJ, Sander C, Zavolan M, Tuschl T.

2007. A mammalian microRNA expression atlas based on small RNA library sequencing. Cell 129:1401-1414.

Lee WT, Chang C. 2004. Magnetic resonance imaging and spectroscopy in assessing 3-nitropropionic acid-induced brain lesions: an animal model of Huntington's disease. Prog Neurobiol 72:87-110.

Levine MS, Cepeda C, Hickey MA, Fleming SM, Chesselet MF. 2004. Genetic mouse models of Huntington's and Parkinson's diseases: illuminating but imperfect. Trends Neurosci 27:691-697.

Li JY, Plomann M, Brundin P. 2003. Huntington's disease: a synaptopathy? Trends Mol Med 9:414-420.

Li S, Li XJ. 2006. Multiple pathways contribute to the pathogenesis of Huntington disease. Mol Neurodegener 1:19.

Li SH, Li XJ. 2004. Huntingtin-protein interactions and the pathogenesis of Huntington's disease. Trends Genet 20:146-154.

Li XJ, Li SH, Sharp AH, Nucifora FC, Jr., Schilling G, Lanahan A, Worley P, Snyder SH, Ross CA. 1995. A huntingtin-associated protein enriched in brain with implications

for pathology. Nature 378:398-402.

Li Y, Lin L, Jin P. 2008. The microRNA pathway and fragile X mental retardation protein. Biochim Biophys Acta.

Lim LP, Lau NC, Garrett-Engele P, Grimson A, Schelter JM, Castle J, Bartel DP, Linsley PS, Johnson JM. 2005. Microarray analysis shows that some microRNAs downregulate large numbers of target mRNAs. Nature 433:769-773.

Lin CH, Tallaksen-Greene S, Chien WM, Cearley JA, Jackson WS, Crouse AB, Ren S, Li XJ, Albin RL, Detloff PJ. 2001. Neurological abnormalities in a knock-in mouse model of Huntington's disease. Hum Mol Genet 10:137-144.

Lione LA, Carter RJ, Hunt MJ, Bates GP, Morton AJ, Dunnett SB. 1999. Selective discrimination learning impairments in mice expressing the human Huntington's disease mutation. J Neurosci 19:10428-10437.

Lois C, Hong EJ, Pease S, Brown EJ, Baltimore D. 2002. Germline transmission and tissue-specific expression of transgenes delivered by lentiviral vectors. Science 295:868-872.

Lukiw WJ. 2007. Micro-RNA speciation in fetal, adult and Alzheimer's disease

hippocampus. Neuroreport 18:297-300.

Lunkes A, Lindenberg KS, Ben-Haiem L, Weber C, Devys D, Landwehrmeyer GB, Mandel JL, Trottier Y. 2002. Proteases acting on mutant huntingtin generate cleaved products that differentially build up cytoplasmic and nuclear inclusions. Mol Cell 10:259-269.

Luthi-Carter R, Hanson SA, Strand AD, Bergstrom DA, Chun W, Peters NL, Woods AM, Chan EY, Kooperberg C, Krainc D, Young AB, Tapscott SJ, Olson JM. 2002a. Dysregulation of gene expression in the R6/2 model of polyglutamine disease: parallel changes in muscle and brain. Hum Mol Genet 11:1911-1926.

Luthi-Carter R, Strand AD, Hanson SA, Kooperberg C, Schilling G, La Spada AR, Merry DE, Young AB, Ross CA, Borchelt DR, Olson JM. 2002b. Polyglutamine and transcription: gene expression changes shared by DRPLA and Huntington's disease mouse models reveal context-independent effects. Hum Mol Genet 11:1927-1937.

Luthra R, Singh RR, Luthra MG, Li YX, Hannah C, Romans AM, Barkoh BA, Chen SS, Ensor J, Maru DM, Broaddus RR, Rashid A, Albarracin CT. 2008. MicroRNA-196a targets annexin A1: a microRNA-mediated mechanism of

annexin A1 downregulation in cancers. Oncogene.

Maat-Schieman M, Roos R, Losekoot M, Dorsman J, Welling-Graafland C, Hegeman-Kleinn I, Broeyer F, Breuning M, van Duinen S. 2007. Neuronal intranuclear and neuropil inclusions for pathological assessment of Huntington's disease. Brain Pathol 17:31-37.

Mangiarini L, Sathasivam K, Seller M, Cozens B, Harper A, Hetherington C, Lawton M, Trottier Y, Lehrach H, Davies SW, Bates GP. 1996. Exon 1 of the HD gene with an expanded CAG repeat is sufficient to cause a progressive neurological phenotype in transgenic mice. Cell 87:493-506.

Manley K, Pugh J, Messer A. 1999. Instability of the CAG repeat in immortalized fibroblast cell cultures from Huntington's disease transgenic mice. Brain Res 835:74-79.

Mantamadiotis T, Lemberger T, Bleckmann SC, Kern H, Kretz O, Martin Villalba A, Tronche F, Kellendonk C, Gau D, Kapfhammer J, Otto C, Schmid W, Schutz G. 2002. Disruption of CREB function in brain leads to neurodegeneration. Nat Genet 31:47-54.

Masaki S, Ohtsuka R, Abe Y, Muta K, Umemura T. 2007. Expression patterns of microRNAs 155 and 451 during normal human erythropoiesis. Biochem Biophys Res Commun 364:509-514.

McCampbell A, Taye AA, Whitty L, Penney E, Steffan JS, Fischbeck KH. 2001. Histone deacetylase inhibitors reduce polyglutamine toxicity. Proc Natl Acad Sci U S A 98:15179-15184.

Melo EO, Canavessi AM, Franco MM, Rumpf R. 2007. Animal transgenesis: state of the art and applications. J Appl Genet 48:47-61.

Merkerova M, Belickova M, Bruchova H. 2008. Differential expression of microRNAs in hematopoietic cell lineages. Eur J Haematol 81:304-310.

Mukhopadhyay D, Jung J, Murmu N, Houchen CW, Dieckgraefe BK, Anant S. 2003. CUGBP2 plays a critical role in apoptosis of breast cancer cells in response to genotoxic injury. Ann N Y Acad Sci 1010:504-509.

Nam EJ, Yoon H, Kim SW, Kim H, Kim YT, Kim JH, Kim JW, Kim S. 2008. MicroRNA expression profiles in serous ovarian carcinoma. Clin Cancer Res 14:2690-2695.

Natarajan G, Ramalingam S, Ramachandran I, May R, Queimado L, Houchen CW, Anant

S. 2008. CUGBP2 downregulation by prostaglandin E2 protects colon cancer cells from radiation-induced mitotic catastrophe. Am J Physiol Gastrointest Liver Physiol 294:G1235-1244.

Niemann H, Kues WA. 2007. Transgenic farm animals: an update. Reprod Fertil Dev 19:762-770.

Nucifora FC, Jr., Sasaki M, Peters MF, Huang H, Cooper JK, Yamada M, Takahashi H, Tsuji S, Troncoso J, Dawson VL, Dawson TM, Ross CA. 2001. Interference by huntingtin and atrophin-1 with cbp-mediated transcription leading to cellular toxicity. Science 291:2423-2428.

Ooi L, Wood IC. 2007. Chromatin crosstalk in development and disease: lessons from REST. Nat Rev Genet 8:544-554.

Pal A, Severin F, Hopfner S, Zerial M. 2008. Regulation of endosome dynamics by Rab5 and Huntingtin-HAP40 effector complex in physiological versus pathological conditions. Methods Enzymol 438:239-257.

Pal A, Severin F, Lommer B, Shevchenko A, Zerial M. 2006. Huntingtin-HAP40 complex is a novel Rab5 effector that regulates early endosome motility and is up-regulated

in Huntington's disease. J Cell Biol 172:605-618.

Perez MK, Paulson HL, Pendse SJ, Saionz SJ, Bonini NM, Pittman RN. 1998. Recruitment and the role of nuclear localization in polyglutamine-mediated aggregation. J Cell Biol 143:1457-1470.

Peters A, Rosene DL, Moss MB, Kemper TL, Abraham CR, Tigges J, Albert MS. 1996. Neurobiological bases of age-related cognitive decline in the rhesus monkey. J Neuropathol Exp Neurol 55:861-874.

Pinkert CA. 2002. Transgenic animal technology : a laboratory handbook, 2nd ed. Amsterdam London: Academic. 359-394 p.

Presty SK, Bachevalier J, Walker LC, Struble RG, Price DL, Mishkin M, Cork LC. 1987. Age differences in recognition memory of the rhesus monkey (Macaca mulatta). Neurobiol Aging 8:435-440.

Qurashi A, Chang S, Peng J. 2007. Role of microRNA pathway in mental retardation. ScientificWorldJournal 7:146-154.

Ravikumar B, Imarisio S, Sarkar S, O'Kane CJ, Rubinsztein DC. 2008. Rab5 modulates aggregation and toxicity of mutant huntingtin through macroautophagy in cell and

fly models of Huntington disease. J Cell Sci 121:1649-1660.

Rong J, Li S, Sheng G, Wu M, Coblitz B, Li M, Fu H, Li XJ. 2007a. 14-3-3 protein interacts with Huntingtin-associated protein 1 and regulates its trafficking. J Biol Chem 282:4748-4756.

Rong J, Li SH, Li XJ. 2007b. Regulation of intracellular HAP1 trafficking. J Neurosci Res 85:3025-3029.

Rong J, McGuire JR, Fang ZH, Sheng G, Shin JY, Li SH, Li XJ. 2006. Regulation of intracellular trafficking of huntingtin-associated protein-1 is critical for TrkA protein levels and neurite outgrowth. J Neurosci 26:6019-6030.

Rosas HD, Hevelone ND, Zaleta AK, Greve DN, Salat DH, Fischl B. 2005. Regional cortical thinning in preclinical Huntington disease and its relationship to cognition. Neurology 65:745-747.

Ryu H, Lee J, Hagerty SW, Soh BY, McAlpin SE, Cormier KA, Smith KM, Ferrante RJ. 2006. ESET/SETDB1 gene expression and histone H3 (K9) trimethylation in Huntington's disease. Proc Natl Acad Sci U S A 103:19176-19181.

Sadri-Vakili G, Bouzou B, Benn CL, Kim MO, Chawla P, Overland RP, Glajch KE, Xia E,

Qiu Z, Hersch SM, Clark TW, Yohrling GJ, Cha JH. 2007. Histones associated with downregulated genes are hypo-acetylated in Huntington's disease models. Hum Mol Genet 16:1293-1306.

Schaefer A, O'Carroll D, Tan CL, Hillman D, Sugimori M, Llinas R, Greengard P. 2007. Cerebellar neurodegeneration in the absence of microRNAs. J Exp Med 204:1553-1558.

Schilling G, Becher MW, Sharp AH, Jinnah HA, Duan K, Kotzuk JA, Slunt HH, Ratovitski T, Cooper JK, Jenkins NA, Copeland NG, Price DL, Ross CA, Borchelt DR. 1999. Intranuclear inclusions and neuritic aggregates in transgenic mice expressing a mutant N-terminal fragment of huntingtin. Hum Mol Genet 8:397-407.

Schilling G, Klevytska A, Tebbenkamp AT, Juenemann K, Cooper J, Gonzales V, Slunt H, Poirer M, Ross CA, Borchelt DR. 2007. Characterization of huntingtin pathologic fragments in human Huntington disease, transgenic mice, and cell models. J Neuropathol Exp Neurol 66:313-320.

Schilling G, Sharp AH, Loev SJ, Wagster MV, Li SH, Stine OC, Ross CA. 1995.

Expression of the Huntington's disease (IT15) protein product in HD patients. Hum Mol Genet 4:1365-1371.

Schroder AR, Shinn P, Chen H, Berry C, Ecker JR, Bushman F. 2002. HIV-1 integration in the human genome favors active genes and local hotspots. Cell 110:521-529.

Sharp AH, Loev SJ, Schilling G, Li SH, Li XJ, Bao J, Wagster MV, Kotzuk JA, Steiner JP, Lo A, et al. 1995. Widespread expression of Huntington's disease gene (IT15) protein product. Neuron 14:1065-1074.

Shehadeh J, Fernandes HB, Zeron Mullins MM, Graham RK, Leavitt BR, Hayden MR, Raymond LA. 2006. Striatal neuronal apoptosis is preferentially enhanced by NMDA receptor activation in YAC transgenic mouse model of Huntington disease. Neurobiol Dis 21:392-403.

Shimohata T, Nakajima T, Yamada M, Uchida C, Onodera O, Naruse S, Kimura T, Koide R, Nozaki K, Sano Y, Ishiguro H, Sakoe K, Ooshima T, Sato A, Ikeuchi T, Oyake M, Sato T, Aoyagi Y, Hozumi I, Nagatsu T, Takiyama Y, Nishizawa M, Goto J, Kanazawa I, Davidson I, Tanese N, Takahashi H, Tsuji S. 2000. Expanded polyglutamine stretches interact with TAFII130, interfering with CREB-dependent

transcription. Nat Genet 26:29-36.

Slow EJ, van Raamsdonk J, Rogers D, Coleman SH, Graham RK, Deng Y, Oh R, Bissada N, Hossain SM, Yang YZ, Li XJ, Simpson EM, Gutekunst CA, Leavitt BR, Hayden MR. 2003. Selective striatal neuronal loss in a YAC128 mouse model of Huntington disease. Hum Mol Genet 12:1555-1567.

Small SA, Chawla MK, Buonocore M, Rapp PR, Barnes CA. 2004. Imaging correlates of brain function in monkeys and rats isolates a hippocampal subregion differentially vulnerable to aging. Proc Natl Acad Sci U S A 101:7181-7186.

Sramka M, Rattaj M, Molina H, Vojtassak J, Belan V, Ruzicky E. 1992. Stereotactic technique and pathophysiological mechanisms of neurotransplantation in Huntington's chorea. Stereotact Funct Neurosurg 58:79-83.

Stack EC, Kubilus JK, Smith K, Cormier K, Del Signore SJ, Guelin E, Ryu H, Hersch SM, Ferrante RJ. 2005. Chronology of behavioral symptoms and neuropathological sequela in R6/2 Huntington's disease transgenic mice. J Comp Neurol 490:354-370.

Steffan JS, Bodai L, Pallos J, Poelman M, McCampbell A, Apostol BL, Kazantsev A,

Schmidt E, Zhu YZ, Greenwald M, Kurokawa R, Housman DE, Jackson GR, Marsh JL, Thompson LM. 2001. Histone deacetylase inhibitors arrest polyglutamine-dependent neurodegeneration in Drosophila. Nature 413:739-743.

Steffan JS, Kazantsev A, Spasic-Boskovic O, Greenwald M, Zhu YZ, Gohler H, Wanker EE, Bates GP, Housman DE, Thompson LM. 2000. The Huntington's disease protein interacts with p53 and CREB-binding protein and represses transcription. Proc Natl Acad Sci U S A 97:6763-6768.

Strehlow AN, Li JZ, Myers RM. 2007. Wild-type huntingtin participates in protein trafficking between the Golgi and the extracellular space. Hum Mol Genet 16:391-409.

Subramaniam D, Natarajan G, Ramalingam S, Ramachandran I, May R, Queimado L, Houchen CW, Anant S. 2008. Translation inhibition during cell cycle arrest and apoptosis: Mcl-1 is a novel target for RNA binding protein CUGBP2. Am J Physiol Gastrointest Liver Physiol 294:G1025-1032.

Sugars KL, Rubinsztein DC. 2003. Transcriptional abnormalities in Huntington disease. Trends Genet 19:233-238.

Szebenyi G, Morfini GA, Babcock A, Gould M, Selkoe K, Stenoien DL, Young M, Faber PW, MacDonald ME, McPhaul MJ, Brady ST. 2003. Neuropathogenic forms of huntingtin and androgen receptor inhibit fast axonal transport. Neuron 40:41-52.

Trottier Y, Devys D, Imbert G, Saudou F, An I, Lutz Y, Weber C, Agid Y, Hirsch EC, Mandel JL. 1995. Cellular localization of the Huntington's disease protein and discrimination of the normal and mutated form. Nat Genet 10:104-110.

van Dellen A, Blakemore C, Deacon R, York D, Hannan AJ. 2000. Delaying the onset of Huntington's in mice. Nature 404:721-722.

van der Burg JM, Bacos K, Wood NI, Lindqvist A, Wierup N, Woodman B, Wamsteeker JI, Smith R, Deierborg T, Kuhar MJ, Bates GP, Mulder H, Erlanson-Albertsson C, Morton AJ, Brundin P, Petersen A, Bjorkqvist M. 2008. Increased metabolism in the R6/2 mouse model of Huntington's disease. Neurobiol Dis 29:41-51.

Van Raamsdonk JM, Metzler M, Slow E, Pearson J, Schwab C, Carroll J, Graham RK, Leavitt BR, Hayden MR. 2007a. Phenotypic abnormalities in the YAC128 mouse model of Huntington disease are penetrant on multiple genetic backgrounds and modulated by strain. Neurobiol Dis 26:189-200.

Van Raamsdonk JM, Pearson J, Slow EJ, Hossain SM, Leavitt BR, Hayden MR. 2005. Cognitive dysfunction precedes neuropathology and motor abnormalities in the YAC128 mouse model of Huntington's disease. J Neurosci 25:4169-4180.

Van Raamsdonk JM, Warby SC, Hayden MR. 2007b. Selective degeneration in YAC mouse models of Huntington disease. Brain Res Bull 72:124-131.

Vo N, Klein ME, Varlamova O, Keller DM, Yamamoto T, Goodman RH, Impey S. 2005. A cAMP-response element binding protein-induced microRNA regulates neuronal morphogenesis. Proc Natl Acad Sci U S A 102:16426-16431.

Vonsattel JP, DiFiglia M. 1998. Huntington disease. J Neuropathol Exp Neurol 57:369-384.

Vonsattel JP, Myers RH, Stevens TJ, Ferrante RJ, Bird ED, Richardson EP, Jr. 1985. Neuropathological classification of Huntington's disease. J Neuropathol Exp Neurol 44:559-577.

Walker FO. 2007a. Huntington's disease. Lancet 369:218-228.

Walker FO. 2007b. Huntington's Disease. Semin Neurol 27:143-150.

Walker LC, Kitt CA, Struble RG, Wagster MV, Price DL, Cork LC. 1988. The neural basis

of memory decline in aged monkeys. Neurobiol Aging 9:657-666.

Wall RJ, Seidel GE, Jr. 1992. Transgenic farm animals - A critical analysis. Theriogenology 38:337-357.

Wang CE, Tydlacka S, Orr AL, Yang SH, Graham RK, Hayden MR, Li S, Chan AW, Li XJ. 2008. Accumulation of N-terminal mutant huntingtin in mouse and monkey models implicated as a pathogenic mechanism in Huntington's disease. Hum Mol Genet 17:2738-2751.

Wang H, Lim PJ, Yin C, Rieckher M, Vogel BE, Monteiro MJ. 2006. Suppression of polyglutamine-induced toxicity in cell and animal models of Huntington's disease by ubiquilin. Hum Mol Genet 15:1025-1041.

Wellington CL, Ellerby LM, Gutekunst CA, Rogers D, Warby S, Graham RK, Loubser O, van Raamsdonk J, Singaraja R, Yang YZ, Gafni J, Bredesen D, Hersch SM, Leavitt BR, Roy S, Nicholson DW, Hayden MR. 2002. Caspase cleavage of mutant huntingtin precedes neurodegeneration in Huntington's disease. J Neurosci 22:7862-7872.

Wheeler VC, Auerbach W, White JK, Srinidhi J, Auerbach A, Ryan A, Duyao MP,

Vrbanac V, Weaver M, Gusella JF, Joyner AL, MacDonald ME. 1999. Length-dependent gametic CAG repeat instability in the Huntington's disease knock-in mouse. Hum Mol Genet 8:115-122.

Wheeler VC, Persichetti F, McNeil SM, Mysore JS, Mysore SS, MacDonald ME, Myers RH, Gusella JF, Wexler NS. 2007. Factors associated with HD CAG repeat instability in Huntington disease. J Med Genet 44:695-701.

Woodman B, Butler R, Landles C, Lupton MK, Tse J, Hockly E, Moffitt H, Sathasivam K, Bates GP. 2007. The Hdh(Q150/Q150) knock-in mouse model of HD and the R6/2 exon 1 model develop comparable and widespread molecular phenotypes. Brain Res Bull 72:83-97.

Xie X, Lu J, Kulbokas EJ, Golub TR, Mootha V, Lindblad-Toh K, Lander ES, Kellis M. 2005. Systematic discovery of regulatory motifs in human promoters and 3' UTRs by comparison of several mammals. Nature 434:338-345.

Yang SH, Agca Y, Cheng PH, Yang JJ, Agca C, Chan AW. 2007. Enhanced transgenesis by intracytoplasmic injection of envelope-free lentivirus. Genesis 45:177-183.

Yang SH, Cheng PH, Banta H, Piotrowska-Nitsche K, Yang JJ, Cheng EC, Snyder B,

Larkin K, Liu J, Orkin J, Fang ZH, Smith Y, Bachevalier J, Zola SM, Li SH, Li XJ, Chan AW. 2008a. Towards a transgenic model of Huntington's disease in a non-human primate. Nature 453:921-924.

Yang SH, Cheng PH, Sullivan RT, Thomas JW, Chan AW. 2008b. Lentiviral integration preferences in transgenic mice. Genesis.

Yee JK, Zaia JA. 2001. Prospects for gene therapy using HIV-based vectors. Somat Cell Mol Genet 26:159-174.

Yekta S, Shih IH, Bartel DP. 2004. MicroRNA-directed cleavage of HOXB8 mRNA. Science 304:594-596.

Yu JY, Chung KH, Deo M, Thompson RC, Turner DL. 2008. MicroRNA miR-124 regulates neurite outgrowth during neuronal differentiation. Exp Cell Res.

Zhao Y, Keating K, Thorpe R. 2007. Comparison of toxicogenomic profiles of two murine strains treated with HIV-1-based vectors for gene therapy. Toxicol Appl Pharmacol 225:189-197.

Zheng P, Wang H, Bavister BD, Ji W. 2001. Maturation of rhesus monkey oocytes in chemically defined culture media and their functional assessment by IVF and

embryo development. Hum Reprod 16:300-305.

Zhu H, Wu H, Liu X, Evans BR, Medina DJ, Liu CG, Yang JM. 2008. Role of MicroRNA miR-27a and miR-451 in the regulation of MDR1/P-glycoprotein expression in human cancer cells. Biochem Pharmacol 76:582-588.

Zuccato C, Belyaev N, Conforti P, Ooi L, Tartari M, Papadimou E, MacDonald M, Fossale E, Zeitlin S, Buckley N, Cattaneo E. 2007. Widespread disruption of repressor element-1 silencing transcription factor/neuron-restrictive silencer factor occupancy at its target genes in Huntington's disease. J Neurosci 27:6972-6983.

Zuccato C, Tartari M, Crotti A, Goffredo D, Valenza M, Conti L, Cataudella T, Leavitt BR, Hayden MR, Timmusk T, Rigamonti D, Cattaneo E. 2003. Huntingtin interacts with REST/NRSF to modulate the transcription of NRSE-controlled neuronal genes. Nat Genet 35:76-83.

PUBLISHED PAPERS

Journal articles

Yang, S. H., P. H. Cheng, J. J. Yang and A. W. S. Chan. 2008. Evaluation of lentiviral transgenesis in transgenic mice. **Transgenic research**. (in revision)

Yang, S. H., P. H. Cheng, R. T. Sullivan, J. W. Thomas, and A. W. S. Chan. 2008. Lentiviral Integration preferences in transgenic mice. **Genesis** (Accepted)

Lorthongpanich, C., **S. H. Yang**, K. Piotrowska-Nitsche, R. Parnpai and A. W. S. Chan. 2008. Chemical enhancement in embryo development and stem cell derivation from single blastomere. **Cloning and Stem Cells** (Accepted)

Piotrowska-Nitsche K., **S. H. Yang**, H. Banta and A. W. S. Chan. 2008. Assisted fertilization and embryonic axis formation in higher primates. **RBM Online** (Accepted)

Wang, C. E., S. Tydlacka, A. L. Orr, **S. H. Yang**, R. K. Graham, M. R. Hayden, S. Li, A. W. S. Chan, X. J. Li. 2008. Accumulation of N-terminal mutant huntingtin in mouse and monkey models implicated as a pathogenic mechanism in Huntington's disease. **Human Molecular Genetics** 17(17):2738-2751.

Yang, S. H., P. H. Cheng, H. Banta, K. Piotrowska-Nitsche, J. J. Yang, E. C. .H. Cheng, B. Snyder, J. Liu, K. Larkin, J. Orkin, Z. Fang, Y. Smith, J. Bachevalier, S. M. Zola, S. Li, X. J. Li and A. W. S. Chan. 2008. Towards a transgenic model of Huntington's Disease in a non-human primate. **Nature** 453: 921-924.

Lorthongpanich, C., **S. H. Yang**, K. Piotrowska-Nitsche, R. Parnpa and A. W. S. Chan. 2008. Development of single mouse blastomeres into blastocysts, outgrowths and the establishment of embryonic stem cells. **Reproduction** 135(6):805-813.

Yang, S. H., Y. Agca, P. H. Cheng, J. J. Yang, C. Agca, and A. W. S. Chan. 2007. Enhanced transgenesis by intracytoplasmic injection of envelope-free lentivirus. **Genesis** 45(4):177-83.

Conference abstracts

Li, X. J., C. E. Wang, A. Orr, J. Wang, S. Tydlacka, **S. H. Yang**, A. W. S. Chan and S. Li. 2008. Neuronal toxicity of cytoplasmic mutant huntingtin. Hereditary Disease Foundation.

Yang, S. H., P. H. Cheng, H. Banta, K. Piotrowska-Nitsche, J. J. Yang, E. C. .H. Cheng, B. Snyder, J. Liu, K. Larkin, J. Orkin, Z. Fang, Y. Smith, J. Bachevalier, S. M. Zola, S. Li, X. J. Li and A. W. S. Chan. 2008. A transgenic nonhuman primate model of Huntington's disease. Hereditary Disease Foundation.

Liu, J., C. Cheng, R. Long, **S. H. Yang**, L. Wang, P. Cheng, J. Yang, D. Wu, S. Brooke, H. Mao, and A. W. S. Chan. 2008. Ferritin transgene functions as an endogenous MRI reporter in embryonic stem cell. The 38th Annual meeting of the Society for Neuroscience. Washington, DC, USA.

Yang, S. H., P. H. Cheng, and A. W. S. Chan. 2008. Gene expression profiles in post-mortem brain tissue and peripheral blood for the non-human primate model of Huntington's disease. The 38th Annual meeting of the Society for Neuroscience. Washington, DC, USA.

Yang, S. H., P. H. Cheng and A. W. S. Chan. 2008. Lentiviral transgenesis in mice and nonhuman primates. The 34th Annual International Embryo Transfer Society (IETS) Conference. Denver, Colorado, USA.

Lorthongpanich, C., **S. H. Yang**, K. Piotrowska-Nitsche and A. W. S. Chan. 2007.

Competence of early embryonic blastomeres for the establishment of embryonic stem cell line. The 63rd annual meeting of American Society of Reproductive Medicine. Washington, DC, USA.

Piotrowska-Nitsche, K., **S. H. Yang**, H. Banta and A. W. S. Chan. 2007. Sperm enters the egg through the mechanical injection does not affect early patterning of the monkey embryos. The 63rd annual meeting of American Society of Reproductive Medicine. Washington, DC, USA.

Lorthongpanich, C., **S. H. Yang**, K. Piotrowska-Nitsche, R. Parnpai and A. W. S. Chan. 2007. Stem Cell Establishment from Single Mouse Blastomere. The 3rd annual meeting of the Asian Reproductive Biotechnology Society. Hanoi, Vietnam, Singapore.